-

Dissertation

Submitted to the Combined

Faculties for the Natural Science and for Mathematics

of the Ruperto-Carola University of Heidelberg, Germany

for the degree of

Doctor of Natural Science

Presented by

Diplom-Pathologist : **Yung-Hui Kuan**

Born in : Taiwan

Oral-examination : Feb. 16 2005

Referees : **Prof. Dr. Dr. h.c. Konrad Beyreuther**
Prof. Dr. Felix Wieland

Characterization of APPBP2/PAT1a
and
Analysis of its interaction with APP family Proteins

Doctoral study in the Molecular Biology
Center of Molecular Biology (ZMBH)
Ruprecht-Karls University of Heidelberg
Germany

Yung-Hui Kuan
(Tweety ^_^)
Pathologist aus Taiwan

Referees: Prof. Dr. Dr. h. c. Konrad Beyreuther
Prof. Dr. Felix Wieland
Prof. Dr. Med. Joachim Kirsch
Prof. Dr. M. Lanzer
Dr. Stefan Kins

Acknowledgements

Since there are tooooooooooo many people that Tweety wants to thank to.....so,

she decided.....to say, " Thanks God !!! " the first .....^_^.....

anybody dares to have any opinion of that.....☺

Then..... I wanna thank Dr. Stefan Kins who tolerated me for 3+ years and gave lots of useful guidance to make this work possible to achieve what it could be now. Thank all the people in the Lab.128, Peter S., Simone E., Anita, Tomas, Annette, Markus U. and Peter P. that helped me when I was yelling around for helps. Thanks Inge who helped me for those experiments on primary neurons and thanks people in the Lab. 129 that also helped me when my experiments needed their advices.

Tweety wanna thank Prof. Beyreuther that formed this group so that 10+? years later Tweety could get a chance to be one of the members(soon will be an ex-☹...). Tweety also wanna thank Prof. Wieland who was willing and patient to listen her boring progress reports but still gave great advices and encouragements. Tweety wanna thank Prof. Kirsch who generously allowed her to use all the equiptments and materials in his group regardless to all her impoliteness. Tweety wanna thank Prof. Lanzer who was willing to spend his time to examine her in the final defense.....so.....as I've said.....there are many.....hardly to list all.....breath a while.....☺.....then, Tweety wanna thank all Paro's that brought so much fun and warmth to her life spending here in this Inst. The last, Tweety really wanna thank all the people in the 1st floor of ZMBH that could stand her cooking and sleeping in the coffee room. Hope may have chances to see any of you somewhere on the earth again.....**Tweety** ..^_^.. **Feb. 2005**

Table of Contents

I. Abbreviations

Terms	
AD	Alzheimer's disease
LOAD	late onset Alzheimer's disease
Aβ	beta amyloid
APP	amyloid precursor protein
APLP1	amyloid precursor protein like protein 1
APLP2	amyloid precursor protein like protein 2
KLC	kinesin light chain
PAT1	protein interacting with APP tail 1
APPBP2	amyloid precursor protein binding protein 2
PAT1a	protein interacting with APP tail 1a
SNPs	single nucleotide polymorphisms
CNS	central nerves system
CA1	Cornu Ammonis 1 (CA1 region of hippocampus)
CA2	Cornu Ammonis 2 (CA2 region of hippocampus)
CA3	Cornu Ammonis 3 (CA3 region of hippocampus)
DG	dentate gyrus
GFAP	glial fibrillary acid protein
GST	glutathione S-transferase
siPAT1a	small interfering APPBP2/PAT1a
BACE1	β- site APP cleaving enzyme-1
CTF	carboxyl terminal fragment
BaSS	basolateral sorting signal
PTB	phospho tyrosin binding domain
NPTY	NPTY motif
PCR	polymerize chain reaction
GFP	green fluorescence protein
HA	hemagglutinin
DIV	day in vitro
ELISA	Enzyme-Linked Immunosorbent Assay
SH-SY5Y	human neuroblastoma cells
CS-GAG	chondroitin sulfate glycosaminoglycan
CRD	cystein rich domain
Zn/Cu-BD	zinc- and copper binding domains
CHD	carbohydrate domain
KPI	Kunitz-type protease inhibitor domain,
OX-2	MRC-OX2 antigen interacting domain
RIP	regulated intramembrane proteolysis

II. Summary

The physiological function and pathogenic role of the Amyloid Precursor Protein (APP) and its homologues, Amyloid Precursor Protein like protein 1 and 2 (APLP1, APLP2), correlate strongly to their subcellular localization. Lines of evidences from Pimplikar and co-workers showed a kinesin light chain (KLC) like protein, termed PAT1 (protein interacting with APP tail 1), interacts with both microtubules and the intracellular domain of APP, in addition, a neuronal function in the microtubule plus end directed translocation of APP toward the plasma membrane was proposed along within their study. However neither expression nor functional studies in neuronal system for PAT1 were done to date.

In this study, we found that the PAT1 sequence exhibits 7 nucleotide exchanges resulting in 6 non-homologous amino acid substitutions, which are likely due to a rarely occurring polymorphism in the APPBP2 gene, therefore in this study, APPBP2 was used to perform further investigation on the interaction with APP and APLPs.

Characterization by Northern analysis reveals that APPBP2/PAT1a is ubiquitously expressed in all tissues examined from Human and Mouse. In situ hybridization and immunohistochemical analysis clearly show a wide overlap of APPBP2/PAT1a with APP/APLPs in mouse brain, and is predominantly expressed by neurons.

Further, this study shows the existence of a common complex containing APP family members and APPBP2/PAT1a in mouse brain. In primary cultured neurons, APPBP2/PAT1a is partly associated with vesicular membranes among soma and neurites, bearing APP, APLP1 and APLP2 suggesting that APPBP2/PAT1a is implicated in the intraneuronal transport of APP/APLPs. The highest degree of colocalization in neurons was observed for APLP2 in comparison to the other family members indicating that APPBP2/PAT1a might interact preferentially with APLP2 *in vivo*. Moreover, data in this study also showed that the PAT1a protein level affects APP/APLPs processing and alters Aβ secretion in stably transfected SH-SY5Y cells.

All together, these data reveal the expression pattern of APPBP2/PAT1a in situ in mouse brain and various tissues among human and mouse, the in vivo interaction of APPBP2/PAT1a with all APP family members in mouse CNS, and co-distribution in late secretory pathway in primary neurons. Besides, this study shows that APPBP2/PAT1a has a regulatory function in APP/APLPs processing and Aβ production suggesting that APPBP2/PAT1a shall be considered as a alternative

novel target for analyzing physiological functions of APP family proteins and further, a potential target for therapeutic approaches to facilitate Aβ production in Alzheimer's disease.

1. Introduction

1.1 Alzheimer's disease

Alzheimer's disease (AD) is pathologically characterized by neurodegeneration, intracellular deposition of Neurofibrillary Tangles (NFTs) and production of extracellular Amyloid Plaques, mainly composed by the hyperphosphorlated tau or a short peptide, beta-amyloid (Aβ), derived from the Amyloid Precursor protein (APP) (Selkoe, 1994). AD lead to progressive loss of cognitive brain functions, deterioration of the patient's personality, and finally to the death due to respiratory failure. Patients with Alzheimer's disease may live for 7 to 10 years after the onset of the disease, some, however, live for up to 20 years.

The era of molecular biology research in AD started with the identification of the main constituent of vascular Amyloid and Amyloid (Glenner and Wong, 1984; Masters et al., 1985). The initial step involves proteolytic cleavages of APP by β- and γ-secretases, releasing short 40, 42 aa peptides (Aß1-40 and 1-42)(for details, see chapter 1.2). Polymerization of Aβ and subsequent neuronal deposit lead to the degeneration of neurons involved in memory and cognition. Aβ deposits also contain anti-chymotrypsin (ACT), and Apolipoprotein (Apo-E) that may promote Aβ polymerization (Aksenova et al. 1996; Harr et al. 1996; Ma et al. 1996), although Aβ deposits or plaques are central to neuropathogenesis and neurodegeneration of AD, it is still not clear how they affect neuronal functions.

Studies on genetic inheritance of AD found that it is a complex neurodegenerative disorder predisposed by multiple genetic factors (Cartier-Harlin et al. 2004; Pastor et al. 2004; Panza et al. 2004). Mutations in APP are known to be associated with autosomal dominant, early onset familial AD (FAD). A number of genes encoding proteins capable of binding to APP have been identified, but their contribution to AD pathobiology remains largely unclear (King et al. 2004). Conceivably, mutations in these genes may play a role in affecting AD susceptibility, which appears to be substantiated by some genetic studies.

Other mutations were found in the Presenilin1 and 2 (PS1, PS2) genes, all of which are directly involved in the generation of Aβ that support the hypothesis of the amyloid cascade and in general lead to an earlier age of onset (reviewed in (Annaert and De Strooper, 2002a). The main effect of mutations in these genes is the

overproduction of Aβ42, which was shown to be especially prone to aggregation (Suzuki et al., 1994). In the pathogenesis of AD, disturbed cellular Calcium homeostasis ((Mattson and Chan, 2003), oxidative stress, and reactive gliosis were observed which might play a major role in the disease process (reviewed in (Small et al., 2001). Moreover, numerous studies found Aß to be toxic to neurons and to induce apoptosis. Although some researchers now believe that oligomeric Aβ42 is the crucial agent causing the disease (reviewed in (Selkoe, 2002), the precise molecular mechanism leading to neurodegenreation in AD remains unclear. It is also unclear so far whether Tau hyperphosphorylation or tangle formation is either the cause or effect of Aß production and deposition. An exciting study in mouse model systems shows that Aß42 injection in the brain of Tau P301L transgenic mice can induce formation of PHFs (Gotz et al., 2001), which puts Aß in the front among the causes of AD pathology.

Recent therapeutic strategies (reviewed in (Janus, 2003) are aiming at preventing Aβ generation by inhibition of APP cleavage (reviewed in (Dewachter and Van Leuven, 2002), degradation of Aβ with enzymes like IDE (Qiu et al., 1998; Vekrellis et al., 2000), or immunization with either humanized antibodies against oligomeric Aβ42, or active immunization with preaggregated Aß peptides (Schenk et al., 1999). Some of these efforts have already shown promising results (Hock et al. 2002 ; Hock et al. 2003) but no applicable therapy is available to date.

1.2. Structure, expression, and processing of the Amyloid Precursor Protein family

Research in the field of AD was strongly stimulated by the discovery and cloning of a protein precursor to Aß, the Amyloid Precursor Protein (APP) (Kang et al., 1987). APP is a Type I transmembrane protein, has one membrane spanning domain, and belongs to a large protein family which consists in mammals besides APP two paralogues, the Amyloid Precursor-like Proteins, APLP1 and APLP2 (Suzuki et al., 1997; Wasco et al., 1992a).

APP is encoded by 18 exons, of which exons 7, 8, and 15 are alternatively spliced. All eight variants have been shown to exist *in vivo* and expression of the different

splice variants is developmentally regulated (Sandbrink et al., 1997). APP resembles a ubiquitously expressed cell surface receptor with a large ectodomain, a single transmembrane domain and a short cytoplasmic tail (Kitaguchi et al., 1988; Tanzi et al., 1988). The major expressed isoforms of APP consist of 695, 751, or 770 amino acids, all of which are N- and O-glycosylated and transported to the cell surface through the secretory pathway (Weidemann et al., 1989). APP695 is predominantly expressed in neurons, while APP751 and 770 are the major species in peripheral tissues and glial cells (Sandbrink et al., 1994). Alternative splicing by omission of exon 15 generates a consensus sequence for chondroitin sulfate glycosaminoglycan (CS-GAG) modification, and the corresponding L-APP Proteoglycans have first been characterized to be expressed in Leukocytes, but are also found in other peripheral cells, and to a minor extend in neurons (Sandbrink et al., 1993).

Their are two paralogues of APP in mammals, Amyloid Precursor-like Proteins, APLP1 and APLP2 (Wasco et al., 1992b; Wasco et al., 1993). Both share high sequence homology and similar protein domain organization with APP (reviewed in (Bayer et al., 1999; Coulson et al., 2000a). On the extracellular side, a Cystein rich domain (CRD) showing Heparin and Collagen binding properties, Zinc- and Copper binding domains (Zn/Cu-BD) within an acidic region, and a Carbohydrate domain are conserved. Moreover, the short intracellular domain exhibits the highest degree of conservation. APP and APLP2 also share an alternatively spliced Kunitz-type protease inhibitor (KPI) domain, while the OX-2 and the Aβ region are unique to APP. (Fig.1.1a)

APLP1 is viewed as the ancestral member of the mammalian APP gene family, since it is closest to the invertebrate homologues (Coulson et al., 2000a) (Fig.1.1b). APLP1 undergoes no alternative splicing and is predominantly expressed in neurons and some glial cell of the central nervous system (Lorent et al., 1995), which is also described for *Drosophila* APPL (Martin-Morris and White, 1990). APLP2 on the other hand, is alternatively spliced and expressed in a similar pattern as APP (Slunt et al., 1994). One notable difference between APP and APLP2 is that the major neuronal form of APLP2 with 763 amino acids contains the KPI domain (Sandbrink et al., 1997).

In the mammalian brain, all APP family members are widely expressed in a similar pattern (Crain et al., 1996; Lorent et al., 1995; McNamara et al., 1998; Wasco et al., 1993). Biochemical analyses have shown presynaptic enrichment for APP (Ferreira

et al., 1993) and APLP2 (Lyckman et al., 1998), while APLP1 was found to be specifically localized to the postsynapse (kim et al. 1995).

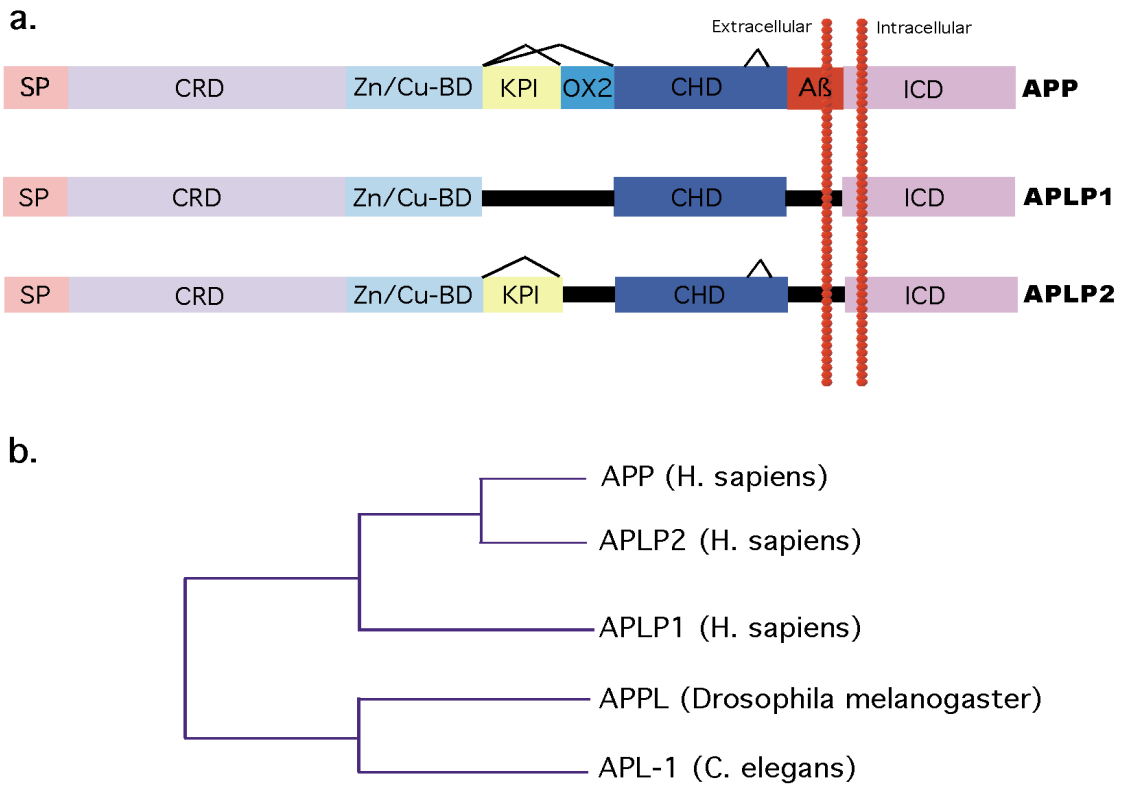

Fig.1.1: APP family proteins. (a) Schematic domain organization of mammalian APP members. SP: signal peptide; CRD: Cystein rich domain; Zu/Cu-BD: an acidic region with Zn-/Cu-binding properties; KPI: kunitz-type proteas inhibitor domain; OX2: MRC-OX2 antigen domain, are found mostly in non-neuronal glial cells; CHD: carbohydrate domain; Aβ**:** β-amyloid domain; ICD: intracellular domain. Brackets indicate alternatively spliced regions. **(b)** Family tree consists of identified APP homologous among 3 different species.

APP is best investigated in regard to its proteolytic cleavage of Aβ, which was found to be derived from its precursor during normal cellular metabolism (Haass et al., 1992; Seubert et al., 1993).(Fig.1.2a) In the amyloidogenic pathway, APP is cleaved by the β- APP cleaving enzyme1 (BACE1) (Hussain et al., 1999; Sinha et al., 1999; Vassar et al., 1999; Yan et al., 1999), resulting in the release of the soluble β-cleaved ectodomain (sAPPβ). Subsequently, the remaining C-terminal fragment is further processed by cleavages at the γ- or ε-sites within the transmembrane region (Weidemann et al., 2002a), thus setting free of the Aβ peptides (Aβ40, Aβ42) and the intracellular domain (APP^{ICD}). The γ-secretase complex, has been reported consisting of at least Presenilin, Nicastrin, Aph-1, and Pen-2 (Edbauer et al., 2003;

Takasugi et al., 2003), is thought to be required for both, γ- and ε-cleavage. The mechanism of this unusual cleavage within a hydrophobic surrounding is still unclear, but might be mediated by two aspartic residues present within the transmembrane region of Presenilin (Wolfe et al., 1999), which may mediate a dual cleavage at the γ- and ε-sites (Schroeter et al., 2003).

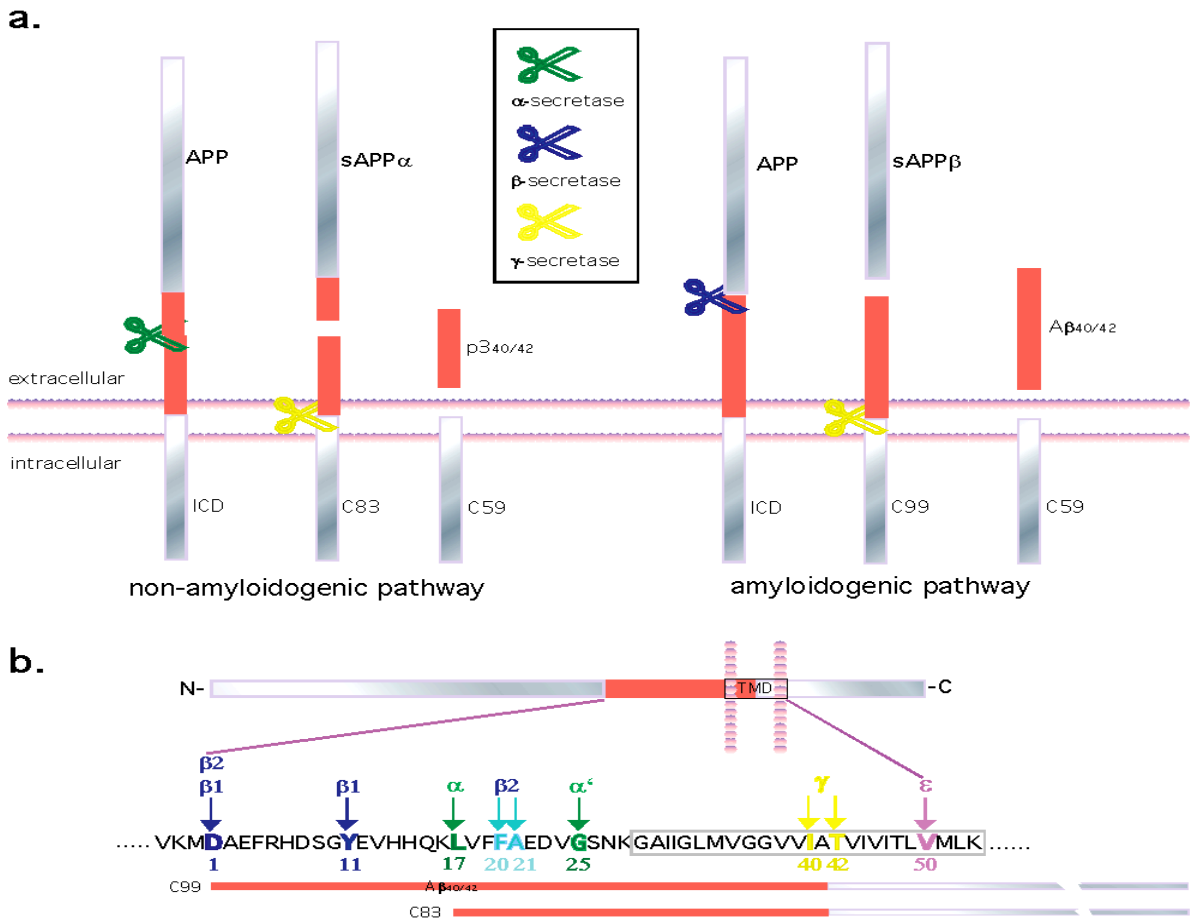

Fig. 1.2 Proteolytic cleavage of APP. (a) APP can be cleaved by α -secretase (left, non-amyloidogenic pathway) or by γ-secretase (upper, amyloidogenic pathway), resulting in the release of the soluble ectodomain. The APP carboxy-terminal fragments (C83 and C99, respectively) are substrates for γ-secretase. The γ-cleavage yields the p3 or Aβ peptides, which are secreted into the extracellular space, and the APP intracellular domain fragment C59, which is released into the cytoplasm. **(b)** Diagram indicates in details, the major and minor cleavage sites of all secretases among Aβ and Transmembrane (TMD) domains. Two variants of β-secretase (β1, β2) may cleave APP within the Aβ domain, C99 is generated by both β1-, β2- cleavages at the same site, and is the majority form of βCTF. The α -secretase also contains two variants (α-,α'-) that may cleave APP within the Aβ domain, C83 is generated by α-cleavage and is the major form of αCTF. Both C99 and C83 become a substrate of γ-secretase.

Alternatively, APP is processed at the α-site, which precludes Aβ generation, and is therefore called the non-amyloidogenic pathway (Fig.1.2a). Subsequently, proteolysis of the remaining α-C-terminal fragment by γ-secretase leads to the release of the APP^{ICD} and a short extracellular peptide (p3) (Eggert et al., 2004a; Walsh et al., 2003a; Weidemann et al., 2002b). The protease activity responsible for α-cleavage is also not clearly identified so far. Several members of the A Disintegrin and the ADAM-Metalloprotease family (A Disintegrin and Metalloprotease family), prominently, MDC-9 (Koike et al., 1999), ADAM-10 (Lammich et al., 1999), and ADAM-17 (Buxbaum et al., 1998) are described to cleave APP through this α-site, suggesting a redundant cleavage system.

All APP family members are cleaved in a very similar way, thus represents another common feature of all APP family members (Fig.1.3), since recent evidence suggests that APLP1 and APLP2 are cleaved by the same proteases as APP (Eggert et al., 2004b; Gu et al., 2001; Scheinfeld et al., 2002a; Walsh et al., 2003b).

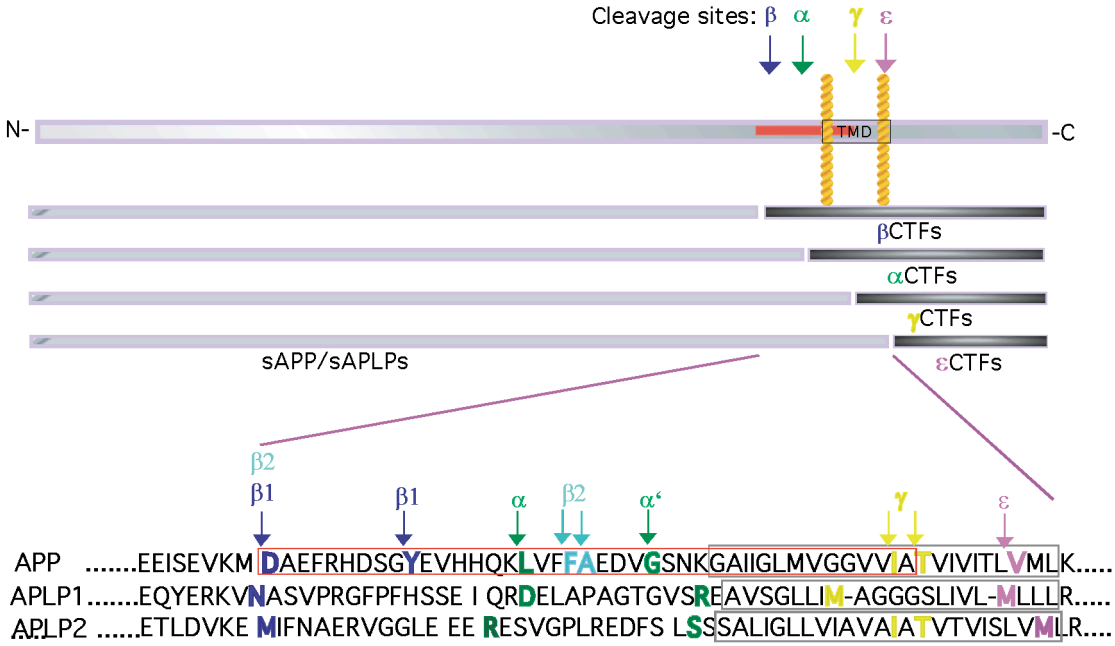

Fig.1.3 Similar cleavage sites of mammalian APP family. The β-, α-, γ-, ε-cleavages are found occurring in all three family proteins. Subsequently cleavages by β- and γ-secretases on APLPs will generate Aβ-like fragements. Subsequently cleavages by α- and γ-secretases on APLPs will generate p3-like fragements. Residues indicating in identical colors represent recognition sites for the same secretases. Red and gray open squares indicate Aβ domain and transmembrane domain (TMD).

An interesting point mentioned by several studies, juxta- and intramembranous cleavage might be a universal signaling mechanism described as regulated intramembrane proteolysis (RIP) (Brown et al., 2000). Quite a number of transmembrane proteins have been identified so far to be cleaved also by Metalloproteases and the γ-secretase complex in a similar manner as APP family proteins (reviewed in Fortini 2002; (De Strooper, 2003). The most prominent example is the Notch receptor, a crucial mediator of cell fate decisions and boundary formation in development ((Selkoe and Kopan, 2003). Notch is initially cleaved by a Furin-like convertase at the S1-site, creating the heterodimeric, mature receptor. In contrast to α-cleavage of APP, S2-site cleavage of Notch by a Metalloprotease is only induced after ligand binding (LaVoie et al. 2003; Kimberly et al 2003), which results in subsequent γ-secretase mediated processing at the S3- and S4-sites, similar to γ- and ε-cleavage of APP. The released Notch intracellular domain is further translocated to the nucleus and can activate transcription of numerous important genes during development stages. These similarities suggested that cleavage of APP may also be regulated by ligands, then mediate its nuclear signaling via the APP^{ICD}. A recent report shows evidences which support this function of APP, the cleaved APP intracellular domain may form nuclear multiprotein complexes then regulate the transcription of its own precursor and several other target genes (von Rotz et al 2004).

1.3. Possible physiological functions of APP family proteins

Over past two decades, numerous biomedical reports have been focused on APP to approach the role for its pathological feature for AD as well as its physiological function, but both still remain unclear. Many functions have been attributed to APP (summarized in (Annaert and De Strooper, 2002a; De Strooper and Annaert, 2000) and morphological investigations have supplied data for APP taking part in neuronal cell adhesion (Breen et al., 1991), neurite outgrowth (Allinquant et al., 1995; Qiu et al., 1995), cell migration (Sabo et al., 2001), fibroblast growth (Ninomiya et al., 1993), and neural progenitor cell proliferation (Caille et al., 2004; Hayashi et al., 1994; Ohsawa et al., 2001). Further evidence for the notion that APP is involved in neurite

outgrowth came from studies with APP-/- primary neuronal cultures exhibiting diminished neurite branching (Perez et al., 1997).

Studies of APP knockout mice and *Drosophila* mutants suggested that APP might play a role in diverse biological processes such as the formation of forebrain commissures, axogenesis and synaptic differentiation, cell adhesion and neuronal cell migration, regulation of apoptosis and possibly also in gene regulation (Annaert and De Strooper, 2002b). However, no obvious structural abnormalities or physiological deficits in brain was observed in APP knock out mice, suggesting that in case APP has a crucial neuronal function, it is compensated by other proteins. Mouse knockouts of APLP1 or APLP2 are viable with very subtle deficits as well, whereas combinations of APLP2 -/- and APP -/- or APLP1 -/- are lethal shortly after birth (Heber et al., 2000; von Koch et al., 1997). Interestingly, APP and APLP1 double knockout mice are viable with no obvious phenotype (Heber et al., 2000) suggesting APLP2 as the essential family member during development. However, the causes of death are still unknown.

Biochemical analyses have shown that APP exhibits properties as a cell adhesion protein, since it is strongly associated with extracellular matrix components (Small et al., 1992). The ectodomains of APP was shown to bind Heparin (Caceres and Brandan, 1997; Clarris et al., 1997; Multhaup, 1994; Multhaup et al., 1995; Williamson et al., 1995) and Collagen (Beher et al., 1996) with high affinity, and form complexes with secreted Cerebroglycan that could be isolated from rat brain (Williamson et al., 1996).

Besides, one study showed that F-spondin, a secreted signaling molecule implicated in neuronal development and repair, binds to the conserved central ectodomains of APP and may inhibit beta-secretase cleavage of APP proposing that F-spondin may be an endogenous regulator of APP cleavage (Ho et al,. 2004). The ectodomains of APP family proteins were also shown to bind Zinc (Bush et al., 1994) and Copper (Simons et al., 2002), and APP is able to reduce bound Cu^{2+} to Cu^{+}(Multhaup et al., 1996).

Structural study of the N-terminal APP Heparin- (Rossjohn et al., 1999) and Copper-binding domains (Barnham et al., 2003) shows corroborating a growth factor- or receptor-like function. An interesting study reported that Fibulin-1 (Ohsawa et al., 2001) which contains repetitive Ca(2+)-binding EGF-like elements, binds to APP at above mentioned growth factor-like domain, forms fibulin-1/sAPP heteromer that

may modulate the neurotrophic activities of APP. Another report showed, APP forms cellular *cis*-Dimers (Scheuermann et al., 2001), which is reminiscent of classical receptor dimerization described for the EGF receptor (reviewed in (Schlessinger, 2002). APP-dimers could be crosslinked in cell lysates and dimerization seems to be mediated by the Collagen binding domain, and possibly also by the Carbohydrate domain (Beher et al., 1996; Scheuermann et al., 2001). However, it is unclear whether dimerization of APP is essential for ligand binding, and if dimerization could influence the distribution of APP.

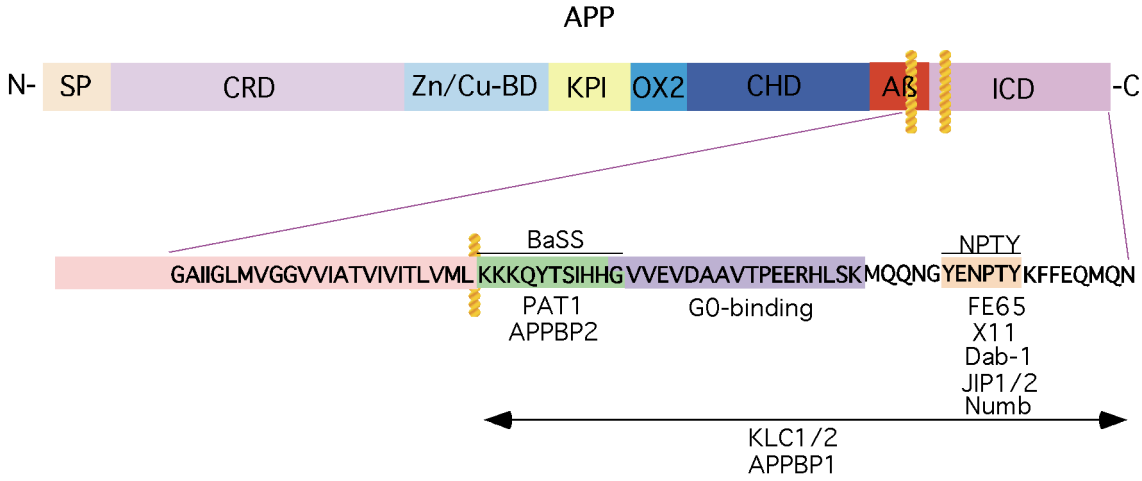

Fig 1.4: Schematic overview of the Intracellular adaptor proteins of APP. PAT1 and APPBP2 are thought to be proteins from the same gene products, and have been identified interacting directly with APP^{ICD} via BaSS (green). G^0 protein has been identified to bind APP^{ICD} through the G^0 binding region (purple). Fe65, X11, Dab-1 and JIP1/2, and Numb have all been identified to bind APP^{ICD} to the NPTY motif (light orange). Both KLC1/2 and APPBP1 have been identified to bind APP^{ICD} as well, but the specific region has not been clarified yet. Note BaSS is located right adjacent to the TMD, at the beginning of APP^{ICD}.

An important perquisite for proper function of APP/APLPs is the correct subcellular localization, which was shown to depend on three different domains: the juxtamembraneouse extra- and intacellular domain, including the Aβ domain (Tienari et al., 1996) and Tyrosine containing BaSS (Haass et al., 1995), respectively, as well as the NPTY-motif, located near to the carboxy terminus(Fig.1.4). The NPTY motif is essential for proper endocytosis of APP/APLPs and it mediates binding to multiple protein partners carrying a phospho tyrosin binding (PTB) domain which play essential roles in signal transduction and protein transport ((King and Scott Turner, 2004). The juxtamembraneouse extracellular domain, including the Abeta domain

was reported as an essential motif for axonal sorting of APP (Tienari et al. 1996), whereas the BaSS was shown to mediate basolateral sorting of APP (De Strooper et al. 1995) in epithelial cells. According to the sorting paradigm of Dotti and Simons (Dotti and Simons, 1990), these two domains might mediate sorting in different directions in neuronal cells as well.

As to date, Disabled-1 (Dab-1) (Homayouni et al., 1999; Howell et al., 1999; Trommsdorff et al., 1998), Shc (Russo et al., 2002; Tarr et al., 2002), JIP1 (Matsuda et al., 2001; Scheinfeld et al., 2002b), X11 (McLoughlin and Miller, 1996; Tomita et al., 1999; Zhang et al., 1997), and Fe65 (Borg et al., 1996; Duilio et al., 1998; Fiore et al., 1995; McLoughlin and Miller, 1996; Trommsdorff et al., 1998; Zambrano et al., 1997) have been described to interact with the NPTY motif of at least one APP family member (Fig.1.4). Binding of some of these intracellular adaptor proteins have been shown to affect the processing of APP. Prominently, X11 and Fe65 seem to have antagonizing effects. While X11 can stabilize the full length APP protein upon overexpression. (Borg et al., 1998; Mueller et al., 2000; Tomita et al., 1999), Fe65 expression and binding seems to increase APP processing and secretion of Aβ (Sabo et al., 2001), suggesting both interaction partners can influence intracellular transport and function in a distinct way. Intriguingly, Fe65 and APP colocalize with β1-Integrins at focal complex adhesion sites, and increase cell motility upon overexpression (Sabo et al., 2001).

An additional proposed function of the APP^{ICD} implies nuclear translocation together with Fe65, where a complex of APP^{ICD}, Fe65 and TIP60, a Histone-Acetyl-Transferase, exhibits transcriptional activity (Cao and Sudhof, 2001). Similar results have been obtained for the APLP1 and APLP2 intracellular domains (Scheinfeld et al., 2002a; Walsh et al., 2003b), while APP might additionally activate transcription in complex with JIP-1 (Scheinfeld et al., 2003). *In vivo* evidence for transcriptional activation of the *kai1* gene by the APP^{ID}/Fe65/Tip60 complex corroborates a function of APP in nuclear signaling (Baek et al., 2002), although there is still some controversy in regard to nuclear translocation of the APP^{ICD} (Cao and Sudhof, 2004; Kinoshita et al., 2002; Muresan and Muresan, 2004).

1.4. APP functions as a cargo receptor, interacts with Kinesin-I in neurons

In neurons, APP is transported within axons by fast anterograde axonal transport from the neuronal cell bodies to the distal never terminals (Koo et al., 1990; Sisodia et al,. 1993). Antisense inhibition using oligonucleotides complementary to kinesin heavy chain coding sequences in hippocampal neurons suggested that axonal transport of APP requires the microtubule-dependant motor protein kinesin-I (Ferreira et al., 1993: Amaratunga et al., 1995; Yamazaki et al., 1995; Kaether et al., 2000). A study using coimmunoprecipitation, sucrose gradient, and direct in vitro binding assay demonstrated that APP forms a complex with the kinesin-I by binding directly to the TPR domain of the kinesin light chain (KLC) subunit (Kamal et al., 2000). Kinesin-I, was the first member of the kinesin superfamily to be identified (Brady et al., 1985; Vale et al., 1985) and is responsible for ATP-dependent movement of vesicular cargoes within cells (reviewed in Goldstein and Philip, 1999; Goldstein and Yang, 2000; Kamal and Goldstein, 2000). Kinesin-I is composed of two components, kinesin heavy chain (KHC) and kinesin light chain (KLC), KLC associates with KHC and tethers membrane vesicles containing a subset of proteins that are transported along the axon from the neuronal cell body to nerve terminals. In addition, within the same study of (Kamal et al., 2000), the author also reported that association of APP with microtubules and axonal transport of APP is greatly decreased in a gene-targeted mouse mutant of the neuronally enriched KLC1 gene, thus led to the proposal of that, one of the normal functions of APP may be as a membrane cargo receptor for kinesin-I and that KLC is important for kinesin-I-driven transport of APP into axons.

Complementary studies revealed that deletion of the *app-like gene (appl)* in the fruit fly, or overexpression of human APP constructs that contained APP or APLP2 cytoplasmic domains, caused aberrant accumulation of transported membrane vesicles within axons (Gunawardena et al., 2001). This phenotype has also been observed in flies that lack kinesin or dynein, a microtubule-activated ATPase that transports membrane vesicles from neuronal dendrites back to the cell body.

Later, a report showed that BACE1 and PS1 are found in membrane vesicles transported along the axons of peripheral and central mouse neurons, and this transport requires APP (Kamal et al., 2001). This study provides complementary

evidence that APP functions as a Kinesin-I membrane receptor to transport an axonal membrane compartment containing the neurotrophin receptor TrkA, the synaptic vesicle-associated phosphoprotein synapsin 1, and the growth-associated protein GAP-43, which regulates cytoskeletal dynamics in neuronal growth cones.
Collectively, with reference to above findings would imply that APP is the receptor for Kinesin-I, however, there is no evidence as yet that APP and KLC directly associate with each other in vivo. On the other hand, the observation that transport of BACE1, PS1, KHC, and KLC still occurs, albeit at lower levels, in the APP-deficient mice, suggesting that APP is unlikely the only cargo receptor for Kinesin-I. It is possible that axonally transported APLP1 and APLP2 (Kamal et al., 2001) might compensate for APP. Moreover, still the evidence of direct binding of APP and KLC can not exclude the existence of indirect binding via adaptor proteins, such as JIPs, It has been shown that APP may bind JIPs via its PTB domain (Matsuda et al., 2001; Scheinfeld et al., 2001), JIPs may bind to the TPR domain of KLC (Verhey et al., 2001) and might mediate APP transports in cells (Fig.1.5).

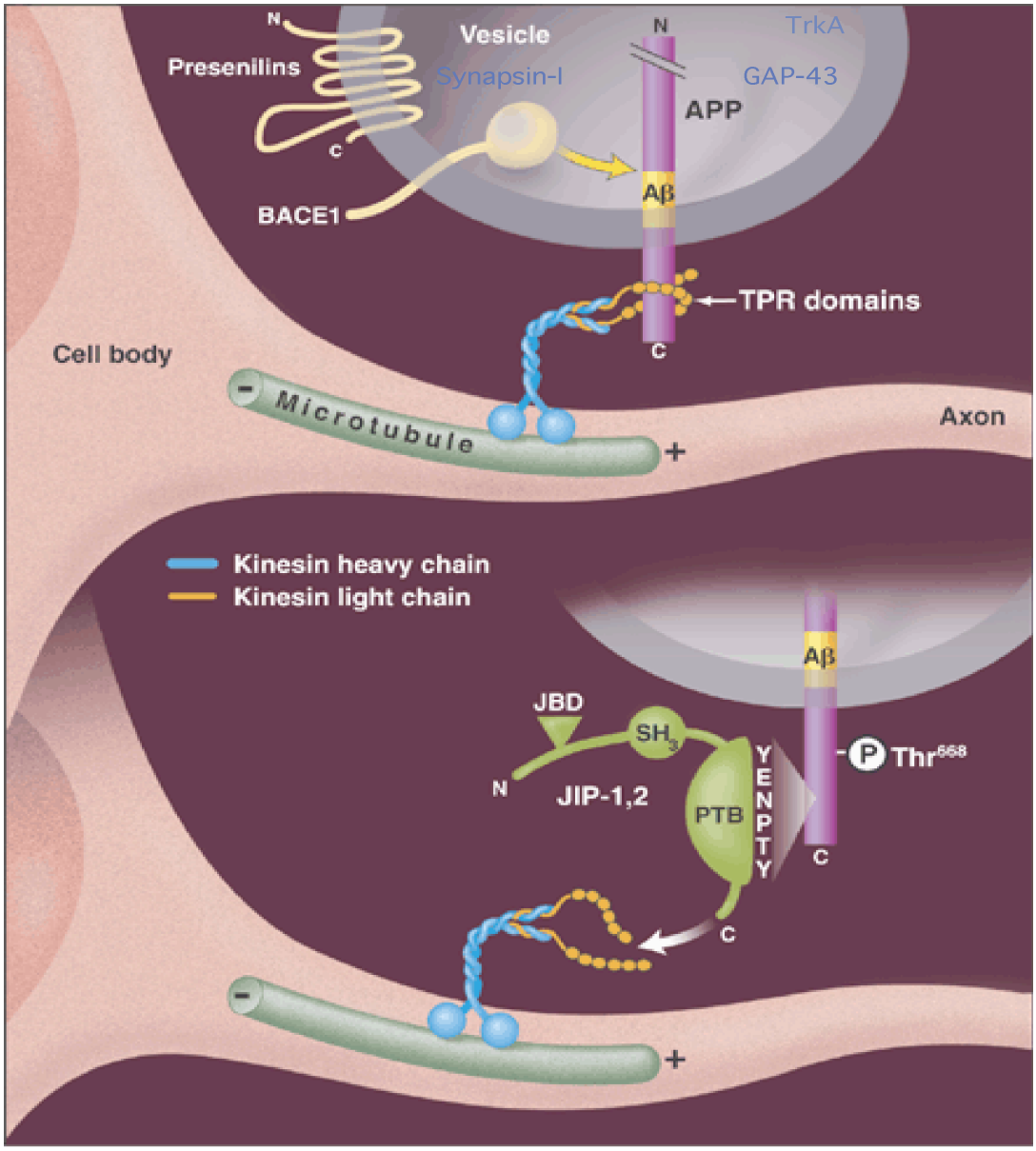

(Sangram S. Sisodia. (2002) *Science*, 295, 805-807)

Fig.1.5: The association of APP with kinesin-I. Membrane vesicles containing protein cargo are transported along axons from the neuronal cell body to nerve terminals. This process is dependent on kinesin-1, which consists of two kinesin heavy chains (KHCs) (blue) and two kinesin light chains (KLCs) (orange). The KLCs are bound to axonal microtubules via the microtubule- and ATP-binding domains of KHC. There are two possible ways in which membrane vesicles containing cargo can associate with kinesin-1. In the first, APP binds directly to the tetratricopeptide (TPR) domains of KLCs, thus linking membrane vesicles to microtubules. In the second, APP or APP carboxyl-terminal fragments could bind to the phosphotyrosine-binding domains of the JIP scaffolding protein family. The JIPs in turn could then bind to the TPR domains of KLC via their carboxyl-terminal regions. In addition, phosphorylation of Thr668 in the APP cytoplasmic domain might serve to modulate the interaction of APP and APP carboxyl-terminal fragments with the KLCs or JIPs.

1.5. Discovery of PAT1 and its relationship with APP

Using yeast two-hybrid screen with the APP-BaSS (amino acid sequence in one letter code KKKQYTSIHHG) fused to the DNA-binding domain of LexA as a bait, Pimplikar an co-works (Zheng et al., 1998) isolated a positive clone from a HeLa cDNA library, and reported it as a kinesin light chain (KLC) – like protein, termed in their article as protein interacting with APP tail 1 (PAT1). Their study showed that, PAT1 interacts with the APP - BaSS (Fig.1.4) but binds poorly when the critical tyrosine is mutated and does not bind the tyrosine - based endocytic signal of APP.

Biochemical assay shows that, PAT1 protein sequence consists of 585 amino acids with a calculated molecular mass of 66.9 kDa and a predicted isoelectric point of 6.9. The N-terminal and C-terminal regions are predicted to form globular structures and a stretch of 35 amino acids is predicted to form 5 heptad repeats that are likely to form a coiled coil, and four imperfect tandem repeats are found toward the C-terminal end of the protein (Fig.1.6a). Reference from their search of public data bases, PAT 1 shows a significant homology to kinesin light chain which is a component of the plus - end directed microtubule - based motor involved in transporting membrane proteins to the basolateral surface in epithelial cells. The region of maximum homology between PAT1 and KLC contains the characteristic four 42-amino acid imperfect tandem repeats conserved in all species of KLCs. Several residues in each repeat are conserved between the KLC and PAT1 sequences. However, the first repeat contains two insertions of 7 and 11 amino acids.

Further characterization of PAT1 shows that it is a cytoplasmic protein, associates with membranes as tested by ultracentrifugation (150,000Xg) and reconfirmed by chemical cross-linking approach. This study also showed that PAT1 may cofractionate with APP-containing vesicles as examined by sucrose density gradient floatation, and bind to microtubules as tested by microtubule binding assay (McIlvian et al., 1994). Cotransfection of PAT1 with a reporter protein shows that PAT 1 is functionally linked with intracellular transport of APP which leads to the proposal, PAT1 is involved in the translocation of APP along microtubules toward the cell surface. (Zheng et al., 1998).

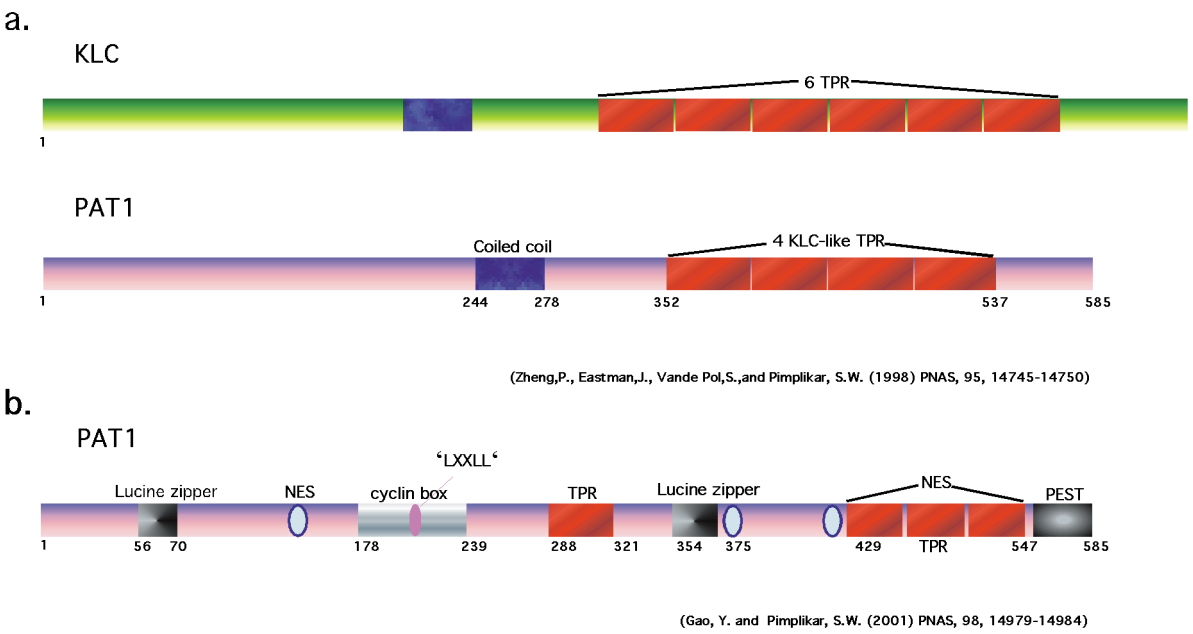

Fig. 1.6: Schematic representation of putative motifs present in PAT1. (a) PAT1 consists of 585 amino acids, a stretch of 35 amino acids was predicted to form a coiled coil domain and 4 KLC-like imperfect tandem repeats were found toward the C-terminal end of the protein. Simplified schematic representation of KLC structure is given to compare the structural similarity proposed by (Zheng et al.,1998). **(b)** PAT1 were predicted to contain several protein-protein-interacting motifs, including two leucine zippers, a cyclin box, a "LXXLL" motif (NR-Box), 4 tetratricopeptide repeat (TPR) domains that also present in kinesin light chain, a proline (P), glutamate (E), serine (S), and threonine (T) rich (PEST) protein-degradation domain, multiple putative nuclear localization signals and leucine-rich nuclear export signals(NESs). Note, in (b), the predicted coiled coil region is missing and the TPR domain are completely shifted in comparison to (a).

Second study of PAT1 published by the same group shows that overexpression of Cγ-59 derived from APP causes disappearance of PAT1 from the nucleus and induces its proteosomal degradation. Treatment of cells with lactacystin, an ubiquitin-proteasome inhibitor, prevents PAT1 degradation and retains its nuclear localization whereas Cγ-57, a minor product of γ-cleavage, is only marginally effective in PAT1 degradation (Gao et al. 2001).

In this study, PAT1 was characterized as a nucleocytoplasmic protein in contradictory to their previous study. They claimed the failure to detect PAT1 signal in the nucleus in the first study presumably was because the tyramide signal-amplification system did not gain access to the nuclear compartment. Further and more detailed sequence analysis predicts the presence of several protein-protein-interacting motifs (Fig.1.6.b). Their predication in this study of PAT1 protein structure showing in

schematic ideograph represent two leucine zipper motifs generally involved in dimerization and also in binding DNA (Alber et al. 1992), a putative cyclin box found in many cyclin-dependent kinases, a "LXXLL" motif (NR-Box) that is present in transcription coregulators (Heery et al. 1997), four tetratricopeptide repeat (TPR) domains that are also present in kinesin light chain (Gindhart et al, 1996), and a proline (P), glutamate (E), serine (S), and threonine (T) rich (PEST) protein-degradation domain (Rechsteiner et al, 1996) at the extreme C terminus that is common in regulatory proteins with high turnover rates. Further they reported evidence for multiple putative nuclear localization signals (NLS) and leucine-rich nuclear export signals (NESs) (Mattaj, et al, 1998). However, the prediction of domains reported in this second study is another contradictory statement to their previous study. They included several novel domains and motifs, and hence changed the putative positions of the TPRs completely. The four imperfect KLC-like tandem repeats were predicted to locate in between aa 352 and aa 537 (1^{st}: aa352-411; 2^{nd}: aa412-453; 3^{rd}: aa454-496; 4^{th}: aa497-537) in the first study, but the four tetratricopeptide tandem repeats (TPR) were indicated to be located at 1^{st}: 288-321; 2^{nd} to 4^{th}(without specifying): aa429-547 (Fig.1.6ab) in the second study of PAT1.

1.6. APPBP2/PAT1a versus PAT1 and Ara67

The name APPBP2 (Amyloid precursor protein-binding protein 2) first appeared in (Monni et al. 2001), which was found in breast cancer cell lines to be one of limited number of highly expressed genes on locus 17q23, a common region of amplification in breast cancers with poor prognosis. Later it was found to exhibit significantly elevated expression in ovarian clear cell adenocarcinomas (Hirasawa et al. 2003) and Neuroblastomas (Saito-Ohara et al. 2003).

Homology search through NCBI GeneBank revealed its synonyms are PAT1, HS.84084, and KIAA0228. Selected protein identity found to be 26.95% among 166aa to mouse Kinesin light chain 1 (mKLC1) (M. musculus sp:O88447), and 24.68% among 228 aa to rat Kinesin light chain C (rKLC C) (R. norvegicus pir:C41539 - C41539) (http://www.ncbi.nlm.nih.gov/UniGene/clust.cgi?ORG=Hs&CID=84084).

Summary in the GeneBank describes: “The protein encoded by this gene interacts with microtubules, is functionally associated with beta-amyloid precursor protein

transport and/or processing. The beta-amyloid precursor protein is a cell surface protein with signal-transducing properties, and it is thought to play a role in the pathogenesis of Alzheimer's disease. This gene has been found to be highly expressed in breast cancer. Multiple polyadenylation sites have been found for this gene“.

Interestingly, among all research articles (Monni et al. 2001; Hirasawa et al. 2003; Saito-Ohara et al. 2003) under the name of APPBP2 that can be found through public resources, neither any binding assay nor any evidence of its interaction with APP were mentioned. In the first appearance (Monni et al. 2001) of such a protein named APPBP2, the author used a combined name as “PAT1/APPBP2” to represent the newly identified gene within their approach, and the listed reference linked to the putative function of APPBP2 is the publication of PAT1, which indicated that PAT1 and APPBP2 were thought to represent the same gene products.

While cloning PAT1, we met difficulties to match the sequences in the data base. Surprisingly, among all independent clones, we consistently found seven nucleotide exchanges, resulting in six amino acid substitutions (F296L, K325R, A337A, S340C, L354V, P369R, N542K,). A sequence (APPBP2 cDNA: NM_006380; aa: NP_006371.2) completely identical with the sequence we amplified from the human brain cDNA library, is annotated to carry these nucleotides as 7 Single Nucleotide Polymorphisms (SNPs) in contrast with PAT1 (Fig.3.1.2). Publications of PAT1 are found to be listed under the references of APPBP2 to represent traceable proposed function. (see http://www.ncbi.nlm.nih.gov/entrez/viewer.fcgi?db=nucleotide&val=18104961).

Sequence analysis of ESTs that are available in the data base, also exhibiting the same 7 SNPs as well, indicate that APPBP2 is the major variant of this gene products.

Since we were unable to match PAT1 but the APPBP2 sequences with the products a mplified from human brain cDNA library, so that the cDNA carries the same coding sequence as APPBP2 is used in this study. We proposed to name newly the target gene product PAT1a in our study is because in our further works on APPBP2, we found the functional similarity on APPBP2 as to PAt1, however there was neither characterization nor functional study were ever done for APPBP2. We think this new name PAT1a should clearly reveal the truth for genetic difference and our findings of functional similarity in between APPBP2 and PAT1.

Interestingly to mention, an androgen receptor associated protein Ara67 was

described to be 99,6% homologous to PAT1 (Zhang et al. 2004), likely represent an additional variant of APPBP2/PAT1a, suggesting a high polymorphism in this gene.

2. Aim of this study

An important prerequisite for proper function of APP/APLPs is their correct subcellular localization, which depends on three different domains: firstly, the juxtamembraneous extracellular region encompassing the Aβ domain is essential for axonal sorting of APP (Tienari et al., 1996). Secondly, the juxtamembraneous intracellular domain, including the tyrosine containing basolateral sorting signal (BaSS), mediates basolateral sorting (Haass et al., 1995). Thirdly, the C-terminal NPTY-motif is essential for endocytosis of APP/APLPs, as well for binding to multiple interaction partners carrying a phosphotyrosine binding (PTB) domain (King and Scott Turner, 2004). In epithelial cells, sorting of APP and APLP2 to the basolateral surface depends on the presence of a BaSS in their cytoplasmic domain, and mutation of the tyrosine residue on the BaSS of APP results in nonpolarized transport of APP in NDCK cells (Haass et al., 1995). According to the sorting paradigm of Dotti and Simons (Dotti and Simons, 1990), the Aβ domain and the BaSS may mediate sorting to different subcellular compartments.

To date, the only indentified partner interacting with the BaSS of APP is PAT1 (protein interacting with APP tail 1). PAT1 has been reported to interact with both microtubules and the BaSS of APP, thus led Pimpliker and co-workers proposed that PAT1 is involved in the translocation of APP along microtubules toward the cell surface (Zheng et al., 1998). However these authors reported only low affinity binding of PAT1 to APP in number, and neither neuronal function of PAT1 nor the existence of in vivo interaction have been tested. Different evidences have shown that both APLP1 and APLP2 share high sequence homology and similar protein domain organizations with APP (Coulson et al., 2000b), have similar subcellular localization ,and are cleaved in a very similar way (Eggert et al., 2004a). It is therefore reasonable to assume that PAT1 might interact with these 2 family members as well.

The aim of this study is to investigate if PAT1 is expressed in central nerves system, then to compare its localization with APP family members and seek in vivo evidence of interactions with each family members. Hence, to investigate whether regulation of this carboxyl terminal interaction partner may affect subcellular trafficking or influence the processing in neuronal cell system. We believe this study will help to gain new knowledge to distinguish the similarities and diversities in the APP family proteins.

This will help to clarify the physiological functions and the pathogenic role of APP, which might contribute new insights to design new therapeutic approaches for AD. (Fig.2).

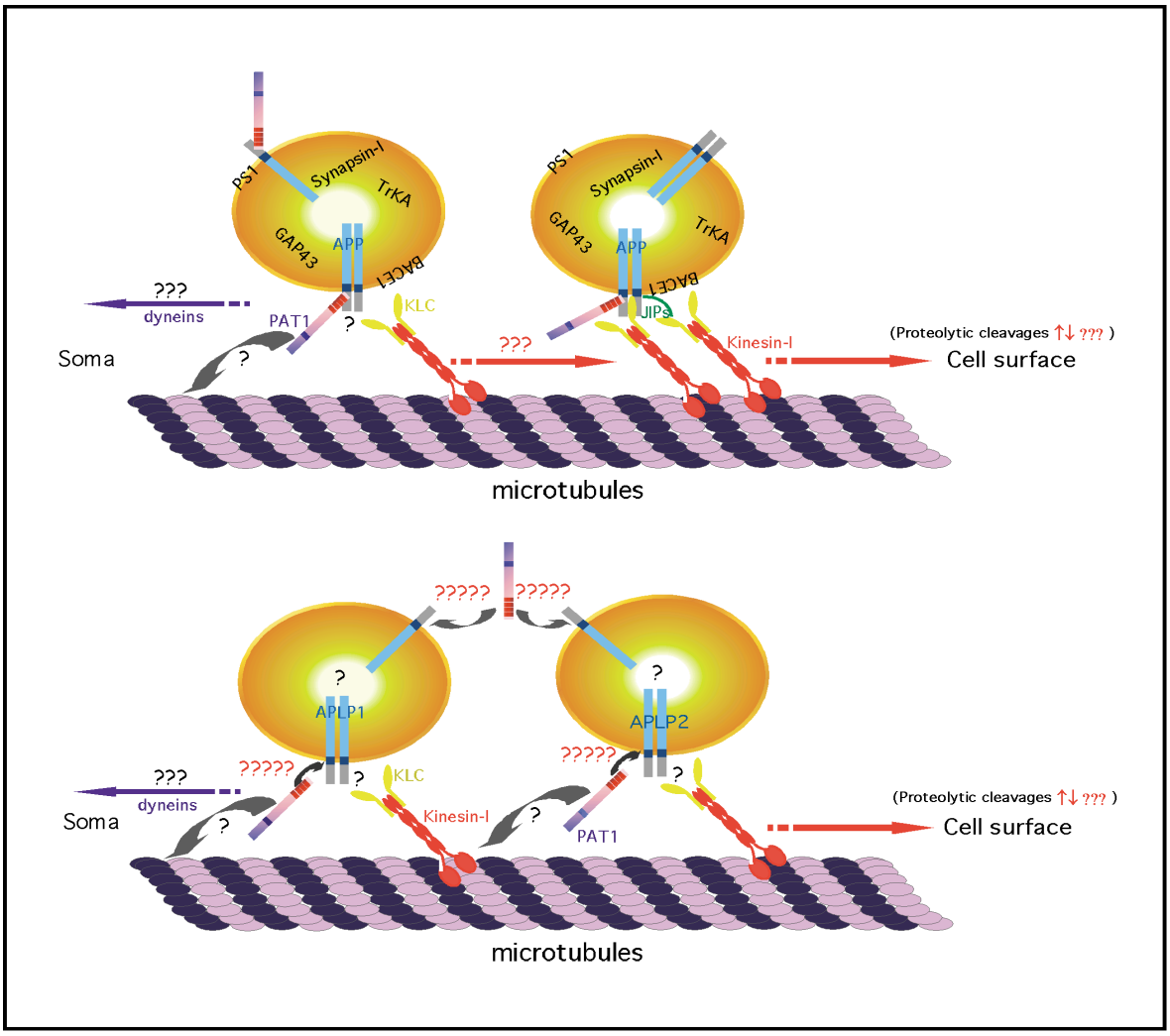

Fig.2: Ideograph of the aim of this study. Based on the studies of PAT1, that was reported as a Kinesin light chain like protein and binds to APP, APP has been shown undergoes fast axonal transport via Kinesin-I. This study will aim on solving the questions marked in red. First, if the binding of PAT1 and APP may be found in vivo and if this affects APP transport and proteolytic cleavages. In parallel, to find if PAT1 also interacts with APP mammalian homologous APLP1, APLP2, and if the interaction affects similarly as to APP.

3. Results

3.1. PAT1 is a rare genetic variant of APPBP2/PAT1a

3.1.1. Alignment result of PCR products

Difficulties occurred while matching clones of PCR product to PAT1 sequence. After discard many clones, we started to doubt that the expected PCR product length is 1758bp, and we found that all of our clones carry at least 7 mutations, which in nowadays is an unexpectedly rare case based on the known quality of biotechnology. We thus aligned all available sequencing results to PAT1 sequence and found 7 common mutations occurred in all clones.

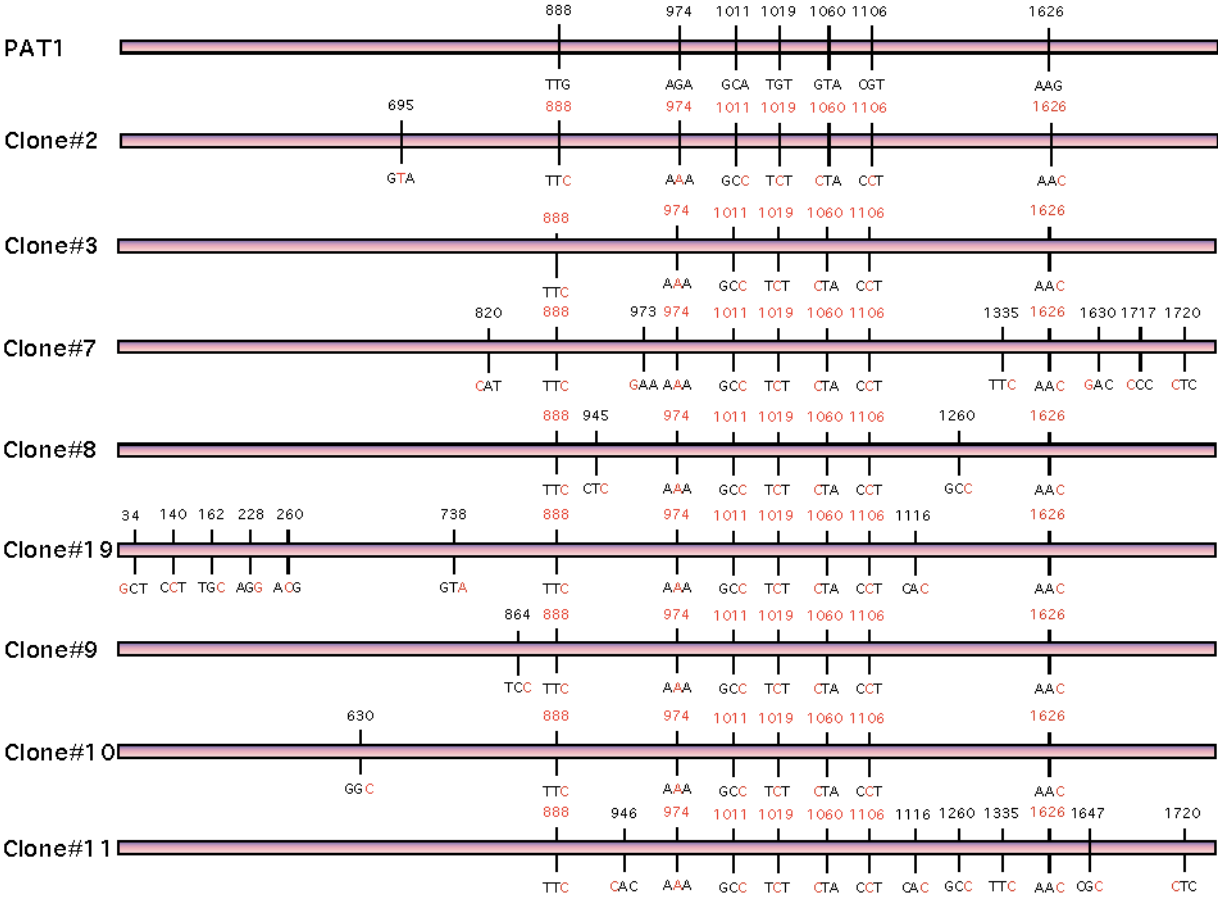

Fig.3.1.1: Schematic representation of sequencing alignment. Different sequences of clones resulted from amplification products of PAT1 were aligned by *SeqMenII* (DNAstar, LASERGENE). Characters in red color indicate the positions of mutated nucleotides aligned to PAT1. Numbers of positions indicate in red color represent mutations that occurred in all clones. Nucleotide change at position1011 will result silent mutation, others will result amino acids changes while translation.

3.1.2. Genetic database analysis of PAT1, APPBP2/PAT1a and related ESTs

Comparison of the PAT1 cDNA sequence (AF017782) with the APPBP2 cDNA (NM_006380) or the genomic sequence (APPBP2; LocusID: 10513) reveals that PAT1 contains seven nucleotide exchanges (888c→g, 974a→g, 1011c→a, 1019c→g, 1060c→g, 1106c→g, 1626c→g), resulting in six non-homologues amino acid substitutions (F296L, K325R, S340C, L354V, P369R, N544K, A337A) (Fig.3.1.2). Six of the seven nucleotide exchanges are annotated as single nucleotide polymorphisms in the database, indicating that PAT1 is a variant of APPBP2. We wanted to amplify the coding region of the PAT1 from a human brain cDNA library but surprisingly found in eight independent clones consistently matching the sequence of APPBP2 among those positions of SNPs, but not the sequence of PAT1, suggesting that the variant PAT1 might occur at low frequency. To test how frequent the SNPs occur, we analyzed 53 ESTs covering the region of PAT1 cDNA containing the nucleotide exchanges. Unexpectedly, all tested EST sequences were identical with the sequence of APPBP2, but none was equal to PAT1, suggesting that the PAT1 sequence, used in previous analysis (Zheng et al.,1998; Gao et al, 2001) carries 6 non-homologous amino acid exchanges and likely represents a very seldom variant of APPBP2 in human brain. For simplification, and as no characterization experiments were done for APPBP2, we think it is more suitable to rename it as PAT1a.

Based on computational analysis of APPBP2/PAT1a, using different programs to predict protein domains (coils, REP, PROSITE (http://www.expasy.ch)), we found significant predictions for one tetratricopeptide repeat (TPR) (aa 429-462), three TPR-like motifs (aa 288-321, 471-505, 514-547), and weak evidences for a coiled coil domain (aa 257-273). These data are widely consistent with the domains of PAT1 predicted by Zheng and coworkers (Zheng et al., 1998) (Fig.1.5a), whereas we found no evidence for the existence of a PEST domain, Leucin-zipper and putative nuclear localization sequences, as postulated by Gao and co-workers (Gao at al., 2001) (Fig.1.5b), which might be explained by the non homologous amino acid exchanges in the PAT1 sequence (Fig.3.1.2).

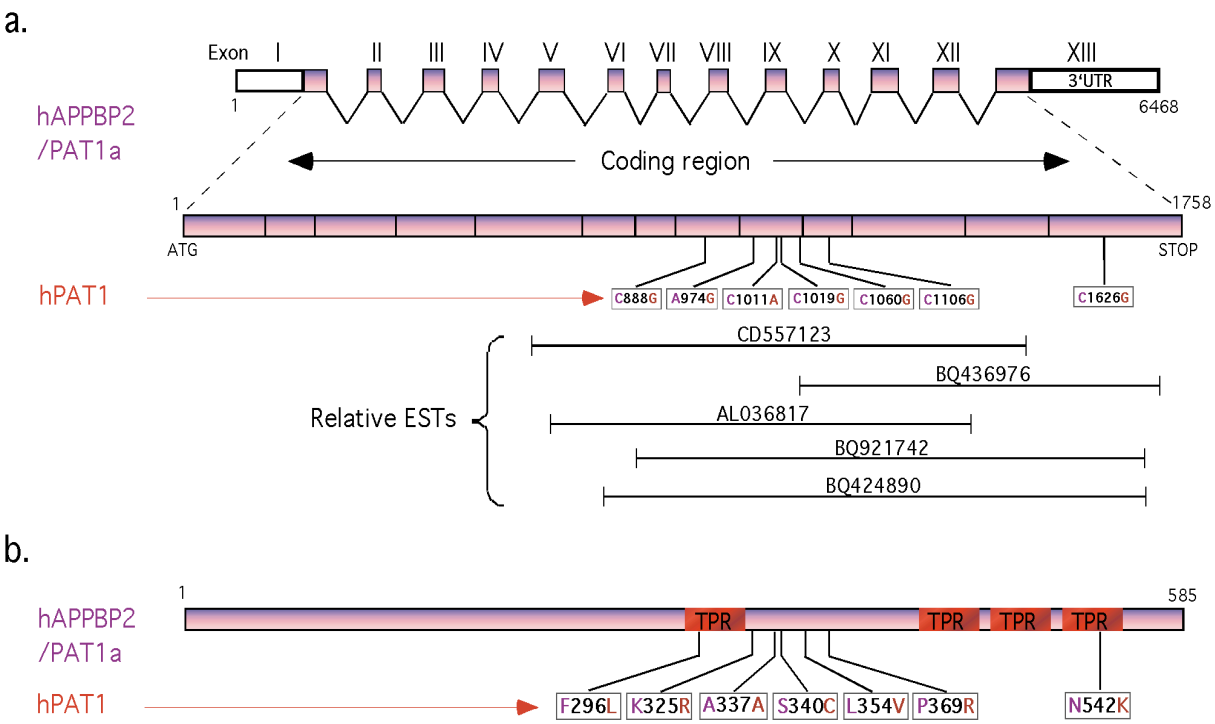

Fig.3.1.2: Schematic representation of the genomic structure, cDNA, and protein organization of APPBP2/PAT1a in comparison to PAT1
(a.) The human APPBP2/PAT1a cDNA has a length of 6468 bp and is genomically represented by 13 exons (I-XIII). Exon boundaries within the coding region of the PAT1a cDNA (1758 bp) are marked. The nucleotide exchanges present in the PAT1 sequence are indicated. Those nucleotide exchanges present in PAT1, which are annotated as single nucleotide polymorphisms (SNPs) in the genomic sequence are marked by an asterisk. The accession numbers and relative positions of five ESTs that correspond to the PAT1a sequence are shown. **(b.)** Protein structure of human APPBP2/PAT1a predicted in this study. The amino acid substitutions in the sequence of APPBP2/PAT1a are given. The positions of predicted helix-loop-helix motifs with a significant homology to tetratricopeptide like repeats (TR) are indicated. Characters indicate in purple or red colors representing hAPPBP2/PAT1a and PAT1 nucleotides or amino acid sequences.

3.2. Northern Analysis of APPBP2/PAT1a in various Human and Mouse tissues

Neuronal function in subcellular transport of APP for PAT1 was proposed (Zheng et al. 1998). However, no study addressing its expression in brain has been performed. To clarify whether APPBP2/PAT1 is expressed in mammalian brains, Northern analysis with a randomly ^{32}P-labelled oligonucleotides and full-length cRNA probes directed against the coding sequence of APPBP2/PAT1a were performed. Since PAT1 and APPBP2/PAT1a are 99% identical,this analysis will detect both transcripts.

Both probes recognized mRNAs with a length of 6.5kb, 4.3kb and 2.3kb in all tissues examined. The transcripts detected at 6.5kb perfectly matched the predicted size of the PAT1a cDNA (6,48kb), which was the same as observed by (Nagase et al. 1996) who detected ubiquitous expression of KIAA0228 as an approximately 6.5-kb transcript. Some lower bands at 6.2 kb (mouse), 4.3kb and 2.3kb (human and mouse) might represent alternatively spliced transcripts, since sequence analysis of the full-length cDNA revealed no sign of alternative initiation on this gene. Our data also revealed high levels of APPBP2/PAT1a transcripts during early development. Interestingly, in the course of development, some variations in the expression level were observed for the longest PAT1a transcript, whereas the expression levels of the 4.3kb transcript remained unchanged. In brief, the Northern data show that the APPBP2/PAT1a gene is expressed in multiple tissues, including brain, and might be differentially spliced in the different tissues and during development.

3.2.1. Expression of PAT1a/APPBP2 transcripts in multiple human tissues

The initiating experiment of this study was to check the expression of APPBP2/PAT1a in humam, Using APPBP2/PAT1 ^{32}P-labelled full-length cRNA probes (hydrolized to~500bp) hybridizated to the human MTNblot (Clontech), the result shows that the APPBP2/PAT1a transcripts may be detected with most pronounced levels in brain, placenta, and kidney in human.

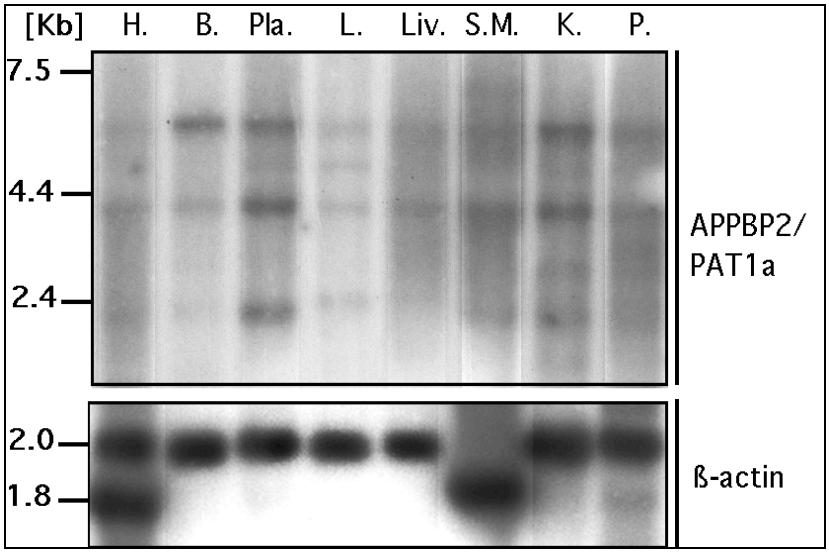

Fig.3.2.1: Northern analysis of APPBP2/PAT1a transcripts in multiple human

tissue. The transcripts detected at ~6.5kb perfectly matched the predicted size of the APPBP2/PAT1a cDNA (6,48kb). The lower bands at 4.3 kb and 2.3 kb might represent alternatively spliced transcripts. (H.: heart; B.: Brain; Pla.: placenta; L.: Lung; Liv.: liver; S.M.: skeleton muscle; K.: kidney; P.: pancreas.) Some lanes with higher background were adjusted to reveal comparable information. Rehybridization with a random ^{32}P-labelled cRNA probe derived from human ß-actin cDNA confirmed that comparable amounts of various mRNA were loaded (lower panels).

3.2.2. Expression of APPBP2/PAT1a transcripts in multiple mouse tissues

Considering for research analysis that may be applicatible on human samples is strictly limited, we thus check the similarity of APPBP2 gene in between human and mouse and found they are 96% identical. To know the expression pattern of APPBP2/PAT1a and if it is expressed in mouse brain, Northern analysis was performed on blots loaded with mRNA samples from multiple mouse tisseus. The APPBP2/PAT1a transcripts were detected with most pronounced levels in heart, brain, spleen, kidney in mice (Fig.3.2.2).

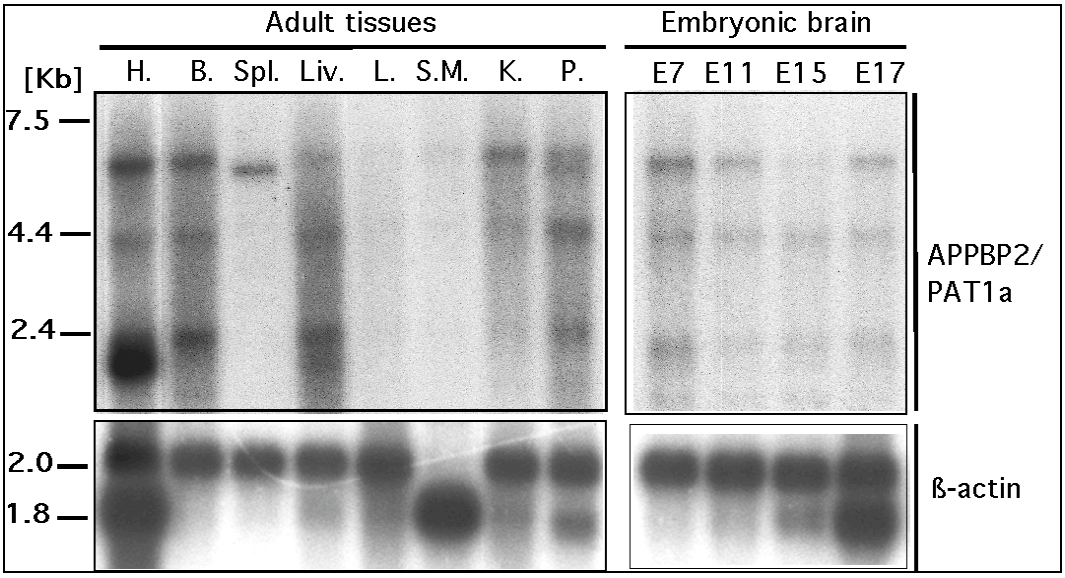

Fig.3.2.2: Northern analysis of APPBP2/PAT1a transcripts in multiple adult mouse tissues and different stages of mouse embryonic brains. The transcripts detected at 6.5 kb perfectly matched the predicted size of the APPBP2/PAT1a cDNA (6,48kb) as mentioned before. Notable,the longest PAT1a transcript in mouse spleen had a size of 6.2 kb instead of 6.5 kb and in testis, two transcripts with a length of 6.5 kb and 6.2 kb were found. Right panel revealed levels of PAT1a transcripts during early development. Interestingly, in the course of development some variations in the expression level were observed. The bands at 6.5kb shows high levels of transcripts at embryonic day 7 (E7, 7 days after gestation), decreased at E11 and significantly at E15,but elevated at later stage.At E11 and E17,the signals were similar, suggesting that this full length APPBP2/PAT1a mRNA level is regulated during embryonic

development. Remarkably, the expression level of the 4.3 kb transcript were equal during development. (H.: heart; B.: Brain; Spl.: spleen; Liv.: liver; L.: Lung; S.M.: skeleton muscle; K.: kidney; P.: pancreas; E#: embryonic stages). Rehybridization with a random ^{32}P-labelled cRNA probe derived from ß-actin cDNA confirmed that comparable amounts of various mRNA were loaded (lower panels).

3.3. *In situ* Analysis of APPBP2/PAT1a transcripts in adult mouse brains

3.3.1. APPBP2/PAT1a is predominantly expressed in neurons in mouse brain

Northern analysis had shown the presence of APPBP2/PAT1a transcripts in the brain, the next would be to verify in detail the cellular expression of APPBP2/PAT1a transcripts in mouse brain, *in situ* hybridization was performed with randomly DIG-labeled cRNA probes (alkaline hydrolyzed to 200-500bp), and the result showed that APPBP2/PAT1a transcripts are widely distributed in brain, predominantly expressed in neurons. The strongest signal was detected in cell-dense areas such as cortex, the Purkinje cell layer in the cerebellum, the dentate gyrus and CA1-3 region in the hippocampus, whereas no significant staining of glial cells was observed(Fig.3.3.1).

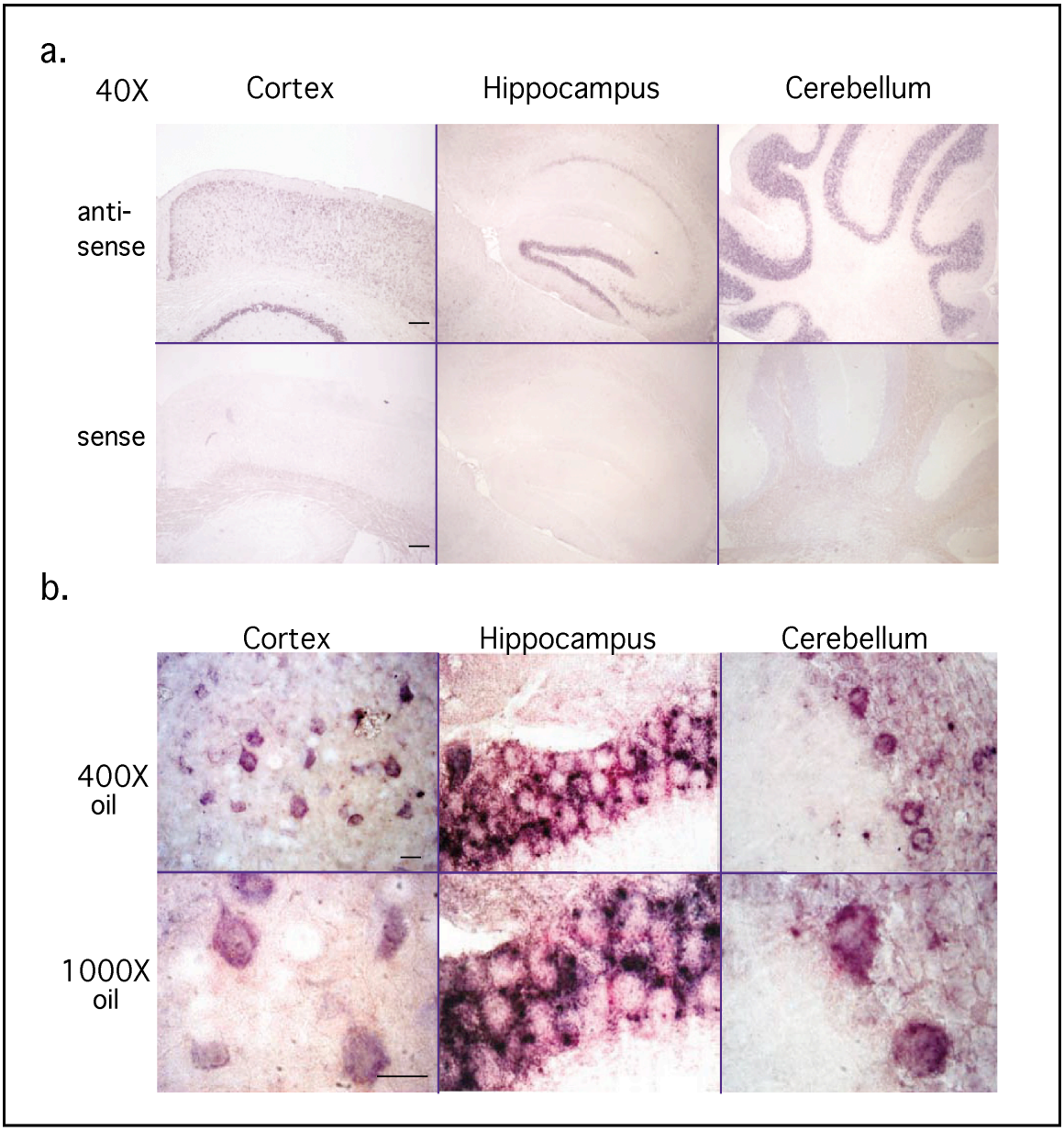

Fig. 3.3.1: *in situ* hybridization analysis of APPBP2/PAT1a transcripts in adult mouse brain. (a)APPBP2/PAT1a transcripts were found widely distributed in brain and are predominantly expressed in neurons. The strongest signal was detected in cell-dense areas such as cortex, the Purkinje cell layer in the cerebellum and the dentate gyrus and CA1-3 region in the hippocampus, whereas no significant staining of glial cells was observed. No significant signal was found using the corresponding sense probe. Bar=200um. **(b.)**High magnification clearly shows a cytosolic pattern, underlining the specificity of the hybridization signals. Bar=50um.

3.3.2. Comparison of APPBP2/PATa expression levels in various sub-regions among adult mouse brain

Distribution of APPBP2/PAT1 transcripts in mouse brain		
Cortex		++++
Corpus Callosum		-
Hippocampus	CA1	++++
	CA2	+++
	CA3	++++
	DG	+++++
Striatum		+
Amygdala		+++
Thalamus		+
Olfactory bulb		+
Cerebellum	Molecular Layer	+
	PC Layer	+++++
	Granular Layer	+++
Brain stem		+
Pons		+

Signal Intensities: -, none
+. low
+++, intermediate
++++, high
+++++, very high

Table 3.3.2: Comparison of signal intensities from *in situ* analysis. Every 3 of whole transverse and saggital sections were observed in identical light path and strength. Cortex, hippocampus and amygdala are affected and known strongly correlated to the progression of AD, whereas brain stem and pons are known not affected in the course of AD.

3.4. Western Analysis of Subcellualr localization of APPBP2/PAT1a in COS-7 cells

3.4.1. Presence of APPBP2/PAT1 in membrane fraction

Primary sequence analysis revealed that APPBP2/PAT1a exhibit no predictable membrane spanning domain, and based on the reported interaction with APP, it was reasonable to assume that APPBP2/PAT1a shall be present in both the cytosolic fraction and the membrane fraction after ultracentrifugation (40,000Xg) of the postnuclear supernatant. To test this, COS-7 cells were transiently transfected with recombinant APPBP2/PAT1a-HA and collected for membrane preparation 24hr post-transfection. Western analysis of the resulting samples were performed and the result showed that APPBP2/PAT1a is partly detectable in membrane fraction as where APP present.

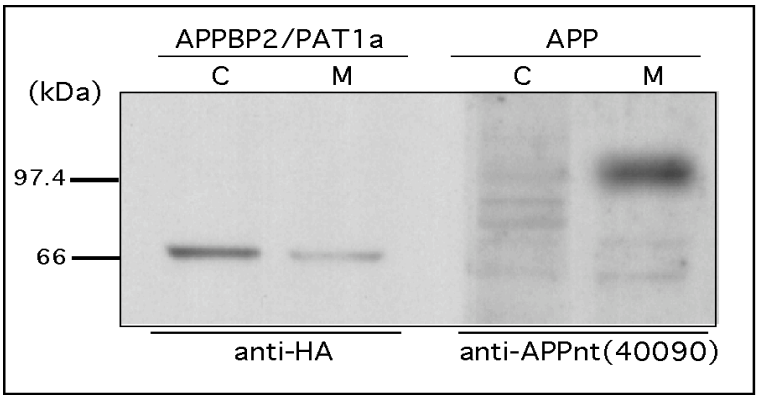

Fig.3.4.1: Western blot the of membrane preparation of APPBP2/PAT1a. APPBP2/PAT1a is partly detectable in membrane pool as where APP is present. (C: cytosolic fraction, M: membrane fraction). APP fractionation was performed in parallel to serve as a preparation control.

3.4.2. Depletion of Membrane bound APPBP2/PAT1a by Carbonate Extraction

With consideration of that, if the presence of APPBP2/PAT1a in the membrane fraction representing the association but not anchoring characters of APPBP2/PAT1a to the subcellular membrane compartments, the treatment of high pH carbonate (pH=11) to the postnuclear supernatant should result the disappearance of APPBP2/PAT1a from the membrane fraction of membrane preparation.

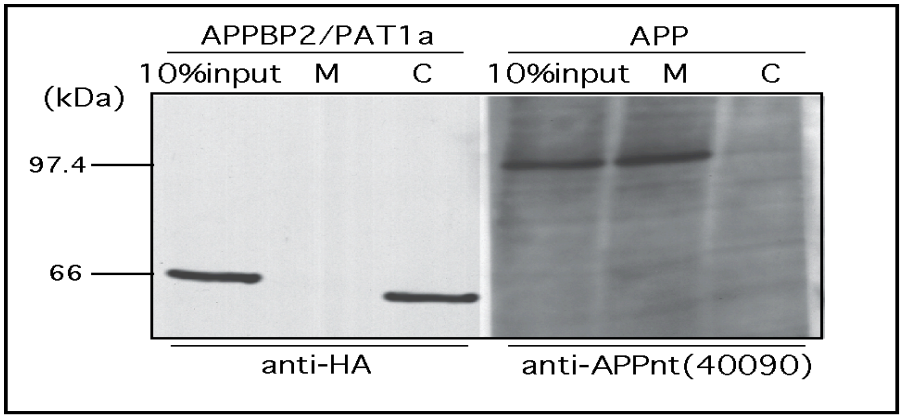

Fig.3.4.2: Western blot of APPBP2/PAT1a after carbonate extraction. APPBP2/PAT1a is an attached membrane protein. Membrane associated APPBP2/PAT1a was deattached from membrane by carbonate treatment (ph=11), could only be detected in the cytosolic fraction (left panel) (C: cytosolic fraction, M: membrane fraction). APP fractionation was performed in parallel to serve as a preparation control.

3.5. Characterization of polyclonal rabbit anti-PAT1a antibody

To extend the expression studies and for further analyzing APPBP2/PAT1a on the protein level, we generated a peptide antibody directed against the carboxy terminus of APPBP2/PAT1a (aa543-572). Like the probes described for Northern and *in situ* Hybridization previously, this antibody likely will detect all APPBP2/PAT1a variants. After collecting the evaluated high titer of anti-PAT1a anti-serum, the anti-PAT1a was affinity purified according to procedures for other well-characterizd antibodies Western analysis of the samples from cells overexpressing APPBP2/PAT1a-HA were performed and the result showed that the purified anti-PAT1a antibody and an anti-HA antibody recognized a major band in Western analysis at approximately ~67kDa in extracts from HEK293, COS-7, Hela, and SH-SY5Y cells expressing recombinant HA-tagged APPBP2/PAT1a, corresponding to the calculated MW (66.9 kDa) in full-length. Importantly, no visible signal was detected with the anti-HA antibody in mock-transfected cells, which indicates its specificity. When anti-PAT1a probed with the extracts from mock transfected cells and wild-type cells in a double loaded amount, it also detected a major band as above, likely representing the endogenous APPBP2/PAT1a in contrast with the pre-immune serum of anti-PAT1a, it did not reveal significant signal within the same source of extracts. Comparing the set of samples loaded with extracts from wild-type and cells expressing recombinant APPBP2/PAT1a, the later revealed a higher intensity of the major band. All of above indicate that, the anti-PAT1a antibody recognize specifically APPBP2/PAT1a in

Western analysis.

The same combination of test were done for immunocytochemical assay as describe above. Comparing anti-PAT1a with commercially well-characterized anti-HA antibodies, the anti-PAT1a could reveal the same cellular staining pattern when applied to cells over expressing recombinant APPBP2/PAT1a carrying HA-tag. Comparing the staining between wild-type and cells over expressing recombinant APPBP2/PAT1a revealed different levels of indirect fluorescence, but stained both the cytosol and the same subcellular compartments. During the generation of the anti-PAT1a antibody, methods that may test the specificity of the anti-PAT1a were chosen and the results are shown in the following:

3.5.1. Anti-PAT1a may bind to selected sequence-specified APPBP2/PAT1a c-terminal epitope at high affinity

In order to collect the highest titer of anti-PAT1a and test its affinity to the selected peptide during production, BIACore Surface Plasma Resonance (SPR) was performed in colaboration with Prof. Multhaup. BIAcore's SPR technology is a label-free technology for monitoring biomolecular interactions as they occur, in our case the interaction would be in between the selected sequence-specified APPBP2/PAT1 peptide and the generated anti-PAT1 antibody. The dection principle relies on surface plasmon resonance(SPR), an electron charge ddensity wave phenomenon that arises at the surface of a metallic film(mostly gold) when light is reflected at the film under specific conditions. What Biacore actually measures is the angle of minimum reflected light intensity. When anti-PAT1 bind to the sensor surface coupled with the selected APPBP2/PAT1 peptide, the concentration and therefore the reflective angle at the surface chenges and an SPR response can be detected. Plotting the response against time during the course of an interaction provides a quantitative measure of the progress of the interaction, the recording plot is called a sensorgram. SPR response values are expressed in resonance units(RU). One RU represents a change of 0.0001° in the angle of the intensity minimum. For most proteins, this is roughly equivalent to a change in concentration of about 1pg/mm^2 on the sensor surface. The exact conversion factor between RU and surface concentration depends on propertiesof the sensor surface (in our case is a thin layer of gold) and the nature of the molecule responsible for the concentration changes.

(Details in Material and methods). The SPR results showed that, the anti-PAT1a antibody binds in an affinity at least 150 pg/mm^2 to the selected APPBP2/PAT1a peptide.

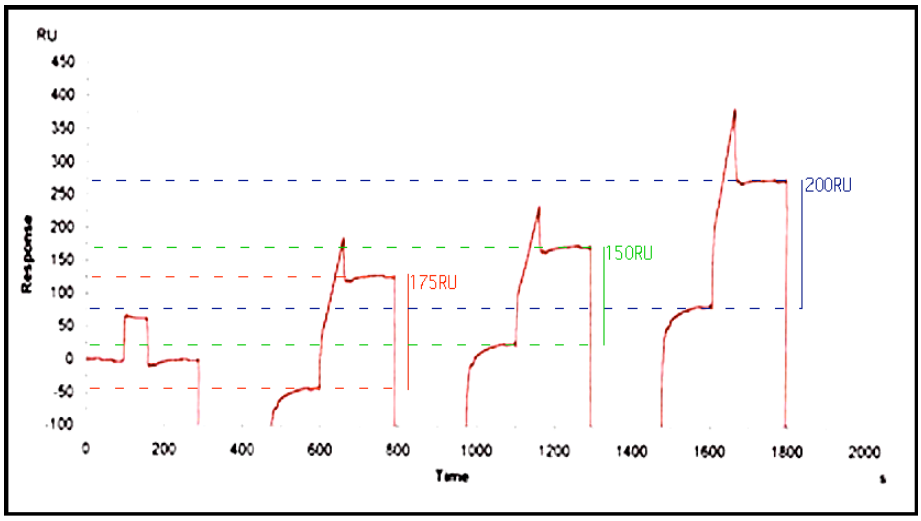

Fig.3.5.1: Result of anti-PAT1a tested by BIACore Surface Plasmon Resonance (SPR). RU: resonance units. Time scale: msec. One RU represents a change of 0.0001° in the angle of the intensity minimum. For most proteins, this is roughly equivalent to a change in concentration of about 1 pg/mm^2. Recording started when the sample anti-PAT1a flow in passing through the sensor surface that coupled with the APPBP2/PAT1a peptide. The difference of RU indicated aside every recording curve represents the affinity of the antibody to the peptide in steady status. The lowest affinity tested (green) was 150 RU, represent the anti-PAT1a may bound in amoung of at least 150pg/ mm^2 to the APPBP2/PAT1a peptide. In practical cases, >50 pg/ mm^2 is thought to interact with good affinity (Edwards, P. R. 1995; Johnsson, B et al., 1991).

3.5.2. Western Analysis of anti-PAT1a compared with anti-HA antibody

Based on positive results from BIAcore SPR test, further test of anti-PAT1a was carried by Western analysis. COS-7 cells were transiently transfected with APPBP2/PAT1a-HA and the cells were harvested 24hr post-transfection.

The recognition pattern of anti-PAT1a with highly expressed APPBP2/PAT1a-HA protein samples in comparision with the well-characterized, commercially available anti-HA antibody (Roche) is showing in (Fig.3.5.2).

3.5.3. Immunocytochemical Analysis of anti-PAT1a compared with anti-HA antibody

To test if anti-PAT1a may be suitable for immunocytochemical approaches,

immunocytochemical staining in comparison with anti-HA antibody to cells collected in parallel within the above mentioned Western analysis was performed. The result revealed positive staining of anti-PAT1a to its target protein APPBP2/PAT1a tagged with a HA-epitope and the same pattern in comparison with the anti-HA antibody.

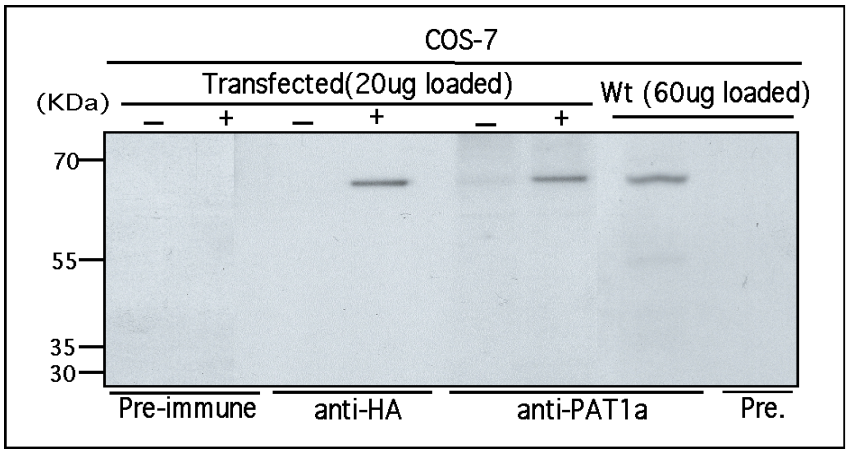

Fig. 3.5.2: Anti-PAT1a recognizes APPBP2/PAT1a with high specificity in Western analysis. The anti-PAT1a antibody and an anti-HA antibody recognized a major band at ~67kDa in extracts of cells expressing recombinant HA-tagged APPBP2/PAT1a (lanes indicated with "+"), which matched to the calculated MW (66.9 kDa). No significant signal was detected with the anti-HA antibody in mock transfected cells (lanes indicated with "–"). The anti-PAT1a antibody recognized the wild type sample loaded in triple amount a major band at ~67 kDa, likely representing the endogenous PAT1a. No bands were detected in lanes probed with pre-immunoserum (Pre.) representing high specificity of anti-PAT1a antibody.

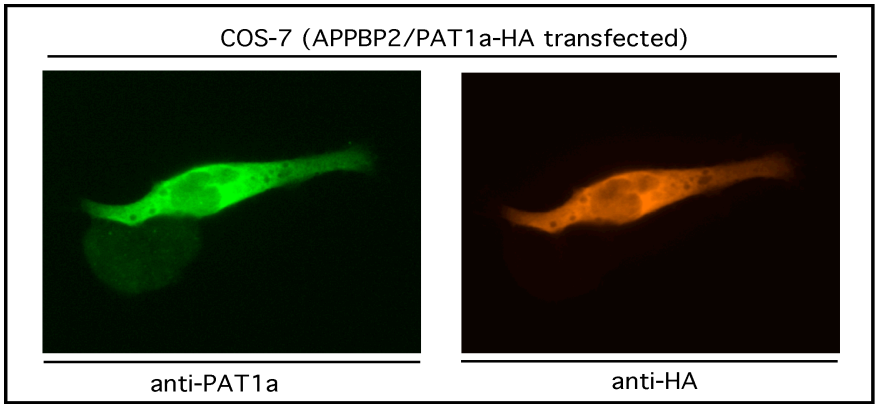

Fig.3.5.3: Anti-PATa shows the same staining pattern as anti-HA antibody. Double staining with the anti-PAT1a (green) and anti-HA (red) antibodis to verify the specificity of anti-PAT1a to APPBP2/PAT1a revealed an identical staining pattern. Note, with the anti-PAT1a antibody staining an adjacent cell with weaker immunoreactivity of anti-PAT1a was detected which might represent the endogenous APPBP2/PAT1a level and reveal the anti-HA has no cross-reactivity to any endogenous protein in this cell type.

3.5.4. Immunopercipetation Analysis of anti-PAT1a antibody

To test if the anti-PAT1a antibody could be utilized for immunoprecipitation (IP) approaches, additional characterization was designed. Our Characterization for immunoprecipitation approach had a convincing result as well. Protein lysates from cells overexpressing the recombinant HA-tagged APPBP1/PAT1a were subjected to immunoprecipitation procedures with either the pre-immunoserum of anti-PAT1a and anti-PAT1a. The resulted immunoprecipitates were analysized and revealed no detectable band from the pre-immunoserum and a clear band from the anti-PAT1a at the expected size in contrast with a lane loaded with 20% input, which indicated that anti-PAT1a could immunoprecipitate its target protein, APPBP2/PAT1a.

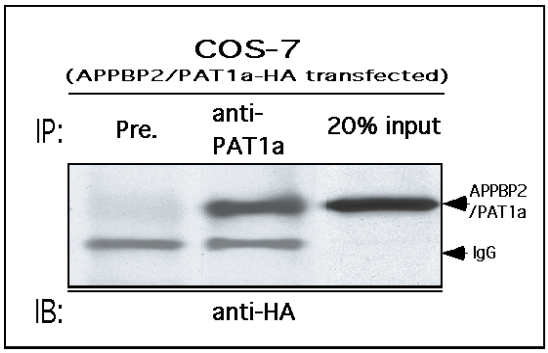

Fig. 3.5.4: The antiPAT1a antibody immunoprecipitates specifically. Anti-PAT1a immunoprecipitates APPBP2/PAT1a-HA protein whereas the immunoprecipitation performed with pre-immune serum(Pre) shows no positive signal in contrast to the lane loaded with 20% input sample. The presence of IgG bends revealed that in our cases there are cross-spices activity occurred between the capturing antibodies for IP and the secondary detection antibodies for IB: immunoblotting.

3.6. Distribution of APPBP2/PAT1a in various cell lines and mouse tissues

Based on the results from characterization of anti-PAT1a, we could conclude that this rabbit anti-PAT1a is specific and suitable to be utilized for approaches on endogenous expression of APPBP2/PAT1a. Prior to this with combined evaluation of BIAcore SPR result, the anti-PAT1a was affinity purified with the same peptide for the immunorization in order to enhanced the purity of this antibody. In previous characterization of anti-PAT1a antibody that showed it recognizes a major band at

~67 kDa, likely representing the endogenous PAT1a, however, in this test the criteria of sample amount loaded was minimal, only to bring visible signals. With reference back to the Northern results, the APPBP2/PAT1a transcripts levels varied highly among tested tissues, it was reasonable to consider an increasing amount of loading samples in order to avoid wrong evaluation of endogenous expressing APPBP2/PAT1a from different cell lines and mouse tissues. After the protein concentration was determined, 80ug/lane of samples were loaded to proceed the analysis of endogenous expression of APPBP2/PAT1a.

3.6.1. Expression pattern of APPBP2/PAT1a differs in different cell lines.

Various cell lines available in our group were used. Lysates from wild type COS-7, HEK293, SH-SY5Y, Hela cells, primary mouse cortical neurons (DIV7) were collected with normal morphological condition. Lysates from different cell lines overexpressing APPBP2/PAT1a-HA except primary neurons were also collected for analysis, since the size of HA epitope is about 3 kDa, the gel system used for this analysis could not differentiate the size difference in between APPBP2/PAT1a and APPBP2/PAT1a-HA, so that the later samples may served to indicate the correct position of bends represent APPBP2/PAT1a.

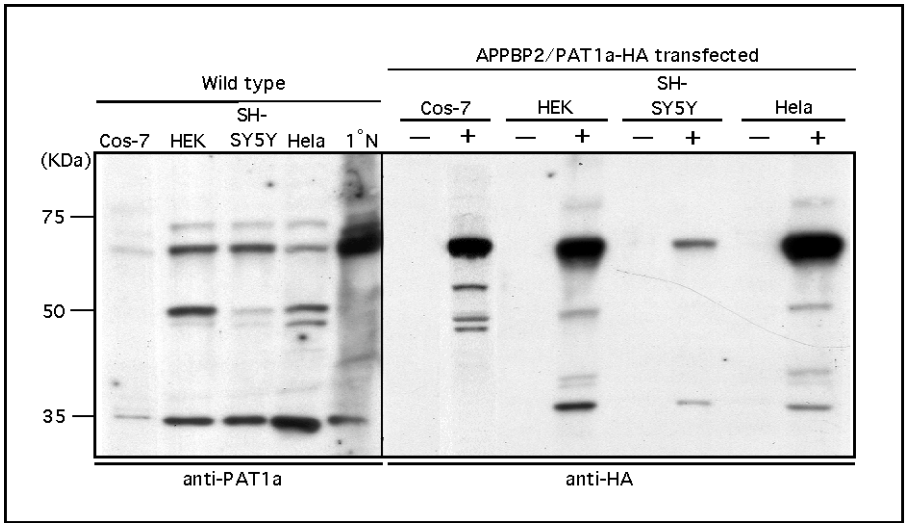

Fig.3.6.1: Western Analysis of endogenous APPBP2/PAT1a and recombinant APPBP2/PAT1a-HA in different cell lines. The anti-HA and anti-PAT1 antibodies recognized in extracts of cells expressing recombinant HA-tagged APPBP2/PAT1a (+) or endogenous APPBP2/PAT1a a major ~67kDa band (arrowhead) and several signals with lower MW, including 47kDa and 35kDa, possibly representing carboxy

terminal cleavage products of APPBP2/PAT1a or putative APPBP2/PAT1a splice variants. No signal was found in non transfected cells (-). Note, that the pattern of low molecular bands varies in the different cell types.

3.6.2. Ubiquitous expression of APPBP2/PAT1a in multiple mouse tissues is in high complexity

In this step, extracts of multiple mouse tissues were subjected for Western analysis using the previousily characterized and affinity purified anti-PAT1a antibody. The result showed that, besides the major band at ~67kDa, additional signals at 72kDa and also at lower molecular weight were detected. The ~67kDa band was found in all tissues, whereas the lower molecular weight forms varied in size between the different tissues and the ~72 kDa band was found only in some tissues. However, based on our results with recombinant APPBP2/PAT1a-HA, we assume that the ~67kDa form represents full length APPBP2/PAT1a, whereas the low molecular weight forms are either cleavage products or due to alternative splicing. The ~72 kDa bands possibly resulted from posttranslational modifications of the ~67kDa band. The expression pattern of the ~67kDa APPBP2/PAT1a form resembles the result of the Northern analysis of APPBP2/PAT1a.

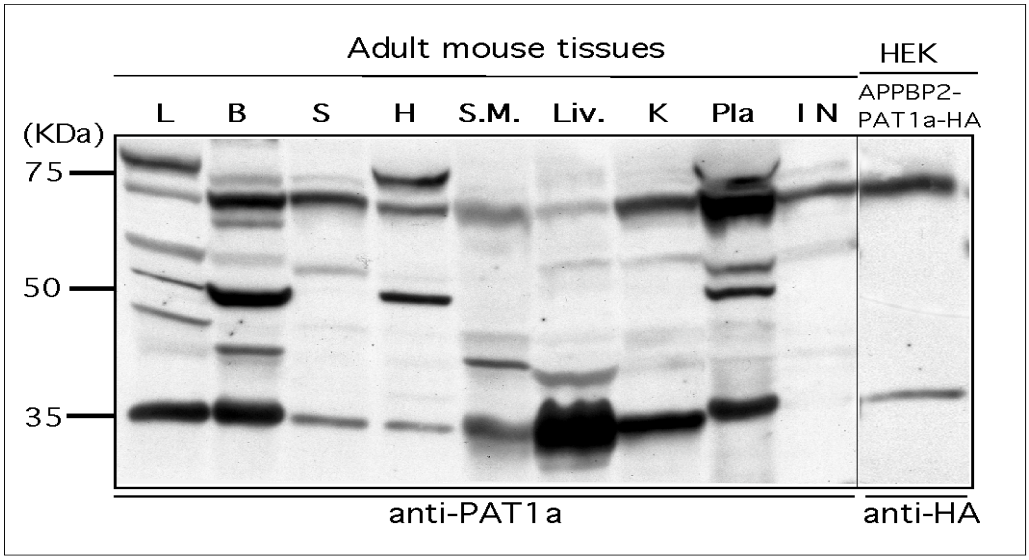

Fig.3.6.2: Western Analysis of PAT1a/APPBP2 among adult mouse tissues. Besides the major band at ~67kDa, additional signals at ~72kDa and also at lower molecular weight were detected. (L: lung; B: brain; S: spleen; H: heart; S.M.: skeleton muscle; Liv: liver; K: kidney; Pla: placenta; 1N: primary neurons). The ~67kDa band was found in all tissues, whereas the lower molecular weight forms varied in size

between the different tissues. However, based on our results with recombinant APPBP2/PAT1a-HA (right most lane), we assume that the ~67kDa form represents full length APPBP2/PAT1aPAT1a, and the low molecular weight forms are either due to posttranslational cleavage or alternative splicing. In contrast with the detection of anti-HA to APPBP2/PAT1-HA, the pattern of low molecular weight bands varied in different cell lines, suggesting that tissue specific or cell type specific cleavages or modifications might occur. Consistent with this assumption, the expression pattern of the ~67kDa APPBP2/PAT1a form resembled the result of the Northern analysis: pronounced levels of PAT1a were detected in brain, placenta, and kidney, whereas only low expression was found in liver and skeletal muscle.

3.7. The distribution of PAT1a overlaps with the expression pattern of APP family proteins

3.7.1. APLP1 is expressed in neurons in mouse brain (reconfirmed)

While looking back for references that described the neuronal expression of APLP1, we found contradictary datas were reported by (Lorent et al, 1995) and (Heber et al 2000; and Thinakaran et al, 1995), Lorent and co-workers reported that APLP1 is expressed in both nourons and glial cells whareas Heber and co-workes, and Thinakaran reported that APLP1 is expressed strickly in nourons. Thus, it needed to be re-investigated, clarifing the statement in protein level. Considering the available materials, we used the commercially well-characterized anti-APLP1 antibody (CT-11), that was raised against the human APLP1 carboxyl terminal residues (640-650aa), which may recognize mouse APLP1 as well. Immunohistochemical and immunohisto fluorescence staining on mouse brain sections were performed, and to ensure any presence of nonspecific reactivity with this antibody, brain sections from APLP1-/- mice were used as control (Fig. 3.7.1).

3.7.2. Overlapped expression of PAT1a/APPBP2 to APP family members in mouse brain is highly susceptible to neurodegeneration in AD

To extend the study of APPBP2/PAT1a expression pattern in protein level, and to investigate if it is distributed in brain regions that highly affected by AD, this is rather an important issue to propose any link to AD pathologenesis. Immunohistochemical analysis of mouse brain sections with anti-PAT1a antibody was performed.

Immunohistochemical analysis of mouse brain sections using anti-PAT1a antibody

revealed a widespread and predominantly neuronal expression. Importantly, there is no obvious significant signal could be detected by using the pre-immunoserum of anti-PAT1a antibody. Interestingly, PAT1a was present both in the soma and distal neurites of pyramidal neurons, whereas in Purkinje cells only the cell body and proximal neurites were stained, suggesting a differential cell type specific expression of PAT1a. Besides this, a weak staining of glial cells was observed, as indicated by colocalization with GFAP. In contrast with *in situ* analysis which has no signal shown on glial cells, we think the possible reasons would be that, the APPBP2/PAT1a mRNA transcripts in glial cells is lower than our detectable range but is sufficient to generate low but detectable APPBP2/PAT1a protein.

The result revealed a widespread predominant neuronal expression with high level in the cortex and hippocampus that are affected in AD, which shows agreement to our *in situ* data (Fig.3.7.2).

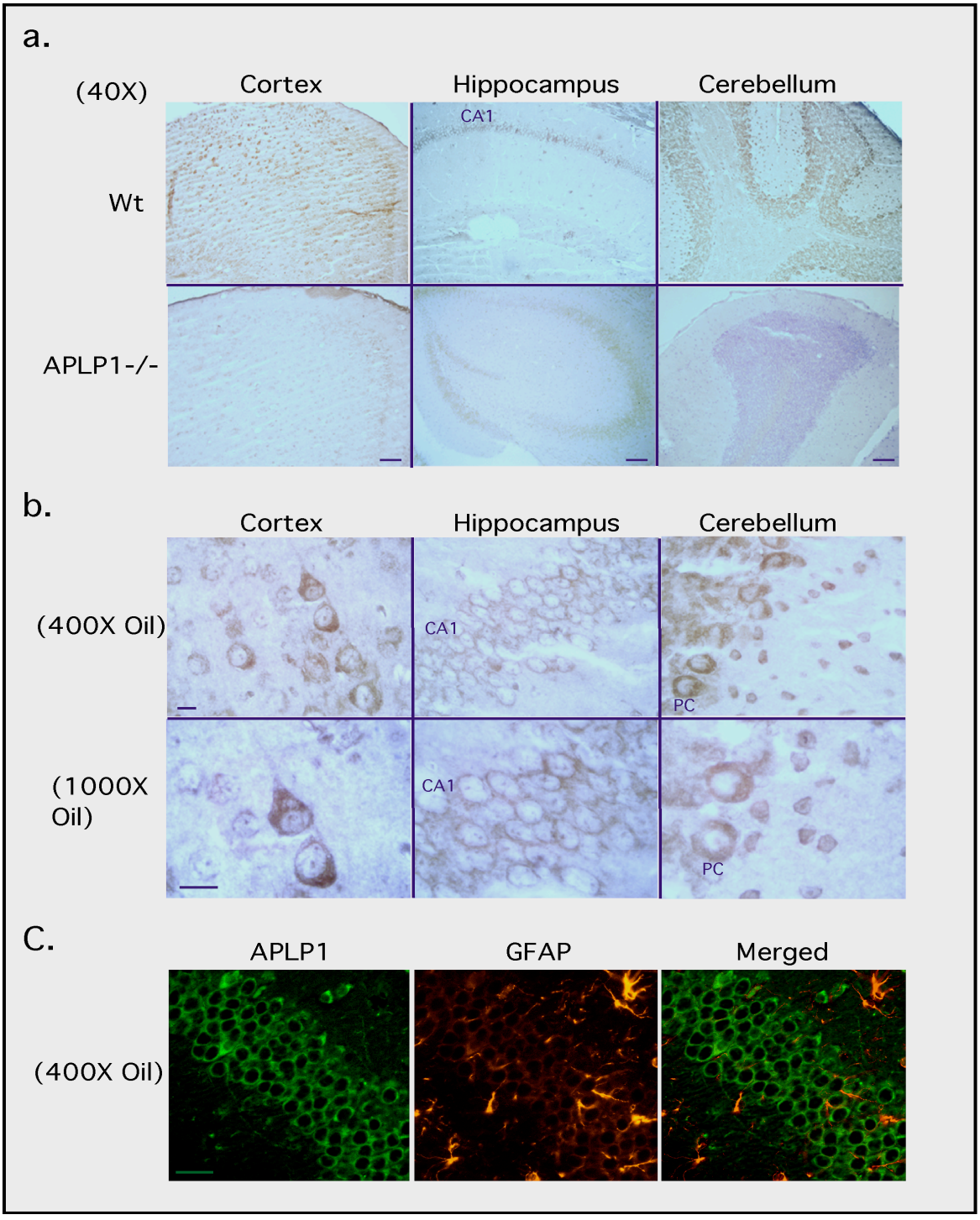

Fig.3.7.1: Immunohistochemical Analysis of APLP1 expression pattern in mouse brain. (a)APLP1 was found widely distributed in mouse brain and the expression is strictly in neurons. The signals were detected and obvious in cell-dense areas such as cortex, the Purkinje cell layer (PC) in the cerebellum and the dentate gyrus and CA1-3 region in the hippocampus, whereas no significant signal was observed on brain sections from APLP-/- mouse. Bar=200um. **(b)**High magnification clearly shows a cytosolic staining with extension to the apical neuritic region. Bar=50um. **(c)** Double staining of APLP1 with GFAP revealed no overlapping expression, agreed with the *in situ* experiment that APLP1 is expressed strictly in neuronal cells. Bar=50um.

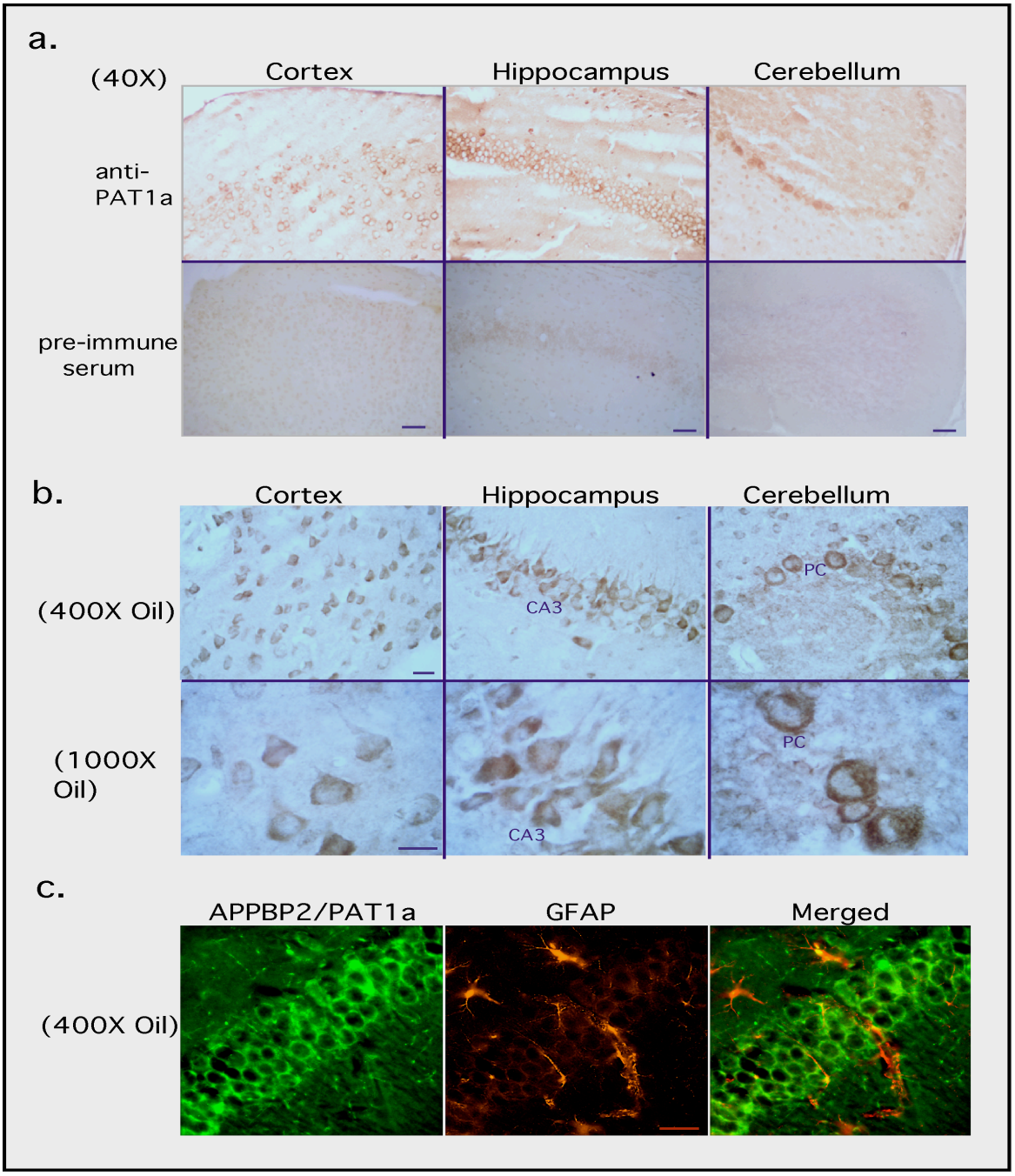

Fig.3.7.2: APPBP2/PAT1a immunohistochemical stain of mouse brain sections. **(a)**APPBP2/PAT1a was found widely distributed in mouse brain and the expression is predominantly in neurons. The signals were detected in cell-dense areas such as cortex, the Purkinje cell layer (PC) in the cerebellum and the dentate gyrus and CA1-3 region in the hippocampus, whereas no significant signal was observed on brain sections that probed with pre-immune serum. Bar=200um. **(b)**High magnification clearly shows a cytosolic staining with extension to the apical neuritic region. Bar=50um. Notably, PAT1a was present in the soma and apical dendrites of pyramidal neurons, whereas in Purkinje cells only the cell body and proximal neurites were stained, suggesting a differential cell type specific expression of APPBP2/PAT1a. **(c)** Double staining of APPBP2/PAT1a with GFAP revealed slightly overlapping expression, suggesting that APPBP2/PAT1a may be expressed in lower level in glial cells. Bar=50um.

3.8. Colocalization of recombinant APPBP2/PAT1a and APP family proteins in subcellualr membrane compartment in primary mouse E14 cortical neurons (DIV 7)

3.8.1. APPBP2/PAT1a is transported to both dendrites and axons

We next investigated the cellular localization of APPBP2/PAT1a-HA in primary neurons. For this purpose, we transfected primary neurons differentiated for 7 days *in vitro* (DIV7), with cDNA encoding HA-tagged APPBP2/PAT1a.

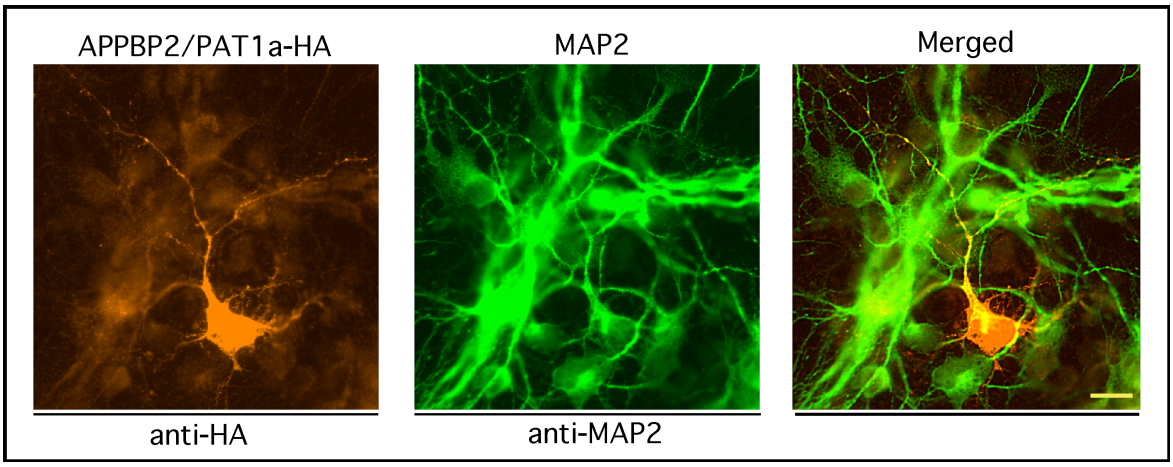

Fig.3.8.1: The subcellular distribution of APPBP2/PAT1a. Besides a diffuse cytosolic staining, we observed a punctate, vesicular APPBP2/PAT1a(Red) immunoreactivity, suggesting that APPBP2/PAT1a is partly associated with intracellular vesicles. We also observed strong APPBP2/PAT1a immunoreactivity in the somatodendritic compartment and in MAP2-negative (green) neurites suggesting that APPBP2/PAT1a is localized to both dendrites and axons. However, we found no accumulation of PAT1a in a specific subcellular compartment, such as the nucleus or the cis/medial Golgi apparatus in neurons. Bar=50um.

3.8.2. Co-localization of APPBP2/PAT1a with APP family proteins in neurons

Concerning whether APPBP2/PAT1a co-localizes with APP, APLP1 or APLP2 in subcellular membrane compartments, mouse primary neurons were transfected with APPBP2/PAT1a-HA and myc-tagged APP, APLP1, or APLP2. The results reveal, PAT1a is associated with APP/APLPs containing vesicles in the early and late secretory pathway suggesting that APPBP2/PAT1a may be implicated in different steps of the subcellular transport of APP, APLP1 and APLP2 from the ER/Golgi to the cell surface. Since antibodies available from different species for indirect

immunoflorescence analysis were limited for APLP1 and APLP2, both have only antibodies derived from rabbits, and our anti-PAT1a was derived from the same species as well, so that this approach could not be done in endogenous levels, we therefore decided to double transfect HA-tagged APPBP2/PAT1a with each myc-tagged APP family members. Analysis regarding the co-localization was done with 20 z-scan sections in 2um depth on every single neuron and the deconvolution enchancement was performed with the highest ranked program. Besides, we focused the localization on the fine structures covering neurites instead of soma region to avoid highly saturated false positive co-distribution signals. As shown in result 3.8., APPBP2/PAT1a associates with vesicular membranes or organelles co-localized with each APP family members in the distal neurites. Remarkably, most of the APLP2 positive vesicular structures co-localized with APPBP2/PAT1a, whereas the APP or APLP1 co-localized only partly, which also agreed with the GST pull-down data from our group that observed the strongest binding for APPBP2/PAT1a and APLP2, suggesting that APPBP2/PAT1a may interact preferentially with APLP2 *in vivo*.

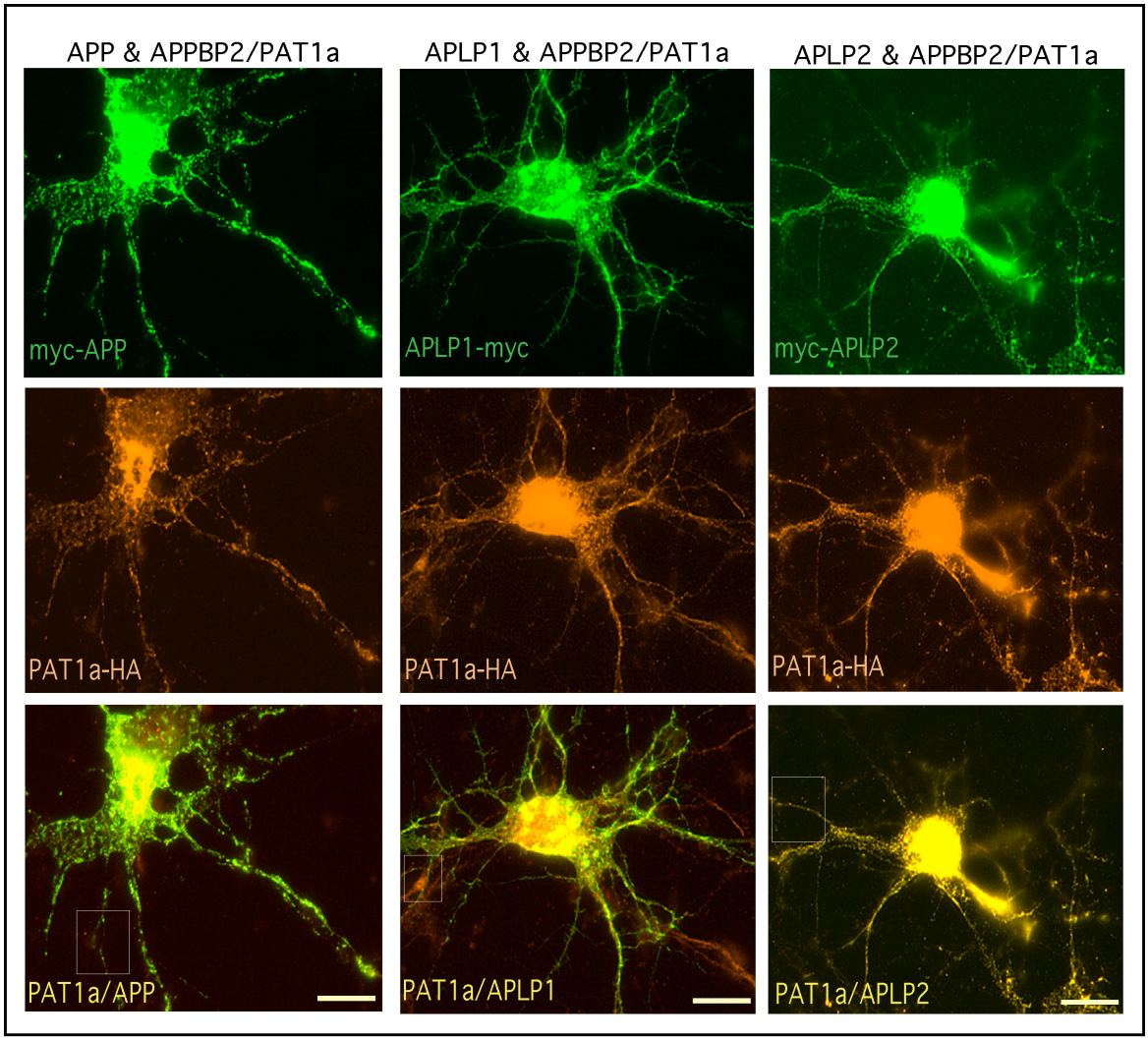

Fig.3.8.2: Overall co-expression of APPBP2/PAT1a and APP family proteins in neurons. Mixed cortical neurons were transfected with cDNAs encoding HA-tagged PAT1a, and myc-tagged APP, APLP1 or APLP2. Cells were stained with the anti-HA (red) and anti-myc (green) antibodies. Immunocytoflurocence analysis revealed a co-staining (yellow) of APPBP2/PAT1a with APP, APLP1, or APLP2 not only in the cell soma, but also in vesicular structures of distal neurites. Remarkably, most of the APLP2 positive vesicular structures co-localized with APPBP2/PAT1a, whereas the overlap of APP or APLP1 staining with that of APPBP2/PAT1a staining was lower. Bar=50um.

3.8.3. APPBP2/PAT1a is co-localized with APP family proteins in subcellular membrane compartments

To show clearly the co-localization of APPBP2/PAT1a in subcellular compartments, enlarged views of selected regions focusing on the distal neurites form the previous overviews (Fig.3.8.2) of whole neurons are showing below:

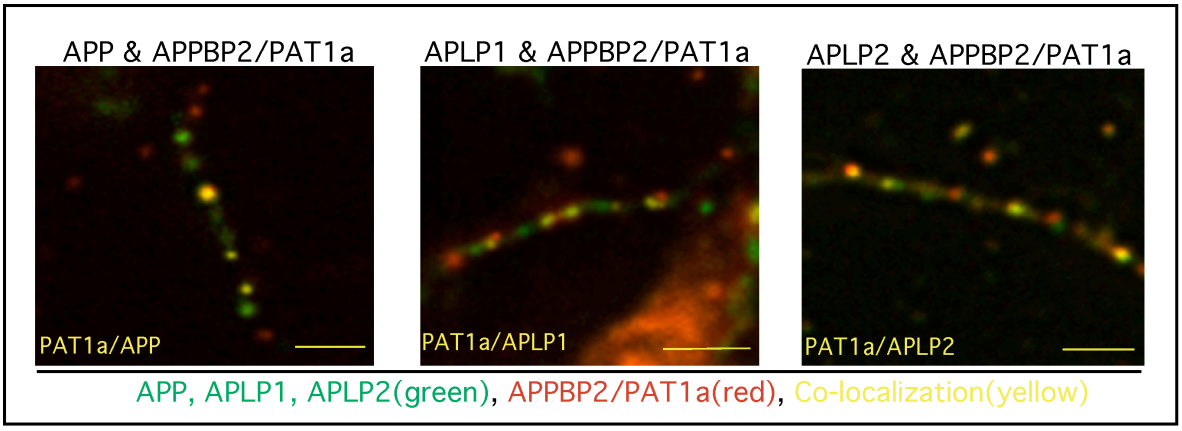

Fig.3.8.3: Detail Co-localization of APPBP2/PAT1a in vesicular structures. Higher magnification of the area marked in the merged images (Fig.3.8.2) by a square. In these enlarged views, subcellular compartments may be seen clearly to reveal the co-distribution (yellow) of APPBP2/PAT1a (red) and APP family proteins (green). However, The specific subcellular compartments could not be differentiated in this study because lack of markers. These structures might present transport vesicles, endosomes or lysosomes. Bar=50um.

3.9. In vivo interaction of APPBP2/PAT1a and APP family proteins in mouse CNS

PAT1 was shown to interact directly with APP in vitro, however further evidence to prove the existence of in vivo interaction was considered necessary for AD researches. Previously, We have shown that APPBP2/PAT1a presents in the membrane fraction of the postnuclear supernatant, and this presence was depleted when the supernatant was subjected to high pH carbonate treatment prior to the membrane preparation. Above lays barely, APPBP2/PAT1a, without any predictable membrane spanning domain, is partly associated with membrane compartments where the APP family proteins also present. While the other works in our group were reconfirming the in vitro binding by Western analysis and in parallel checking if the other two mammalian homologous of APP might interact with APPBP2/PAT1a in vitro as well since they are from an highly conserved gene family, this study moved on directly to analyse the in vivo interactions between APPBP2/PAT1a and APP family members in mouse central nerves system. Co-immunoprecipitation approaches were performed to answer these questions. The anti-PAT1a antibodies has been characterized well that can immunoprecipitate it target protein APPBP2/PAT1a, we

utilized it as the capturing antibody to precipitate the immunocomplexes that associate with APPBP2/PAT1a in adult mouse brain. Pre-immune serum of anti-PAT1a was used to serve as a control experiment, which may indicate if the presence of any APP family proteins was resulted by non-specific co-precipitation. Comparative quantification of the interacting affinity among different family members was not performed because of that, for APLPs, the capturing antibodies and detection antibodies are from the same species, whereas in the experiment of APP were different. Using same species of capturing and detection antibodies in co-immunoprecipitation would reveal uniformed strong bands of immunoglobulins, in our case, would overlap with bands of each APP family members. We thus have to couple the capturing antibodies for co-immunoprecipitating APLPs which most likely would cause an non-equal amount of capturing antibodies used while performing the experiments and therefore would result an unreliable quantification.

The co-immunoprecipitation experiments clearly revealed that all three members exist in a common complex with APPBP2/PAT1a *in vivo* in the mouse central nerves system, which agreed with the data from our group that shows, in vitro synthesized APPBP2/PAT1a could be pulled down by in vitro translated GST-fused intracellular domains of APP, APLP1 and APLP2 (Tomas Grübl unpublished data).

3.9.1. APP can be co-immunoprecipitated with APPBP2/PAT1a from in vivo sample source.

Started with APP, mouse brains were collected and homogenized as described in Meterials and methods. Co-immunoprecipitation was performed with anti-PAT1a as the capturing antibody, Pre-immune serum and sepharose beads only(-) severed as controls in parallel. Western analysis (IB) of the immunoprecipitates was done with monoclony mouse anti-APP (22C11) since there was no cross reactivity of mouse anti-IgG to rabbit IgG (anti-PAT1a) observed in our system. We performed 2 methods, one set, the IP capturing antibodies were uncoupled to the protein A Sepharose beads, the other set, the capturing antibodies were covalently coupled to saphorose beads prior to the immunoprecipitation reaction.

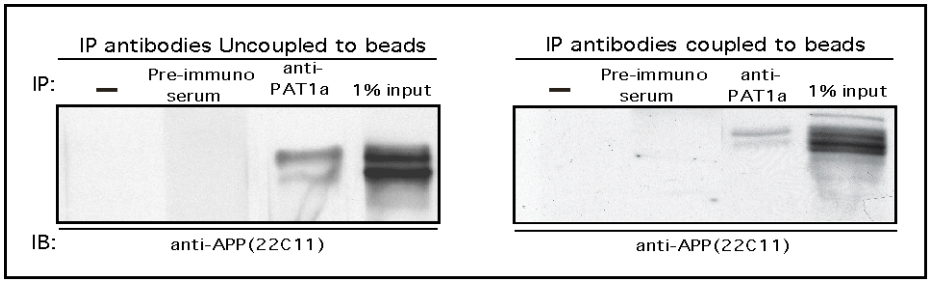

Fig.3.9.1: Presence of APP in the immunocomplexes of anti-PAT1a. APP was co-immunoprecipitated with the anti-PAT1a antibody, but not in the absence of IP antibody (-) or with the adjacent pre-immuno serum. Comparison between two sets of results revealed that the technical difference would cause non quantifiable binding ratio between APPBP2/PAT1a and APP. In the case of uncoupled IP antibodies (left panel), it revealed about 0.3% of APP binds to APPBP2/PAT1a (left panel) whereas when the antibodies were coupled to the Sepharose beads (right panel), it revealed only 0.1% of APP binds to APPBP2/PAT1 in mouse brain, this most likely was caused by the loss of antibody while coupling.

3.9.2. APLPs can be co-immunoprecipitated with APPBP2/PAT1a from in vivo sample source.

After fonud the evidence of in vivo interation between APPBP2/PAT1a and APP, the next is to test if APPBP2/PAT1a also interacts with APLPs, co-immunoprecipitation was also performed with the capturing anti-PAT1a antibody and pre-immuno serum coupled to the Sepharose beeds. Mouse brains were collected and homogenized in lysis buffer as described in Meterials and methods, then proceed to the immunoprecipitation reaction. Western analysis of the immunoprecipitates showed that bothe APLP1, APLP2 present in anti-PAT1a immuno complexes.

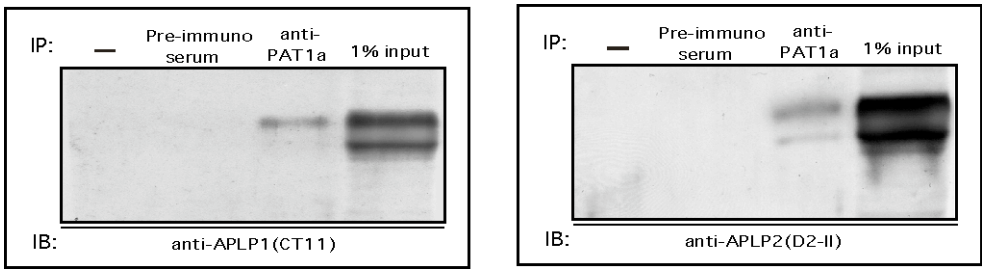

Fig.3.9.2: Presence of APLPs in the immunocomplexes of anti-PAT1a. APLPs were co-immunoprecipitated with the anti-PAT1a antibody, but not in the absence of IP antibody (-) or with the adjacent pre-immuno serum. Approximately, 0.2% of APLP1 may bind to APPBP2/PAT1a (left panel), 0.1% of APLP1 may bind to APPBP2/PAT1a (right panel) in mouse brain. Note, these experiments were performed with the coupled capturing antibodies to the Sepharose beads.

3.10. Processing of APP family proteins may be affected by regulation of APPBP2/ PAT1a levels

To test the consequences of the interaction between APPBP2/PAT1a and APP family proteins, the influence of APPBP2/PAT1a on APP/APLPs processing was examined. If APPBP2/PAT1a has a function in the control of the subcellular transport of APP/APLPs, it should affect their proteolytic cleavages. We used neuroblastoma cells (SH-SY5Y) stably expressing APP, APLP1 or APLP2 fused to a tandemly repeated z domain (2z) of proteinn A, which facilitates the detection of the APP/APLPs C-terminal fragments (CTFs) (Eggert et al., 2004a; Weidemann et al., 2002c). These cells expressing APP-, APLP1- or APLP2-2Z were transiently transfected with cDNAs encoding APPBP2/PAT1a-HA, an empty vector (mock) or small interfering APPBP2/PAT1a (siPAT1a), which causes a reduction of PAT1a protein level of about 50%-70% (Fig.3.10.1). Cells co-expressing APPBP2/PAT1a-HA produce elevated levels of sAPP, sAPLP1 and sAPLP2, as well as increased amounts of c-terminal fragments, whereas the reduction of the APPBP2/PAT1a levels led to decreased secretion of sAPP/APLPs and less CTF production (Fig.3.10.2). All detected CTFs were reduced to a similar extent, suggesting that PAT1a facilitates the transport of APP/APLPs towards the late secretory pathway, where α- and β-cleavage take place.

3.10.1. Alteration of APPBP2/ PAT1a by small interfering application

To move further for functional study of APPBP2/PAT1a, establish a system that may allow us to regulate the APPBP2/PAT1a levels was necessary. We applied both small interfering RNA (siRNA) and antisense techniques to modulate the endogenous APPBP2/PAT1a level. We found the siRNA technique could affect more than the antisense application in the human neuroblastoma cell line (SH-SY5Y), we thus utilized it to perform our analysis on the processing of APP family proteins.

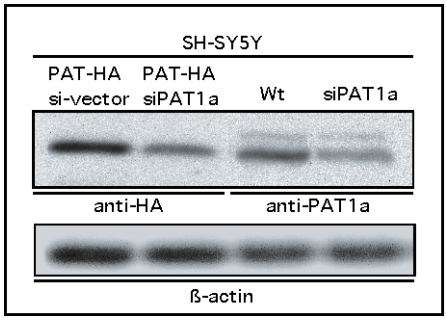

Fig. 30.10.1: Western analysis of down regulation of APPBP2/PAT1a. siPAT1a may down regulate both recombinant and endogenous APPBP2/PAT1a (upper panel). The siPAT1a co-transfected with APPBP2/PAT1a-HA caused a suppression of recombinant APPBP2/PAT1a-HA about 70% and caused a suppression of the endogenous APPBP2/PAT1a level about 50% in SH-SY5Y cells, whereas the β-actin level remained unchanged (lower panel).

3.10.2. APPBP2/PAT1a affects APP/APLPs processing

The influence of APPBP2/PAT1a on the generation of CTFs and secreted forms of APP/APLPs (sAPP, sAPLP1 and sAPLP2) was analyzed in SH-SY5Y cells that were stably expressing APP-, APLP1- or APLP2-2z constracts and transiently transfect with APPBP2/PAT1-HA (PAT1a-HA) cDNA, empty vectors (mock) or small interfering APPBP2/PAT1a (siPAT1a) vector. After 48h, medium containing sAPP, sAPLP1, or sAPLP2, and the cell extracts containing full length (fl) and carboxyl terminal fragments (CTFs) of APP, APLP1 and APLP2 were subjected to Western analyses. Cells co-expressing APPBP2/PAT1a-HA produce elevated levels of sAPP, sAPLP1 and sAPLP2, as well as increased amounts of C-terminal fragments, whereas the reduction of the APPBP2/PAT1a levels led to decreased secretion of sAPP/APLPs and less CTF production (Fig.3.10.2).

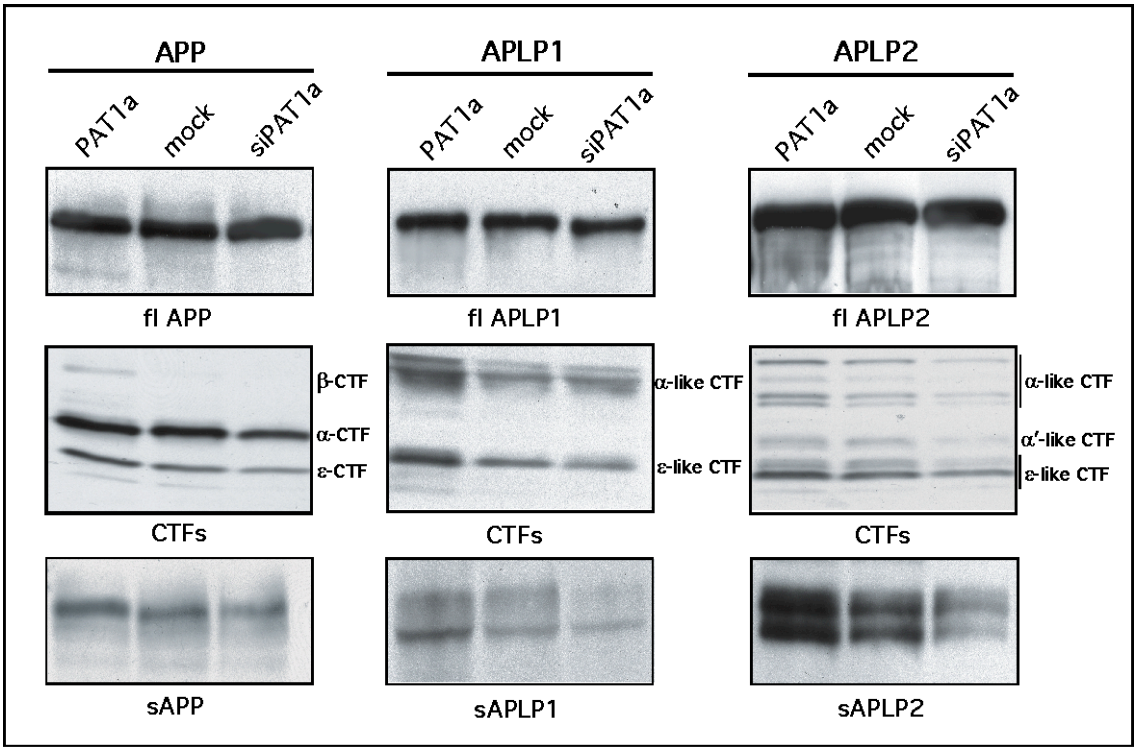

Fig.3.10.2: Western Analysis of APP family proteins after up/down regulation of APPBP2/PAT1a. The influence of APPBP2/PAT1a on the generation of CTFs and secreted forms of APP/APLPs (sAPP, sAPLP1 and sAPLP2) was analyzed. Regulation of APPBP2/PAT1a were designed to transiently transfect APPBP2/PAT1a cDNA, empty vectors (mock) or small interferring APPBP2/PAT1a cDNA (siPAT1a). After 48h, medium containing sAPP, sAPLP1, or sAPLP2, and the cell extracts containing full length (fl) and carboxyl terminal fragments (CTFs) of APP, APLP1 and APLP2 were analyzed. The full length of each proteins were normalized to the same amount (the upper most panel), to allow determination of the change of the generated CTFs and s-forms of each family proteins. Interestingly, we observed that cells co-expressing PAT1a produce elevated levels of sAPP, sAPLP1 and sAPLP2, as well as increased amounts of C-terminal fragments, whereas the reduction of the APPBP2/PAT1a levels led to decreased secretion of sAPP/APLPs and less CTF production. Notably, all detected CTFs were reduced to a similar extent, suggesting that the transport of APP/APLPs towards the late secretory pathway, where α- and β-cleavage take place, might be facilitated by APPBP2/PAT1a.

3.10.3. Quantification of the effects on the processing of APP family proteins

Quantification based on densitometric measurements were done by measuring the intensity of each bend resulted from above Western analysis. The results revealed significant influences.

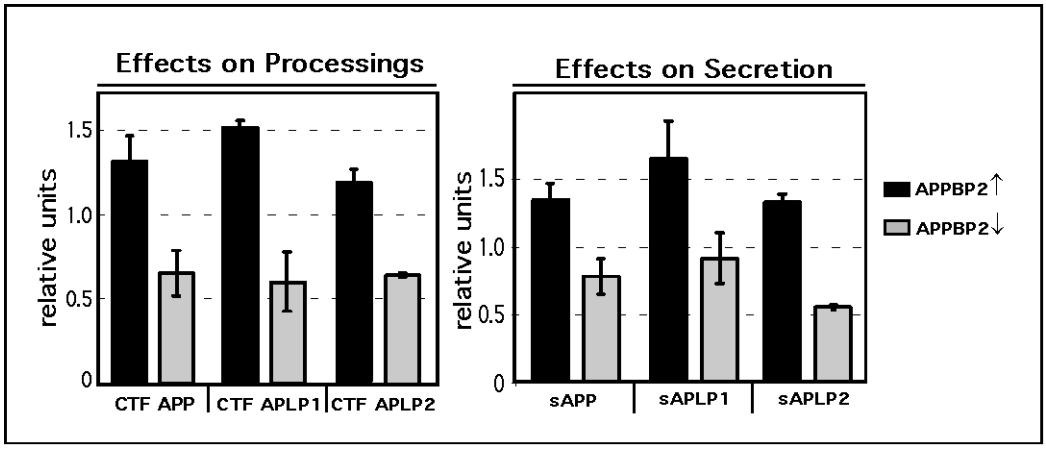

Fig.3.10.3: The amounts of sAPP/APLPs and CTFs generated in APPBP2/PAT1a overexpressing cells (black bars), mock transfected cells and siPAT1a treated cells (gray bars) were quantified. The relative amounts of CTFs and secreted fragments in comparison to mock transfected cells (set to 1) are shown. APP/APLPs fl protein levels varied in the range of less than +/- 5%. Error bars show standard deviations of the mean (n=3).

3.10.4. Quantification of the effects on Aβ production

To determine the effects on Aβ secretion, sandwich ELISA were performed with the medium collected from the cells that were examined for the influence on the processing by regulating the APPBP2/PAT1a levels. As mentioned before, the medium were collected 48hr post-transfection (affecting period 48hr), alternatively, the media were changed 36 hr post-transfection, then collected for analysis at the 48th hr post-transfection (affecting period 36-48 hr) for the ELSIA. Since we observed the peak of siPAT1a influence occurred during this period, thus was reasonable to think the maximal influence by regulating APPBP2/PAT1a should present in the same period as well. Our results proved the consideration, and reveal that regulation of APPBP2/PAT1a level favors the generation of Aβ42 than Aβ40 and the effects on Aβ42 is stranger than Aβ40.

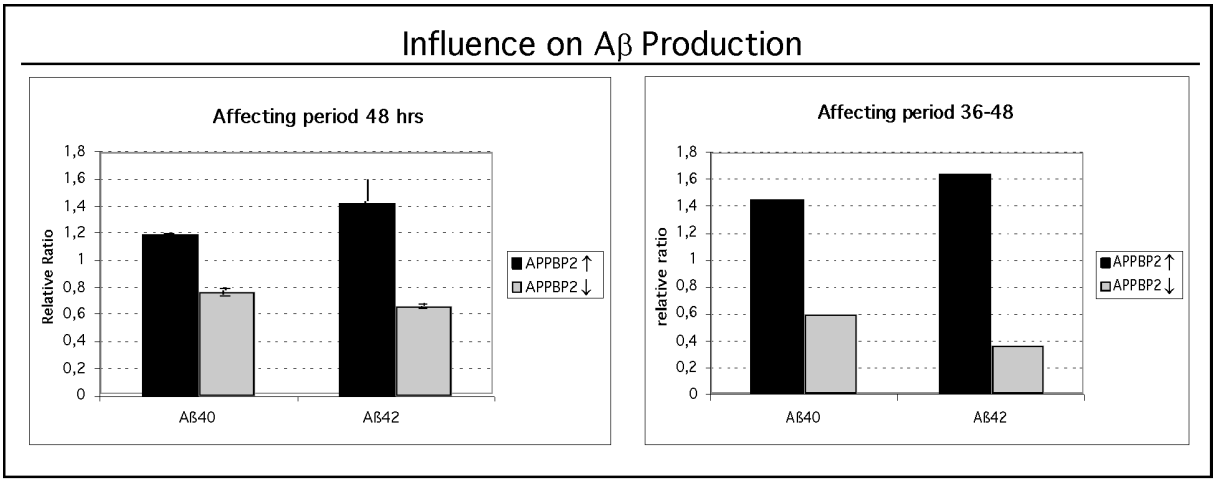

Fig.3.10.4: Quantification of the influence on Aβ production., Medium from the experiments of APP processing containing Aβ were collected as mentioned. The amounts of Aβ in APPBP2 overexpressing cells (black bars), mock transfected cells and siPAT1a treated cells (gray bars) were quantified. The relative amounts of Aβ in comparison to mock transfected cells (set to 1) are shown. The APP/APLPs full-length (fl) protein levels varied in the range of less than +/- 5% was checked in (Fig.3.10.3). Error bars show standard deviations of the mean (n=3).

.

4. Discussion

4.1. Why is PAT1 a rare variant of its representative gene in human brain?

Starting cloning of PAT1, we found all of our resulted PCR products containing constantly several mutations in alignment to PAT1 sequence. Database analysis revealed that the sequence of PAT1 results from an infrequent polymorphism of the APPBP2 gene. We cannot exclude that this could be resulted from different sources of cDNA that were used as templates while performing amplification. PAT1 was amplified from Hela cell cDNA (Zheng et al., 1998), and our APPBP2/PAT1a was amplified from human brain cDNA library. Interestingly, an androgen receptor associated protein (Ara67) was amplified from human testis cDNA library and described in recent (Zhang et al. 2004), which is 99,6% homologous to PAT1, this likely represents an additional variant of APPBP2/PAT1a, suggesting a high polymorphism in this gene.

Considering for AD research, we recommend, the accurate genetic information obtained from human brain shall be a more appropriate source. We also analyzed 53 ESTs covering the region of PAT1 cDNA containing the nucleotide exchanges. Unexpectedly, all tested EST sequences were identical with the sequence of APPBP2, but none was equal to PAT1, suggesting that the PAT1 sequence likely represents a rare variant of APPBP2. From some personal conversations with other groups that ever interested in working on PAT1, we found they all failed to reconfirm the interaction by western analysis with the recombinant PAT1 provided by (Zheng et al., 1998), which probably would explain why no occurrence of any following study could be found to date, this might due to the 6 amino acids exchange in between PAT1 and APPBP2/PAT1a. Further investigations shall be necessary to determine the precise frequency and to test whether these exchanges will result a consequence on the binding properties to APP/APLPs and if these polymorphisms might affect the risk for AD. In this context it will be further interesting to test the specific characteristics of the putative APPBP2/PAT1a splice variants.

4.2. APPBP2/PAT1a has 3 transcripts and is highly expressed in the areas where severely affected in the course of AD.

A neuronal function in subcellular transport of APP for PAT1 was proposed (Zheng et al. 1998). However, no study addressing its expression in brain has been performed. Therefore, analysis the neuronal expression of APPBP2/PAT1 is rather an important issue to propose any link to AD pathology.

Northern analysis In this study shows that APPBP2/PAT1a gene may encode three transcripts with the length of 6.5 kb, 4.3kb and 2.3kb. In contrast with all published Northern analysis of PAT1 among different cancer cell lines (Maarit, Cancer Research 2000); or its synonyms KIAA0228 (Nagase et al. 1996) including different human and mouse tissue and nonepithelial cells; or its variant Ara67 (Zhang et al. 2004) including human tissues and multiple cell lines. Our result reveal the same pattern and clear bands, which provide further specific data of APPBP2/PAT1a transcripts in natural sources from various human and mouse tissues. Worth to mention, our result shows that the APPBP2/PAT1a transcripts may be detected with most pronounced levels in brain, placenta, and kidney in human which differs from the study done by (Zhang et al. 2004). In their study, they concluded, “strong expression of Ara67/PAT1 transcripts were seen in skeletal muscle, placenta, and, heart “. Reference back to the figure of their Northern data, we found, the author did not normalize the expression levels to the control ß-actin transcripts which exhibited in diverse levels while our detection of ß-actin transcripts exhibited comparable amounts of mRNA that were loaded.

APP was shown to be expressed in both neurons and glial cells among all regions in the brain, when affected by AD, was observed to be up regulated in the frontal cortex and the hippocampus (Cras et al., 1991). The regional, subcellular distribution of APLP1 and APLP2 was shown to overlap with each other and with APP (McNamara et al., 1998), but cellular expression of APLP1 was shown strickly in the neurons (Thinakaran G, 1995; reconfirmed in this study). In AD brain, both were examined to accumulate in the large dystrophic neurites in a subset of senile plaques (Bayer et al., 1997; Crain et al., 1996; McNamara et al., 1998). Our in situ hybridization shows that, all 3 transcripts of of APPBP2/PAT1a detected in the Northern analysis are distributed in mouse brain predominantly in neurons and widely overlaps with the expression of APP/APLPs and is highly expressed in the areas that are severely

affected in the course of AD (Table 3.3.2).

4.3. Do we have a specific and reliable polycoloned anti-APPBP2/PAT1a antibody?

As shown in the Results 3.5., the BIACore SPR result revealed, the generated anti-PAT1a antibody has relatively high affinity to the selected peptide from standard technical views, it surely can recognize the epitope selected from APPBP2/PAT1a, and most likely will recognize APPBP2/PAT1a. Western analysis of the recognition of anti-PAT1 to its target protein revealed a predominant band at the expected size, and the immunoprecipitation test showed that the anti-PAT1a may bind to APPBP2/PAT1a under non-denatured condition. Immunocytofluorescence analysis revealed the anti-PAT1a may exhibit the same staining pattern as anti-HA antibody.
In brief, we did BIAcore SPR analysis, test for immunoprecipitation, Western and immunocytochemical analysis, plus the affinity purification to ensure the anti-PAT1a is in a high quality of specificity. Although there are other techniques that may be apply to characterize an antibody, such as ELISA and pre-absorption, that represent similar principles as BIAcore and Affinity purification. With all the characterization works done for anti-PAT1a, we believe, this anti-PAT1a antibody reveals high specificity to not only its antigen, the selected peptide of APPBP2/PATa, but also to the target protein, APPBP2/PAT1a, and its other full-length variants or cleavage products containing the selected epitope.

4.4. Expression of APPBP2/PAT1a proteins in vivo is in high complexcity

The anti-PAT1a and anti-HA antibodies both recognized a major band at approximately 67kDa in extracts from different cells expressing recombinant HA-tagged APPBP2/PAT1a, corresponding to the calculated MW (66.9 kDa). In addition, we also observed lower molecular weight minor bands with both antibodies, which we believe, may be carboxyl terminal cleavage products or represent spliced variants

of APPBP2/PAT1a since at least 3 transcripts were consistently found in a detectable range among all Northern analysis of the same gene transcripts. As the protein pattern of low molecular weight bands varied in different cell lines, indicated that APPBP2/PAT1a is possibly differentially spliced or processed in different cell types.
With reference to all different Northern data showing in the other references and in this study, it clearly revealed that APPBP2/PAT1a transcripts contain three splicing variants, so that is reasonable to believe, likely may result at least three protein products if all in nature are being encoded for protein production. Mature proteins often accomplished with posttranslational modification, and hence may be subjected under goes processing for physiological functioning. Concerning all above possibilities thus made difficulties to predict band pattern that can be detected by Western analysis when the sample sources are from highly complicated organisms. In additional, protein products lack of the selected epitope for antibody generation would result no appearance to the analysis, which will reveal less unique band pattern comparing with Northern analysis. However, we still cannot exclude any specific cross reactivity that may occur during probing the characterized specific anti-body to denatured protein samples for western analysis. If this could come to an argument after carefully characterized the specificity of an antibody, then would argue a huge pool of existing antibodies, since it is also possible, a specific cross reactivity occurs on expected size of the target protein. Our over expression and down regulation of APPBP2/Protein have proved the anti-PAT1a is surely specific to APPBP2/PAT1a since the detection intensity varies when regulating APPBP2/PAT1 protein levels. We thus believe that the in vivo APPBP2/PAT1a protein expression is rather complicated.

4.5. APP family members can be detected in APPBP2/PAT1a immunocomplexes and observed existing in the same subcellular membrane compartments

Pimplikar and co-works only provided the in vitro interaction, which brought reasonable doubts if the evidence was too weak and might be in a false positive range when applying in vitro binding assay. Concerning the matter of fact, evidence of *in vivo* interaction is thus valuable to address better links of APPBP2/PAT1a to

APP pathological role of AD.

This study clearly shows that the subcellular co-localization of APPBP2/PAT1a and APP family members in primary mouse neurons were observed in membrane compartments, and all three members exist in a common complex with APPBP2/PAT1a *in vivo* in the mouse central nerves system by co-immunoprecipitation experiments, which agreed with the data from our group that shows, in vitro synthesized APPBP2/PAT1a could be pulled down by in vitro translated GST-fused intracellular domains of APP, APLP1 and APLP2 (Tomas Grübl unpublished data). In conclusion, our data suggest that APPBP2/PAT1a is associated with membranes containing APP/APLPs, indicating that APPBP2/PAT1a may be implicated in different steps of the subcellular transport of APP, APLP1 and APLP2 from the ER/Golgi to the cell surface and/or futher to endosomes.

4.6. The processing of APP family members and production of Abeta are influenced by regulating APPBP2/PAT1a levels

This study shows that cells co-expressing APPBP2/PAT1a produce elevated levels of sAPP, sAPLP1 and sAPLP2, as well as increased amounts of C-terminal fragments, whereas the reduction of the APPBP2/PAT1a levels led to decreased secretion of sAPP/APLPs and less CTFs production. Since α- and β- cleaved CTFs were reduced to a similar extent. Combine with the reported properties of PAT1, a KLC-like protein interacting with the BaSS of APP suggesting that, APPBP2/PAT1a facilitates the transport of APP/APLPs towards the late secretory pathway, where α- and β-cleavages take place.

Neurons are thought to be the main source of Aβ in brain (Turner et al., 2003) and as this study reveals that APPBP2/PAT1a affects APP/APLP processing in neuronal cells, it is feasible that APPBP2/PAT1a has a regulatory function in Abeta generation. Our sandwich ELISA results proved this proposal, the modulation of APPBP2/PAT1a level not only affect the Aβ production but surprisingly favor particularly the production of Aβ42. Thus, APPBP2/PAT1a is likely involved in the carboxy-terminal cleavage of APP in both normal and pathological states. Since there may be different γ-secretaseprotein complexes involved in the generation of Aβ40 and Aβ42 (Klafki et al., 1996; Skovronsky et al,. 2000), it is interesting to speculate that

elevated APPBP2/PAT1a may increase the ratio of Aβ42/Aβ40 by preferentially encouraging the activity of the 42-specific γ-secretase, suggesting a function of APPBP2/PAT1a in regulating APP/APLPs in neurons.

4.7. Possible roles of interaction between APPBP2/PAT1a and APP family proteins

It has been shown that in MDCK cells APP and APLP2 are transported to the basolateral membrane (Haass et al., 1994; Lo et al., 1995) and in agreement with the finding by Pimplikar and co-workers that the APPBP2/PAT1a binds to the BaSS of APP, and with reference to data from our group that APPBP2/PAT1a also binds to the BASS of APLPs. Thus APPBP2/PAT1a might be involved in subcellular targeting of APP/APLPs. However, the molecular mechanisms underlying the APPBP2/PAT1a function in subcellular sorting still remain to be investigated. Intriguingly, PAT1a was recently identified as an androgen receptor (AR) associated protein, suppressing the nuclear import of the AR (Zhang et al, 2004)The nuclear import of the AR depends on homo-dimerization (Langley et al., 1995), implicating that the suppression of nuclear import might be mediated by inhibition of the homo-dimerization of the AR. APP was also shown to form homo-dimers, and the dimerization was shown to affect processing (Scheuermann et al, 2001). A similar mechanism was proposed for APLP1 and APLP2 (Scheuermann et al, 2001). Thus, it is reasonable that APPBP2/PAT1a might suppress homo-dimerization of APP/APLPs, possibly causing an altered subcellular transport to the cell surface or membrane compartments where secretase activity and proteasomal cleavage occur, resulting in effects on APP/APLPs proteolytic cleavages.

Furthermore, (i) a conformational change in the juxtamembraneouse intacellular domain of APP/APLPs that contains the APPBP2/PAT1a-binding region, BaSS, or (ii) an alteration in maturation of APP/APLPs caused by sorting variation, leading to different membrane compartments, or (iii)an alteration of phosphorylation, or (iv) either the binding capacity or the sorting change may facilitate proteasomal cleavage of the cytosolic domain of APP so that altering gamma-secretase cleavage, or all of above may occur when modulating the level of this binding partner, since all of above possible roles have been proposed or shown in neurons with another intacellular

domain binding partner of APP, Fe65 (Ando et al., 2001).

4.8. Conclusion and future views

Based on all the known knowledge of PAT1, and APPBP2/PAT1a shown in this study, APPBP2/PAT1a widely overlaps with the expression pattern of APP, APLP1 and APLP2 and is predominantly expressed with relatively high level in the neurons that located in the mouse brain regions where in human was shown severely affected by AD in the brain. Further investigation of the expression of APPBP2/PAT1a and its different polymorphisms on AD brains in comparison with normal samples will be a necessary step to clarify this interpretation.

APPBP2/PAT1a exhibits structural similarity to KLC, associates with membrane compartments in the late secretory pathway bearing APP/APLPs and interacts directly with the BaSS of APP/APLPs *in vitro*. Further analysis of what have been reported for the interaction between KLC and APP is necessary to clarify if APPBP2/PAT1a is functionally similar to KLC and might compete the binding or compensate the function of KLC in APP/APLPs transport. Although the BaSS has been shown responsible for the sorting of APP, APLP2 to the basolateral surface in polarized epithelial cells, no evidence has been shown that it may facilitate the sorting to any particular subcellular region in neuronal cells. Variation of subcellular distribution of APP/APLPs by APPBP2/PAT1a in neuronal cells thus likely depends on other mechanisms instead of depending on the property of BaSS. Combination of different analysis of APPBP2/PAT1a on possible influences such as the dimerization, phosphorylation of APP/APLPs, shall be design to advance the knowledge toward its physiological function.

Evidence is provided that APPBP2/PAT1a may alter the proteolytic conversion of all APP family members and the ratio of Ab42/Ab40, indicating it may be a regulator of the physiological function of the APP family members and might have an important pathological role in AD. Further study will be necessary on whether the binding of APPBP2/PAT1a to APP/APLPs changes the polarity when APP/APLPs vesicles undergoes fusion to the plasma membrane, thus altering the secretase activity *in vitro*. *in vivo* studies on mice with a deletion in the APPBP2/PAT1a gene crossed with APP transgenic mice may address these questions and will be important for a more

detailed understanding of the role of APPBP2/PAT1a in AD.

5. Materials and Methods

5.1. Chemicals

Acetic anhydride	Fluka
Agar	Difco, Augsburg
Agarose	Invitrogen
Amberlite	Merck
6-Aminohexane acid	Merck-Schuchardt, Hohenbrunn
Ampicillin	Biomol, Hamburg
Ammoniumperoxodisulfate(APS)	Roth, Karlsruhe
Bacto Tryptone	Difco, Augsburg
Bacto Yeast Extract	Difco, Augsburg
Benzonase	Merck, Darmstadt
Bicinchinonic acid	Sigma, Deisenhofen
Boric acid	J.T.Baker, Deventer, Holland
Bovine serum albumne (BSA)	Roth, Karlsruhe
Bromo-Chloro-Indolyl Phosphate (BCIP)	Roche
Bromophenol-blue	Serva, Heidelberg
Calciumchloride ($CaCl_2$)	J.T.Baker, Deventer, Holland
Coppersulfate ($CuSO_4$)	Sigma, Deisenhofen
$CuSO_4$ solution (4%)	Sigma, Deisenhofen
Dextransulfate	Sigma
DMSO (Dimethylsulfoxide)	Sigma, Deisenhofen
Disodiumhydrogenphosphate (Na_2HPO4)	Merck, Darmstadt
DTT (Dithiothreitol)	Serva, Heidelberg
EDTA (Ethylendiaminetatracetate)	Roth, Karlsruhe
Ficoll P-400	Amersham
Ethanol	Riedel-de-Haen, Seelze
Ethidiumbromide	Sigma, Deisenhofen
Formamid	Merck
G418-sulfate	PAA Laboratories
L-Glutamate acid	Sigma, Deisenhofen
L-Glutamine (200 mM)	Sigma, Deisenhofen
Glycerol	Roth, Karlsruhe
Hydrochloric acid 37%	Merck, Darmstadt
Hygromycin B	PAA Laboratories
IPTG (Isopropylthiogalactoside)	Biomol, Hamburg
Isopropanol	Roth,Karlsruhe
Kanamycin	Sigma, Deisenhofen
Levamisol	Fluka
β-Mercaptoethanol	Sigma, Deisenhofen
Methanol	Merck, Darmstadt
Milk powder	Roth, Karlsruhe
MOPS (3-(N-morpholine)propane sulfonic acid)	Sigma, Deisenhofen
Natriumchloride (NaCl)	J.T.Baker, Deventer, Holland
Nitroblue-Tetrazolium (NBT)	Roche
Nonidet P40 (NP-40)	Fluka, Neu-Ulm
Penicillin-Streptomycin	Sigma, Deisenhofen
PMSF (Phenylmethylsulfonylfluoride)	Serva, Heidelberg

Poly-L-Lysine (PLL)	Sigma, Deisenhofen
Polyoxyethylen-sorbitan-monolaurate(Tween20)	Sigma, Deisenhofen
Polyvinylpyrrolidone	Sigma
Protogel (30 % (W/V) Acrylamide; 0,8 %(W/V) Bisacrylamide)	National Diagnostics
D(+)-Saccharose	Roth, Karlsruhe
Sodiumazide (NaN_3)	Sigma, Deisenhofen
Sodiumdihydrogenphosphate (NaH_2PO4)	Merck, Darmstadt
SDS (Sodiumdodecylsulfate)	Sigma, Deisenhofen
Sodiumpyruvate	Sigma, Deisenhofen
Sucrose	Sigma, Deisenhofen
TMEDA (N,N,N',N'-Tetramethylenediamine)	Sigma, Deisenhofen
Tricine	Biomol, Hamburg
Triethanolamine (TEA)	Fluka
Tris-HCl	Sigma, Deisenhofen
Urea	Roth, Karlsruhe
Xylene	Sigma

5.2. Materials

1 kb (+) DNA-ladder	Invitrogen
Phenobarbital sodium injection	Abbott Laboratories
Antigen unmasking solution	Vector
B27 supplement	Invitrogen
Biomax MR single emulsion films	Amersham (Kodak)
Bis-Tris-Gels 4-12%	Invitrogen
BSA standard solution	Pierce
Complete Protease Inhibitor Cocktail	Roche Molecular Diagnostics
CSPD, ready to use	Roche
3,3'-Diaminobenzidine	Sigma Deisenhofen
Dulbecco's Modified Eagle's Medium (DMEM)	Sigma Deisenhofen
DMEM/F-12 (1:1)	Invitrogen
ECL solution	Amersham
Expand Long Template PCR System	Roche
F-12/HAM nutrient mixture	Sigma, Deisenhofen
Fetal calf serum (FCS)	PAA Laboratories or Biochrom AG
Freund's Adjuvant complete or incomplete	Sigma, Deisenhofen
FuGene 6 Transfection Reagent	Roche
Glutathione Sepharose 4 Fast Flow	Amersham
Hepes Buffer (1M)	Sigma, Deisenhofen
High Fidelity Polymerase Chain Reaction Mix	Roche
Hyperfilm ECL	Amersham
Human brain cDNA	Clontech
Human MTN™ Blot	BD Bioscience
In vitro transcription kit (DIG labeling)	Roche
Lipofectamine Plus / Lipofectamine 2000	Invitrogen
[α^{32}P]CTP 40 mCi/ml;	Amersham
Mimimum Essential Medium Eagle (MEM)	Sigma, Deisenhofen
Mouse Embryo MTN™ Blot	BD Bioscience

Mouse MTN™ Blot	BD Bioscience
N2-supplement	Invitrogen
Neurobasal Media	Invitrogen
Nitrocellulose Protran 0,4 µm	Schleicher & Schuell
Non-Essential Amino Acid Solution (100 x)	Sigma, Deisenhofen
Normal sheep serum	Dako
Nucleobond AX-Kit	Macherey & Nagel
OPTI-MEM	Invitrogen
Pfu-DNA-Polymerase	Invitrogen
Prestained Protein marker: Rainbow low	Amersham
Prestained Protein marker: Rainbow high	Amersham
Prestained Protein Marker: Rainbow broad range	Amersham
Protein A-Sepharose	Amersham
ProFound™ Co-Immunoprecipitation Kit	Pierce
Qia Maxi Prep Kit	Qiagen
Qia Spin Mini Prep Kit	Qiagen
Qia Quick Gel Extraction Kit	Qiagen
Quick Ligation Kit	New England Biolabs (NEB)
Ouick Spin Columns	Roche
RNAse free Proteinase K	Roche
Sea-Blocking	Pierce
SP6/T7 Transcription Kit	Roche
StabilCoat	SurModics
StreptABComplex/HRP	DakoCytomation
Stratavidin-HRP	Amersham
SulfoLink® Kit	Pierce
T4-DNA-Ligase	Invitrogen
Taq-DNA-Polymerase	Invitrogen
1-Step™ Ultra TMB-ELISA	Pierce
TOPO-cloning kit	Invitrogen
Trypsin-EDTA	Sigma, Deisenhofen
Yeast RNA	Roche

**Restriction enzymes were purchased from Roche Molecular Diagnostics or New England Biolabs (NEB).

**Cell culture dishes and flasks purchased from Sarstedt, Falcon, Costar, or Greiner.

**Plasticware was purchased from Sarstedt, Falcon, or Eppendorf.

5.3. Cell lines

DH5α: E. coli supE44 ΔlacU169 (80 lacZΔM15) hsdR17 recA1 endA1 gyrA96, thi-1

XL 1-Blue : E.coli Tn10 pro A^+B^+ lac/^{q} Δ(lacZ)M15/recA1 endA1 gyrA96(Nal') thi hsdR17 ($r_k^- m_k^+$) glnV44 relA1 lac

COS-7: African green monkey kidney epithelial cell line (Gluzman, 1981)

SH-SY5Y: Human neuroblastoma (Ross et al., 1983)

HEK 293: Human embryonic kidney tumor, SV40-transformed

HeLa: Human epithelial adenocarcinoma cells from cervix

5.4. Antibodies

Name	Protein(Epitope)	WB	IP (ul)	IC/IH	Reference
Anti-DIG-AP	**DIG,Fab Fragments**	-	-	1:200	Roche
AP-20	**MAP2**	-	-	1:400	Sigma
Anti-PAT1a	**hAPPBP2/PAT1a (aa542-572)**	1:500 (purified)	10 20	1:50	obtained from Dr.S.Kins
22734	**hAPP695** (ectodomain)	-	5	-	obtained from Prof. G.Multhaup
40090	**hAPP695** (ectodomain)	1:8000	-	-	obtained from G. Multhaup
42464	**hAPLP1** (499-557 aa)	1:5000	-	-	(Ida et al., 1996)
42476	**hAPLP2** (608-662 aa)	1:5000	-	-	Eggert et al. 2004
CT-11	**hAPLP1** (640-650 aa)	1:10000	-	1:2000	Calbiochem
CT-12	**hAPLP2** (752-763 aa)	1:10000	-	1:2000	Calbiochem
D2-II	**hAPLP2-751**	1:10000	-	1:2000	Calbiochem
G2-10	**Aβ 40**	ELISA	5ug/ml		(Ida et al., 1996)
G2-13	**Aβ 42**	ELISA	5ug/ml		(Ida et al., 1996)
$WO_{2\text{-Biotin}}$	**Aβ** (1-16 aa)	ELISA	1ug/ml	-	(Ida et al., 1996)
22C11	**hAPP** (66-81aa)	1:10000	-	-	(Weidemann et al., 1989)
3F10	**rat αHA**	1:5000	-	1:200	Roche
9E10	**mouse αmyc**	-	-	1:100	Roche
9E10	**mouse αmyc**	-	-	1:100	Santa Cruz
IB4	**GFAP**	-	-	1:200	BD Bioscience
SDL.3D10	**β-Tubulin III**	1:1.000	-	-	Sigma
TUB 2.1	**β-Tubulin**	1:1.000	-	-	Sigma

**For Enhanced Chemical Luminescence (ECL) detection after Western blotting, appropriate Horseradish-Peroxidase (HRP) coupled anti-mouse (Promega), anti-rabbit (Promega), or anti-rat (DAKO) antibodies were used as a 1:10.000 dilution.

**For immunocytochemistry, corresponding Alexa488, Alexa568, Alexa594, or Alexa633 fluorescent dye-coupled, goat secondary antibodies were purchased from Molecular Probes and used as a 1:200 dilution.

**For Immunohistochemical stain with DAB detection, Biotinylated anti-rabbit IgG(H+L) was used at dilution 1:200.

5.5. Plasmids

pCDNA 3.1(+)-Hygro	Invitrogen
pCR II-TOPO	Invitrogen
pcDNA3.1-V5/HIS6-TOPO	Invitrogen
pSilencerTM 1.0-U6 siRNA vector	Ambion

pCEP4-APP695, -APLP1, and -APLP2-2Z constructs have been previously described (Eggert et al., 2004b) and have been kindly provided by S. Eggert. The myc-APP, APLP1-, -APLP2 constructs were kindly obtained from Dr. Peter Soba.

5.6. Generation of PAT1, and PAT1a/APPBP2 Constructs

5.6.1. Primer selection

On the bases of the human PAT1 sequence information, primers were synthesized flanking the coding region of human PAT1. All primers were synthesized by MWG Biotech.

Primire name	Sequence (5' → 3')	Description
PAT1-5'-1	GAA GGA AGA TGG CGG CCG TGG	hPAT1 mutagenesis
PAT1-3'-1	CCT CAG CAG CTC GGT CCC TCG ACA TTC TG	hPAT1 mutagenesis
PAT1 150s	GGA CGC TTA TGT CAA CTG	sequencing
PAT1 150as	CAG TTG ACA TAA GCG TCC	sequencing
PAT1 391s	CAG ATG CAG GCT GGT ACA	sequencing
PAT1 391as	TGT ACC AGC CTG CAT CTG	sequencing
PAT1 709s	CAG CAG GCT TAC CAG TGA	sequencing
PAT1 709as	TCA CTG GTA AGC CTG CTG	sequencing
PAT1 979s	TCC ACG TAG CAA CAG CTC	sequencing
PAT1 979as	GAG CTG TTG CTA CGT GGA	sequencing
PAT1 1224s	TTG CAC CTG TCT TCA CTC	sequencing
PAT1 1224as	GAG TGA AGA CAG GTG CAA	sequencing
PAT1-Sub-S1	AAT TGG TAC CGC CGC CAC CAT GGC GGC CGT GGA ACT AGA GTG	hPAT1 mutagenesis inclu. Kozak seq.
PAT1-Sub-AS2	GTA ATT GCG GCC GCT CAA GCG TCT TAG GGG ACG TCG TAT GGG TAG CAG CAC GGT CCC TCG ACA TTC TG	hPAT1 mutagenesis inclu. HA epitope.

5.6.2. Amplification of PAT1orf by Polymerase Chain Reaction(PCR)

With consideration for AD researches, accurate genetic information from human brain shall be an appropriate source, Human cDNA library obtained from Clontech was used as a template to amplify our target protein PAT1.

Reaction Mixture		End.con.	Program steps	
Template 1ng/ul	2 ul	40 pg/ul	94 ºC 2 min	
10X PCR buffer 3	5 ul	1X	94 ºC 15 sec	25X
dNTP Mix (12.5mM)	2 ul	500 uM	62 ºC 1 min	
PAT1-5'-1 (5pmol/ul)	4 ul	0.4 pmol/ul	68 ºC 2 min	
PAT1-3'-1 (5pmol/ul)	4 ul	0.4 pmol/ul	68 ºC 7 min	
2d.H_2O	32.25 ul		4 ºC ∞	
Enzyme	0.75 ul	2.5 units		

5.6.3. Generation of siPAT1a construct in *pSilencer*™

For down regulation of PAT1a, the siPAT1a inserts were generated as described in (Zhang et al., 2004) and subcloned into p*Silencer*™ 1.0-U6 siRNA Expression Vector (Ambion).

5.7. DNA methods

5.7.1. Ethanol precipitation of DNA

Solutions: 3 M Sodium acetate pH 5.2
100 % Ethanol
70 % Ethanol
TE-buffer (pH 8.0): 10 mM Tris/HCl pH 8.0
1 mM EDTA pH 8.0

1/10 Vol. of 3 M Sodium acetate, pH 5.2 and 2.5 Vol. 100 % Ethanol (-20 °C) was added to the DNA sample, mixed well, and incubated for 30 min at -20°C. The precipitated DNA was centrifuged for 20 min at 4 °C/13.000 rpm, washed with icecold 70 % Ethanol, and centrifuged for 5 min at 4 °C/13.000 rpm. The supernatant was removed, and the precipitated DNA was air-dried and diluted in TE-buffer or H_2O.

5.7.2. PCR (Polymerase chain reaction)

DNA was amplified by PCR using *Taq, Pfu*, or *High Fidelity Taq/Pwo* (Roche), as appropriate. Specific sense and antisense oligonucleotide primers flanking the desired target sequence were used.

A typical PCR reaction was prepared as follows:

10-100 ng	DNA template
1 µl	Polymerase (1 U)
5 µl	10 x reaction buffer
1 µl	10 mM dNTP (Desoxy-Nucleotide-Triphosphate)-Mix: (dATP, dTTP, dGTP, dCTP)
2 µl	sense-Primer, 10 pM
2 µl	anti-sense-Primer, 10 pM
add 50 µl	H_2O

PCR parameters were adjusted to the appropriate conditions. Generally, 25-35 cycles were used for amplification.

5.7.3. Colony PCR

Colony PCR allows screening of a large number of transformed *E. coli* colonies for positive clones before isolation from small scale cultures of these cells.

Colonies were picked with a sterile toothpick and dipped three times in 25 _l dd H_2O. To break the cell walls and release plasmid DNA, the mixture was boiled at 95°C for 5 min prior to the PCR. *Taq*-Polymerase, dNTPs, $MgCl_2$, and buffer were added, together with specific primers for the transformed plasmid. The PCR products were analyzed on an agarose gel. In parallel, small scale liquid cultures were inoculated with the colonies for isolation of plasmid DNA, and incubated on a shaker at 37° in LB-medium containing the appropriate antibiotic for selection.

5.7.4. Restriction digestion of DNA

A typical reaction was prepared as follows:

1.0 µg	DNA plasmid
3 µl	10x reaction buffer
0.5 – 1.0 µl	Restriction enzyme (5-10 U)
ad 30 µl	H_2O

The reaction was incubated at the appropriate temperature (generally 37 °C) for 1-2 h.

5.7.5. Analysis of DNA fragments on Agarose gels (Meyers et al., 1976)

Solutions:	1 x TAE buffer:
	40 mM Tris-acetate
	1 mM EDTA pH 8.0
Ethidiumbromide stock:	10 mg/ml (use 1:10.000)
6 x DNA sample buffer:	0.25 % (w/v) Bromophenol-blue
	60 % Glycerol (w/v)
	1mM EDTA pH 8.0

Depending on the size of the DNA fragments, appropriate 0.8-2 % (w/v) Agarose gels were used for separation. The Agarose was dissolved in 1xTAE buffer by boiling in a microvave oven. Ethidiumbromide was added to a final concentration of 1 µg/ml, and the solution was poured into a gel chamber. Samples supplemented with DNA sample buffer and, for comparison, a 1kb DNA ladder were loaded, and electrophoresis was performed at 100-200V.

After separation, the gels were photographed and printed with a RAYTEST IDA (Image and Documentation analysis) gel documentation device. The DNA fragments were cut out from the gel under UV light (254 nm) and transferred into an Eppendorf tube. To purify DNA fragments from agarose, the QIAquick gel extraction kit (Qiagen) was used according to the manufacturer's protocol. The DNA was eluted in 30 ul H_2O pH=8.4.

5.7.6. Ligation

A typical ligation reaction was prepared as follows:

300 ng	DNA insert fragment
30 ng	DNA vector fragment
4 µl	5x T4-DNA-Ligase buffer
1 µl	T4-DNA-Ligase
ad 20 µl	H_2O

Insert DNA was generally used in a 5-10 fold excess of vector DNA. The ligation reaction was incubated for 2-3h at 16°C.

Alternatively, the Quick Ligation kit was used according to the manufacturers protocol (NEB). The ligation reaction was then incubated for 15-30 min at room temperature.

5.7.7. Preparation of bactrial agar plates (Sambrook, 1989)

Solutions: LB-(Luria-Bertani) Medium:

0,5 % (w/v) NaCl

1% (w/v) Bacto-Tryptone

0.5 % (w/v) yeast extract

20 mM Tris/HCl pH 7.5

The pH value was adjusted to 7.0 with NaOH.

2x YT-Medium: 1% (w/v) NaCl

1.6 % (w/v) Bacto-Tryptone

1% (w/v) yeast extract

20 mM Tris/HCl pH 7.5

The pH value was adjusted to 7.0 with NaOH

Bacto-Agar

Ampicillin stock (100 mg/ml): use 1:1.000

Kanamycin stock (50 mg/ml): use 1:1.000

For agar plates, 7.5g bacto-agar was added to 500 ml LB or 2xYT medium, and autoclaved. After cooling to 60°C, the appropriate antibiotic was added to a final concentration of 100ug/ml for Ampicillin or 50ug/ml for Kanamycin, respectively. The liquid medium was poured into 10 cm culture dishes and allowed to cool to room temperature. The agar plates were stored upside down at 4°C and covered from light.

5.7.8. Chemo-competent E. coli generated with the RbCl method

RFI buffer: 100 mM RbCl

50 mM $MnCl_2$ x 4 H_2O

30 mM Potassium acetate

10 mM $CaCl_2$ x 2 H_2O

15 % Glycerol (w/v)

The pH value was adjusted to 5.8 with acidic acid. The buffer was sterile filtered, and 50 ml aliquots were stored at -20 °C.

RFII buffer: 10 mM MOPS (3-(N-Morpholino)-propanesulfonic acid)

10 mM RbCl

75 mM $CaCl_2$ x 2 H2O

15 % Glycerol (w/v)

The pH value was adjusted to 6.8 with NaOH. The buffer was sterile filtered, and 15 ml aliquots were stored at -20 °C.

SOB-Med.: 20 g Bacto-Tryptone
5 g Bacto-yeast extract
0.5 g NaCl
add 1L dd H_2O

The components were dissolved and 10 ml of a 250mM KCl solution were added. The pH value was adjusted to 7.0 with NaOH and the water was added to a final volume of 1L. Immediately before use, 5 ml of a 2M $MgCl_2$ solution were added.

SOC-medium: identical to SOB-medium; additionally, 20 ml of a 1 M sterile filtered Glucose solution were added before use.

A single colony (E. coli DH5α) was inoculated into 2 ml SOC-medium and incubated for 2h at 37°C under vigorous shaking. Afterwards, 500ul were inoculated into 50 ml SOB-medium and incubated at 37°C, until an OD (600 nm) ~0.5-0.6 was reached. The following steps were conducted at 4 °C with pre-cooled material. The culture was transferred to 50 ml Falcon tubes and incubated for 15 min at 4 °C, and centrifuged at 3000rpm/4 °C (Heraeus centrifuge) for 10min. The sedimented cells were resuspended in 17 ml RFI buffer and incubated on ice for 30min. The cells were again centrifuged at 3000rpm/4°C (Heraeus centrifuge) for 10min, resuspended in 4 ml RFII buffer, and incubated on ice for 15min. Aliquots of 200ul were transferred into Eppendorf tubes and shock frozen in liquid nitrogen. Competent DH5α were stored at -80°C.

5.7.9. Transformation of chemo-competent E. coli

LB-medium

Chemo-competent DH5α

Bacterial agar plates

Chemo-competent cells were treated according to (Hanahan, 1985). Cells were thawed on ice, and DNA (5-200ng) was added to a 100ul cell aliquot, and incubated for 15 min on ice. Cells were heat shocked for 45-60 s at 42°C, and cooled on ice for 5 min. 900ul LB medium were added and cells were incubated for 45-60min at 37°C on a roller shaker. Afterwards, different aliquots were plated on bacterial agar plates (50-500ul) and incubated over night at 37°C.

5.7.10. Liquid cultures of bacteria

LB medium

Small scale liquid cultures

A single colony was inoculated into 2-3ml LB medium supplemented with the appropriate antibiotic, and incubated over night at 37°C under vigorous shaking. The bacterial culture was used for small scale DNA preparation (Mini Prep).

Large scale liquid cultures

For large scale DNA preparation (MaxiPrep), a 1 ml pre-culture was inoculated into 200 ml LB-medium supplemented with the appropriate antibiotic, and incubated over night at 37°C under vigorous shaking.

5.7.11. Small scale DNA preparation (Mini Prep)

For small scale DNA preparation (1-5 ug), the Qiagen MiniPrep Kit was used.

Buffers were supplied by Qiagen

S1: 50 mM Tris/HCl, 10 mM EDTA, 100 µg RNase A / ml, pH 8.0

S2: 200 mM NaOH, 1% SDS

S3: 2.80 M Potassium acetate pH 5.1

70 % Ethanol

TE-buffer pH 8.0: 10 mM Tris/HCl pH 8.0, 1 mM EDTA pH 8.0

Small scale liquid cultures (1-2 ml) were transferred into an Eppendorf tube and centrifuged at 6000rpm for 5 min. Cells were resuspended in 100 ul S1 buffer and further processed according to the manufacturer's protocol.

5.7.12. Large scale DNA preparation (Maxi Prep)

For large scale DNA preparation (200-500 ug), the Qiagen Maxi Prep kit, or the Nucleobond AX-500 kit (Macherey & Nagel) were used.

S1: 50 mM Tris/HCl, 10 mM EDTA, 100 µg RNase A/ml pH 8.0

S2: 200 mM NaOH, 1% SDS

S3: 2.80 M Potassium acetate pH 5.1

N2: 100 mM Tris, 15 % Ethanol and 900 mM KCl pH 6.3

N3: 100 mM Tris, 15 % Ethanol und 1150 mM KCl pH 6.3

N5: 100 mM Tris, 15 % Ethanol und 1000 mM KCl pH 8.5

Isopropanol p.a.

3M Sodium acetate pH 5.2

100 % Ethanol p.a. (-20°C)

70 % Ethanol p.a. (-20°C)

TE-buffer pH 8.0: 10 mM Tris/HCl pH 8.0, 1 mM EDTA pH 8.0

A large scale bacterial culture was centrifuged for 10 min at 6000 rpm/4°C (Beckmann JA-2, rotor JA 10-158). Cells were resuspended in 12ml S1 buffer and further processed according to the manufacturer's protocol. For low copy plasmids, double buffer amounts were used.

Further, the DNA precipitated with Isopropanol was dissolved in 500ul H_2O and precipitated again with Ethanol as described. After centrifugation, the precipitated DNA was washed with 70% Ethanol once and centrifuged for 5 min at 13.000 rpm. The DNA pellet was air-dried and dissolved in TE-buffer or H_2O.

5.7.13. Photometric analysis of DNA concentrations

Concentrations of DNA were measured with a spectral photometer (Biorad Smart Spec 3000) at a wavelength of 260 nm. Generally, the DNA was diluted to 1:100 in H_2O for measurement.

A rule of thumb:	ssDNA or ssRNA:	A_{260nm}(1cm)= 1	c ~ 40 µg/ml
	dsDNA:	A_{260nm}(1cm)= 1	c ~ 50 µg/ml

The purity of the DNA samples was determined by measuring the A_{280nm} and A_{310nm}, which correspond to the absorption maxima of proteins and polysaccharides. For pure DNA, the A_{260nm}/A_{280nm} ratio is supposed to be between 1.8 and 2.0, with no absorption at A_{310nm}.

5.7.14. Phenol-chloroform extraction of DNA

An equivalent volume of Phenol-Chloroform-Isoamylalcohol (25:24:1) was added to a DNA solution in TE buffer or H_2O, and thoroughly vortexed for at least 1 min. The emulsion was centrifuged for 10 min at 14.000xg to achieve a separation of the phases. The aquatic, DNA containing phase on top was carefully transferred into a new Eppendorf tube. The procedure was repeated once, and the DNA was precipitated with Ethanol as described and dissolved in TE-buffer or H_2O.

5.8. Northern Analysis

Northern analysis. Blots with samples from different tissues and developmental stages obtained from human and Balb/c mice were purchased from Clontech. Experiments were performed under the User Manual

5.8.1. Probe synthesis, ^{32}P labeling and Alkaline Hydrolysis

Full-length random ^{32}P-labeled cRNA probes were synthesized by using SP6/T7 Transcription Kit (Roche) following the instruction manual. Alkaline hydrolysis was done at 65°C, 12min. this should bring the probe length ~500bp

5.8.2. Count of radioactivity on synthesized probes

Measuring the radioactivity with counter and apply ^{32}P >1x10^{6} cpm/ml to the membrand for hybridization.

5.8.3. Hybridization and Washing

*Add the 15 ml of RNA probe-containing hybridization Buffer to the hybridization tube, avoid air bubbles and cap it.

*Incubate with gentle rocking for o/n at 42°C.

5.8.4. Capture of radioactive signals

Autoradiography was done with exposing the blot to Biomax MR films (Kodak) at -70 °C for at least 20 hrs.

5.8.5. Striping and storage of MTN Blots

To reprobe the Northern blot, shake the membrane slowly in Stripping Buffer 0.1%SDS in 2XSSC for 10min at 90°C. Then, shake vigorously for 15 min at room temperature in 2 X SSC/0.1% (w/v) SDS.

5.8.6. Generation of control β-actin probe

Human β-actin orf was amplified by PCR and TA-cloning into pCRII-TOPO vector. Probe thynthesis was done by using the same kit which was used to generated the APPBP2/PAT1a cRNA probe.

5.9. *In situ* Hybridization Analysis

9-12 month-old wild type mice (C57Bl6) brain sections were prepared as described in (19). Hybridization procedures were done by reference to the published protocols (20) and performed with random DIG-labeled alkaline hydrolyzed full-length APPBP2/PAT1a cRNA probes (->500bp). Signals were visualized with alkaline phosphate system (Roche), Image acquisition was performed with Olympus BX60,

Coupled CCD camera (Olympus), and program Studio Lite (Pixera).

5.9.1. Buffers

3M Natriumacetat pH=5.2
10X PBS: 137mM NaCl, 2.7 mM KCl, 10 mM Na_2HPO_4,
2mM KH_2PO_4
50X Denhard'S: Ficol 1g, PVP 1g, BSA Fraction 1g
in 10ml ddH_2O
20XSSC: 3M NaCl, 0.3M Na-citrate
1M Levamisol
0.1M TEA
10% Triton X-100
Buffer 1: 100mM Tris-HCl pH=7.5, 150mM NaCl
Buffer 2: 100mM Tris-HCl pH=9.5, 100mM NaCl
Buffer 3: 10mM Tris-HCl pH=8.1, 1mM EDTA

5.9.2. Transcadiac perfusion for tissue fixation

9-12 month-old wild type mice (C57Bl6) were anesthetized with 0.1 ml Pentobarbital Sodium sol. and transcaeiac perfused with 300ml 1XPBS, 300ml ice-cold 4%PFA, using 23G needle and perfusion pump set speed15ml/min.

5.9.3. Brain removal and Paraffin embedding

4% PFA fixed mice brains were removed and proceeded to post-fixation at 4°C for 4 hr with shaking. Paraffin embedding were done with HypercenterXP embedding machine and follwing the intruction manual.

5.9.4. Sectioning, De-wax and Rehydration

Sections were cut in 7um thickness and place onto PLL coted glass slides. Dry slide in an oven 52°C overnight. Dewaxed with fresh Xylene 2X 10 min at RT. Rehydrated as following:

100% EtOH 5min
95% EtOH 5min
70% EtOH 5min
50% EtOH 5min
1XPBS 5min x 2

5.9.5. Probe synthesis, DIG labeling and Alkaline Hydrolysis

Probes were thynesized by DIG- RNA labeling kit (Roche) following the instruction manual. Alkaline hydrolysis was done at 65°C, 12 min, and stopped by adding 1/20 0.5mM EDTA.

5.9.6. Measurement of DIG amount on synthesized probes

Measurement of DIG amount along with the synthesized cRNA probes was performed by using CSPD kit as following the instruction manual.

5.9.7. Section pretreatments and Hybridization Procedures

Continuing the 5.9.6. and proceeding as following:

post fixation with 4%PFA 10min RT

Wash with 1X PBS 5min x 3

0.1M HCl 10 min

wash with 1X PBS min x 3

Proteinase K (10ug/ml) treatment at 37°C, 10 min

Wash with 1X PBS 5 min x 3

0.1M TEA 45ml + 750 acetic anhydride 20min

Wash with 1X PBS 5min x 3

Calculate dilution factors by CSPD measurement result and dilute the cRNA probes in hybridization buffer

Denature at 85°C 10 min

hybridization at 42°C overnight

5.9.8. Detection of DIG signals

wash with Buffer 1 5min x 3

Incubate with blocking sol.(buffer1+ 5% NSS) 30 min, RT

Wash with Buffer 1 5min x 3

Incubate with anti-Dig 1:200 in buffer 1 + 2% NSS, 1 hr RT

Wash with Buffer 1 5 min x 3

Incubate with Buffer 2 10 min RT

Incubate with detection sol. (20 ul NBT/BCIP in 5ml Buffer2),

-optimalzed by individual experiment

Stopped with Buffer 3

Wash with dd H_2O 5min x 3

5.9.9. Mount sections and Image Acquisition

Sections were mounted with Mowil sol. and proper size coverslips. Image acquisition was performed with Olympus BX60, Coupled CCD camera (Olympus), and program Studio Lite (Pixera).

5.10. Generation of polyclone rabbit anti-PAT1a/APPBP2 antibodies

5.10.1. Selection of sequence-specific residue on APPBP2/PAT1a

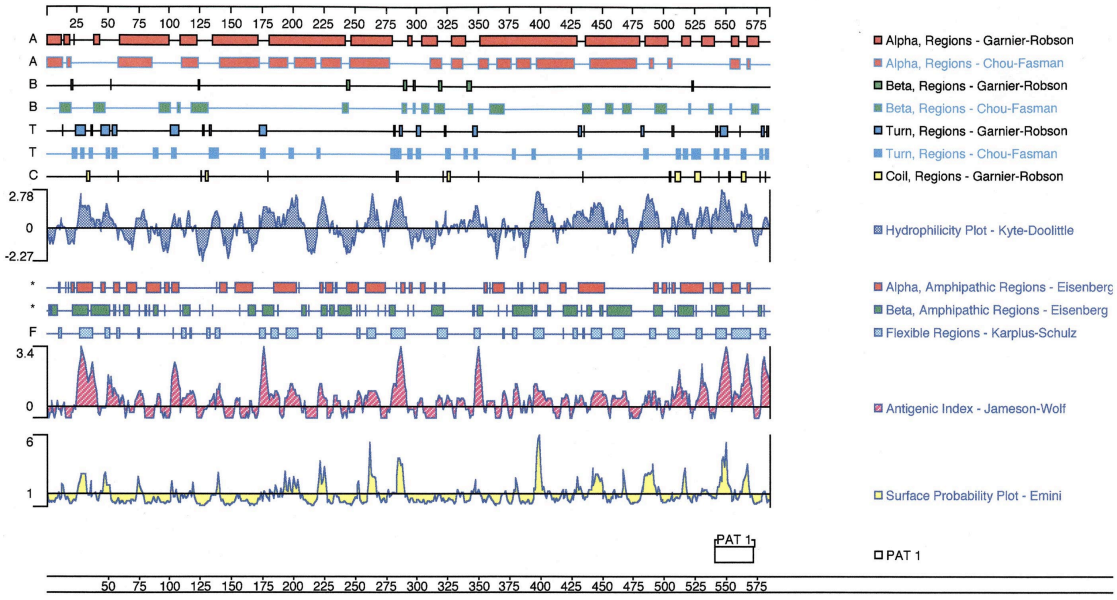

5.10.2. Peptide synthesis

Selected sequence: Anti-PAT1ct: at position 541-573,

-CKWNRLRDRQYSVTDALEDVSTSPQSTEEVVQ-

The peptide was synthesized by Peptide Speciality Laboratories GmbH

Coupled peptide with KLH was done by using KLH coupling kit (Pierce)

5.10.3 Immunorization

Injection of the anti-PAT1a peptide was performed by animal facillity of ZMBH, every 2 weeks.

5.10.4. Anti-Serum collection

Following 7 days after every injections, 15 ml anti-serum were collected and centrifuged at 5000 rpm, 4°C, 15 min. The upper phase (serum) were collected and aliqued 0.5 ml for long term storage.

5.10.5. Affinity screen by BIACore Surface Plasmon Resonance (SPR)

Surface plasmon resonance is a phenomenon which occurs when light is reflected off thin metal films. A fraction of the light energy incident at a sharply defined angle can interact with the delocalised electrons in the metal film (plasmon) thus reducing the reflected light intensity. The precise angle of incidence at which this occurs is determined by a number of factors, but in the Pharmacia BIA devices the principal

determinant becomes the refractive index close to the *backside* of the metal film, to which target molecules are immobilised and addressed by ligands in a mobile phase running along a flow cell. If binding occurs to the immobilised target the local refractive index changes, leading to a change in SPR angle, which can be monitored in real-time by detecting changes in the intensity of the reflected light, producing a sensorgram. The rates of change of the SPR signal can be analysed to yield apparent rate constants for the association and dissociation phases of the reaction. The ratio of these values gives the apparent equilibrium constant (affinity). The size of the change in SPR signal is directly proportional to the mass being immobilised and can thus be interpreted crudely in terms of the stoichiometry of the interaction. Signals are easily obtained from sub-microgram quantities of material. Since the SPR signal depends only on binding to the immobilised template, it is also possible to study binding events from molecules in extracts; i.e. it is not necessary to have highly purified components.

Surface plasmon resonance detection unit. L: light source, D: photodiode array, P: prism, S: sensor surface, F: flow cell. The two dark lines in the reflected beam projected on to the detector symbolise the light intensity drop following the resonance phenomenon at time = t1 and t2. The line projected at t1 corresponds to the situation before binding of antigens to the antibodies on the surface and t2 is the position of resonance after binding.

5.11. Cell Cultures and Transfections

5.11.1. Preparation of culture mediums

COS-7 & Hela: 10% FCS in DMEM+ 1%P/S

SH-SY5Y: F12 250ml+MEM 250ml+L-Glutamine 6ml+P/S 6ml
+Non.Essential aa. 6ml+10%FCS+1&P/S

HEK293: 10%FCS+0.1%Non-Essential aa.+1%P/S in DMEM

5.11.2. Maintainace of cell lines

Freezing of cells for long term storage

Freezing medium: 10 % (v/v) DMSO in growth medium with 20 % FCS and w/o antibiotics

Cells at 70-90 % confluency were used for freezing. Cells from a 10 cm dish were trypsinized as described and transferred into 15 ml tubes with 10 ml of fresh medium. The cells were sedimented at 300x g for 5 min and resuspended in 3-4.5 ml freezing medium. 1.5ml aliquots were transferred into cryovials (Nunc), and incubated on ice for 1-1.5 h. The vials were then stored at -80 °C over night, and then transferred into a liquid nitrogen tank for long term storage.

Alternatively, vials were directly incubated in a cryobox (Nunc) containing Isopropanol at 80°C over night, and afterwards transferred into a liquid nitrogen tank as well.

Thawing of frozen cells

Cells frozen in liquid nitrogen were quickly thawed at 37 °C in a water bath. Cells were then transferred into a 10 cm dish with 10 ml fresh growth medium and equally distributed with gentle shaking. The medium was replaced the next day to remove residual DMSO.

Alternatively, thawed cells were transferred into 15 ml tubes with 10 ml of fresh medium and centrifuged at 300x g for 5 min. The cells were resuspended in 5 ml normal growth medium, and transferred to 10 cm culture dishes with 10 ml of fresh growth medium. Cells were further cultured as described.

5.11.3. Transfection methods used in this study

Transfection of COS-7, HEK293 and HeLa cells with Lipofectamine Plus

OptiMEM (Invitrogen)

Lipofectamine Plus (Invitrogen)

Fatal calf serum (FCS)

Generally, 6cm dishes with cells at 80-90 % confluency were transfected. In an Eppendorf tube, 2ug DNA were mixed with 250 ul OptiMEM and 15ul Plus reagent. After 15 min incubation, 5µl Lipofectamine in 250ul OptiMEM were added, inverted several times, and incubated for 15min.

Cells were washed with OptiMEM once and 2 ml OptiMEM were added. The Lipofectamine/DNA mixture was added dropwise to the cells and incubated for 3-4 h at 37°C and 5 % CO_2. Afterwards, the reagent was removed and fresh normal growth serum was added. After 24h, the cells were either harvested for analysis or passaged and selected for stable expression. For this purpose, the growth medium was supplemented either with 500 µg/ml G418 or 250 µg/ml Hygromycin, depending on the transfected plasmid. The cells were further cultivated as described.

Transfection of SH-SY5Y cells with FuGene 6

OptiMEM (Invitrogen)

Lipofectamine (Invitrogen)

Plus-reagent (Invitrogen)

In an Eppendorf tube, 5ug DNA were mixed with 750ul OptiMEM and 20ul Plus –reagent. After 15min incubation, 30ul FuGene6 in 750ul OptiMEM were added, inverted several times, and incubated for 15min. A 10cm dish with SH-SY5Y cells at 70-80 % confluency was washed with 1x PBS twice and 5 ml OptiMEM were added. The FuGene6/DNA mixture was added dropwise to the cells and incubated for 3h at 37°C and 5 % CO_2. Afterwards, 5ml OptiMEM and FCS to a final concentration of 10% were added. The next day, appropriate growth medium containing either 500 µg/ml G418 or 250 µg/ml Hygromycin, depending on the transfected plasmid, was added to select transfected cells for stable expression. The cells were further cultivated as described.

5.12. Western Analysis

5.12.1. Collection of cell and tissue lysates

Cell lysis

1x PBS

Lysis buffer: 50 mM Tris pH 7.4

150 mM NaCl

2 mM EDTA

1 % NP-40

Complete Protease Inhibitor Mix (Roche)

2x SDS sample buffer

Cells were washed once with cold PBS, scraped in 500 ul 1x PBS, and transferred into an Eppendorf tube. Residual cells in the dish were scraped again in 500 ul 1x PBS, and transferred into the same tube. Cells were centrifuged at 300x g for 5 min, the PBS was removed, and an appropriate amount (50-500 ul) of cell lysis buffer supplemented with Complete Protease Inhibitors was added. Cells were resuspended in the lysis buffer and incubated for 20 min on ice. The lysate was cleared from debris and nuclei by centrifugation at 16.000x g for 10 min. The

supernatant was used immediately for immunoprecipitation, or denatured with the appropriate amount of 2x SDS sample buffer. Alternatively, cell lysates were stored at -80°C for later use.

5.12.2. Measurement of protein concentration

BioRad *DC* protein assay (Biorad)

Bicinchoninic acid (BCA) (Sigma)

4% $CuSO_4$ solution (Sigma)

BSA (Bovine Serum Albumin) standard solutions (0, 0.1, 0.2, 0.3, 0.4, 0.5, 0.6, 0.8, 1.0 mg/ml).

ELISA 96-well plate (Greiner)

The protein concentration of lysate supernatants was determined using the BioRad *DC* protein assay (Biorad) or a BCA assay (Sigma) according to the manufacturer´s protocol.

The BioRad *DC* protein assay is based on a Lowry assay (Lowry et al., 1951), where proteins react with an alkaline copper tartrate solution and reduce the added folin reagent. The reduced folin species have a characteristic blue color with an absorption maximum of 750 nm.

The BCA assay is based on a quantitatively catalyzed reaction of the BCA-Cu^{2+}-complex to the reduced BCA-Cu^{+}-complex, which is accompanied by a color change with an absorption maximum at 550 nm.

For the BCA assay, 20ul of each BSA standard solution and cell lysate (1:10 dilution) were pippeted into the ELISA plate in triplicates. The 4 % $CuSO_4$ solution was diluted 1:40 with the BCA solution, and 200ul of the mixture were added to the standards and lysates. The plate was incubated for 15 min at 37°C, and further 15 min at room temperature on a horizontal shaker.

Absorption was measured with a microplate-reader (BIO-RAD, model 450) at 550 nm, and protein concentrations were calculated with the BSA standard curve.

5.12.3. Preparation of SDS-PAGE

Discontinous SDS-Polyacrylamide gel electrophoresis (SDS-PAGE)

Tris-Tricine gels were prepared according to (Laemmli, 1970).

Buffers: 30 % (w/v) Acrylamide; 0.8 % (w/v) Bisacrylamide (Protogel)

separation gel buffer: 2 M Tris/HCl, pH 8.8

Stacking gel buffer: 1 M Tris/HCl, pH 6.8

20 % (w/v) SDS (Sodium dodecylsulfate)

10 % (w/v) APS (Ammoniumperoxodisulfate)

TMEDA

1 x running buffer: 25 mM Tris-base, 192 mM Glycine, 0.1 % SDS

Separating gel:

Gel percentage	**Protogel (ml)**	**2 M Tris, pH 8.8 (ml)**	**20 % SDS (ml)**	**ddH_2O (ml)**	**10 % APS (ml)**	**TMEDA (ml)**	**Final volume (ml)**
15 %	15	5.6	0.15	9.1	0.1	0.02	30
8 %	8	5.6	0.15	16.1	0.1	0.02	30

Stacking gel:

Protogel (ml)	**1 M Tris, pH 6.8 (ml)**	**20 % SDS (ml)**	**ddH_2O (ml)**	**10 % APS (ml)**	**TMEDA (ml)**	**Final volume (ml)**
1.67	1.25	0.05	7.00	0.05	0.015	10.035

Elektrophoresis was performed over night at 70-90 V.

Precut glass plates (20 x 20 cm) were assembled with Teflon spacers (1 mm) and a silicon tube and used for casting the gel.

Tris-Tricine-PAGE

Tris-Tricine gels were prepared according to (Schagger and von Jagow, 1987).

Cathode buffer: 0.1 M Tris, 0.1 M Tricin, 0.1% SDS

Anode buffer: 0.2 M Tris/HCl pH 8.9

Gel buffer: 3 M Tris, 0.3 % SDS, pH 8.45

	Stacking gel 4% T 3 % C	**Separating gel 10 % T 3 %C**	**Separating gel 16.5 % T 3 % C**	**Separating gel 16.5 % T 6 % C**
49,5 % T solution 3 % C solution	1 ml	6.1 ml	10 ml	-
49,5 % T solution 6 % C solution	-	-	-	10 ml
Gel buffer	3.1 ml	10 ml	10 ml	10 ml
Glycerol	-	4 g	4 g	4 g
ad H_2O	12.5 ml	30 ml	30 ml	30 ml
10 % (w/v) APS	150 µl	150 µl	150 µl	150 µl
TMEDA	20 µl	20 µl	20 µl	20 µl

[T = Acrylamide; C = Bisacrylamide]

Alternatively, for separation of small molecular weight proteins, precast 10-20 % Tris-Tricine gels (Invitrogen) were run with 1x cathode buffer for 90 min at 140 V.

Bis-Tris-HCl polyacrylamide gel electrophoresis

Separation of proteins by electrophoresis was also carried out using precast 4-12 % Bis-Tris gels (Invitrogen).

20 x MES buffer: 1 M MES, 1 M Tris base, 69.3 mM SDS, 20.5 mM EDTA

20x MOPS buffer: 1 M MOPS, 1 M Tris base, 69.3 mM SDS, 20.5mM EDTA.

Depending on the molecular weight of the protein of interest, 1x MOPS (50-100 kDa) or 1x MES (10-50 kDa) running buffer were used due to different separation properties.

5.12.4. Transfer of proteins on to Nitrocellulose Membrane

Proteins separated by SDS-PAGE were transferred from the gel to a nitrocellulose membrane by electrophoresis (Western blotting).

Cathode buffer: 25 mM Tris base, 40 mM 6-Aminohexane acid, 20 % Methanol

Anode buffer I: 30 mM Tris base, 20 % Methanol

Anoden buffer II: 300 mM Tris base, 20 % Methanol

Nine sheets of Whatman paper were cut according to the gel size and three sheets were soaked with each buffer. A nitrocellulose membrane was also presoaked in Anode I buffer. The blot was assembled on a semi-dry apperature as follows:

Cathode (-)

3 Whatman sheets soaked with cathode buffer

SDS gel

Nitrocellulose soaked with Anode I buffer

3 Whatman sheets soaked with anode I buffer

3 Whatman sheets soaked with anode II buffer

Anode (+)

The proteins were blotted for 1-1.5 h at 1 mA/cm^2.

5.12.5. Western blotting (wet blot)

Transfer buffer: 192 mM Glycin, 25 mM Tris-Base, 20 % Methanol

Following SDS-PAGE, the gel was equilibrated in transfer buffer for 5 min. Whatman sheets and a nitrocellulose membrane were cut to the size of the gel and soaked in

transfer buffer. The gel and the membrane were sandwiched between soaked pieces of sponge pads, Whatman paper, and perforated plastic plates as follows:

Anode (+)

Sponge pad

2 Whatman sheets

Nitrocellulose

SDS gel

2 Whatman sheets

Sponge pad

Cathode (-)

The transfer was performed in a blotting tank (Biorad) for 1-3 h at 380 mA at 4°C.

5.12.6. Signal detection by Enhanced Chemo-lumicent system

10x PBS

10x TBST (Tris buffered saline Tween): 100 mM Tris/HCl

1.5 M NaCl

0.5 % Tween 20

ECL-Kit (Amersham)

After western blot transfer of the proteins to the nitrocellulose membrane, the membrane was blocked for 1 h in 1x TBST/5 % (w/v) skimmed milk. The primary antibody was diluted in 1x TBST to an appropriate concentration and the blot was incubated either for 2-4 h at room temperature or overnight at 4 °C. The membrane was washed twice with 1x TBST, and further incubated two times in 1x TBST for 10 min. Incubation of the blot with the secondary antibody conjugated to horseradish peroxidase (HRP, dilution 1:10.000) was carried out for 1 h at room temperature. The membrane was again washed twice with 1x TBST, and further incubated two times in 1x TBST for 10 min. The protein of interest was detected by enhanced chemical luminescence (ECL) utilizing the reaction of Luminol and H_2O_2, which is catalyzed by HRP. For this purpose, the membrane was incubated with the ECL (Amersham) reagent for 1 min and the chemifluorescent signal was visualized by exposure of Hyperfilm ECL (Amersham) films.

5.12.7. Reprobing of Western blot membranes

Stripping buffer: 62.5 mM Tris/HCl pH 6.7

100 mM β-Mercaptoethanol

2 % SDS

For reprobing the membrane with different antibodies, the previously applied antibodies had to be removed first. For this purpose, stripping buffer was preheated to 80 °C. The membrane was incubated with 100-200 ml preheated stripping buffer on a horizontal shaker until room temperature was reached (30-45 min). The membrane was further incubated several times with 1x TBST, until no residual β-Mercaptoethanol could be detected (3-5 times). The blot was again blocked in 1x TBST/5 % (w/v) skimmed milk for 1 h, and a new primary antibody could be applied as described.

5.13. Immunohistochemical Stain

Brains from 9 to 12-month-old wild-type (C57Bl6) and APLP1-/- mice were used. Animals were prepared the same as described in (19). After the post fixation, paraffin sections were treated with Antigen Unmasking Solution (Vector Laboratories). Neurons were fixed with 4% PFA and permeabilized with 0.1%NP-40/PBS. The staining was performed using the published procedures (22). For DAB detection, StreptABComplex/HRP kit (DAKO Diagnostic) was used. Image acquisition of DAB signals were performed the same as described in the ISH. The fluorescent signals were visualized with the Axiovert 200M Inverted Microscope (Zeiss), supplied with CCD Camera (Hamamatsu) and images were acquired and enhanced using the MetaMorph Imaging System (Universal Imaging Co.).

5.14. Culture and transfection of Mouse embryonic cortical neurons

5.14.1. Preparation of culture mediums

Neurobasal+Glutamate culture medium: neurobasal medium 200 ml, B-27 supplement 4 ml, 200mM L-Glutamin 500 ul, 25 mM Glumate 200 ul

Neurobasal-Glutamate culture medium: neurobasal medium 200 ml, B-27 supplement 4 ml, 200mM L-Glutamin 500 ul

10X HBSS

5.14.2. Animal and tissue preparation

Mouse was anesthetized with overdosed CO_2, then E14 brain were removed and placed in 10cm-dish with proper amount of 1X HBSS. Isolated embryonic cortexs were trypsinized at 37°C 15 min. Wash with 1X HBSS 5 times, plate into desired sized dishes, cultured with Neurobasal+Glutamate culture medium.

5.14.3. Transfection procedures

Thansfection of primary neurons in this study were all done by using Lipofectamine2000 and following with the instruction manual.

5.15. Immunocytochemical Stain

5.15.1. Fixation of cells

Cells expressing APPBP2/PAT1a-HA or co-expressing with APP family proteins, myc-APP, APLP1-myc, and myc-APLP2, were grown on cover slips, harvested and fixed with 4% Paraformaldehyde in 1xPBS for 10-30 min.

5.15.2. Staining procedures

Cells were permeabilized in 1x PBS + 0.1% Triton X-100 for 15 min and blocked with 5% normal goat serum in 1x PBS for 1h. Incubation with primary antibody over night at 4°C. The next day, cells were incubated with the appropriate secondary antibodies coupled to Alexa 488 and Alexa 594 fluorescent dyes (Molecular Probes) for 1h at room temperature, and mounted in Mowiol. Omission of primary antibodies was used as a control to verify specificity and showed only very low background staining.

5.15.3. Signal Visualization and Image acquisition

The fluorescent signals were visualized with the Axiovert 200M Inverted Microscope (Zeiss) supplied with CCD Camera (Hamamatsu), and images were acquired and enhanced using the MetaMorph Imaging System (Universal Imaging Co.).

5.16. Immunoprecipitation and Co-Immunoprecipitation

5.16.1. Buffer preparation

Washing buffer A (Wash A): 10 mM Tris/ HCl pH 7.5

150 mM NaCl

5mM EDTA

0.2 % NP40

Washing buffer B (Wash B): like Wash A, but with 500 mM NaCl instead

Washing buffer C (Wash C): 10 mM Tris/HCl pH 7.5

2x SDS sample buffer

5.16.2. Coupling antibodies to Agarose beads

Coupling of anti-PAT1a antibody to sepharose beads by using ProFund co-Immunoprecipitation Kit (Pierce) were done with following the instruction manual.

5.16.3. Procedures

Protein A sepharose (Amersham) as a 50 % slurry in Wash A, 0.02% NaN_3

If not stated otherwise, proteins from brain or cell lysates were precipitated with appropriate antibodies and 30 ul ProteinA beads. Medium aliquots were cleared from cell debris by centrifugation at 15000xg for 10min. Protein lysates (minimum sample volume was 500ul) were generally preincubated for 1h at 4°C with 10ul of ProteinA sepharose to reduce unspecific binding. Equally, antibodies were prebound to 30ul of ProteinA sepharose in 500ul Wash A by incubating on an overhead shaker for 1h at room temperature. The sepharose beads were sedimented at 15000xg for 30s, and the cell lysate supernatant was transferred to the prebound antibody beads. The samples were incubated for 23 h at room temperature, or over night at4 °C. The sepharose beads were centrifuged at 15000xg for 30s, and washed three times with Wash A buffer. In case of unspecific binding, additional washing steps with Wash B and Wash C were performed. The buffer was completely removed with a Hamilton syringe, and the Sepharose beads were denatured in 2x SDS sample buffer for 10min at 95°C. The samples were further analyzed by SDS-PAGE and Western blotting.

5.17. ELISA

5.17.1 Buffers

Carbonate Buffer: 25 mM Na_2CO_3, 75 mM $NaHCO_3$ in 1000 dd H_2O

10X Wash Buffer: 9.5 mM $NaH_2PO_4xH_2O$, 6.8 mM $Na_2HPO_4x2H_20$, 137 mM NaCl, 1% (v/v) Tween 20 in 1000 ml dd H_2O

10X PBS (80mM): 9.5 mM $NaH_2PO_4xH_2O$, 6.8 mM $Na_2HPO_4x2H_20$, 137 mM NaCl

Liquor Buffer: 1.5 % BSA, 0.5% Tween 20, 100ml 80 mM PBS

HRP Buffer: 0.1% BAS, 0.1%(v/v) Tween 20 in 100 ml 80 mM PBS

Stop solution: 1M H_2SO_4

5.17.2. Procedures

Coating capturing antibodies:

G2-10 85ug/ml), G2-13 (5ug/ml) in 110ul Carbonate Buffer/well

Incubate at 37°C 2hr

Wash with wash buffer 5min x 3

Blocking with StabilCoat (SurModics) 110ul/well Rt 2hr

Wash with wash buffer 5min x 3

Preparing reaction mixture:

WO_2-Biotin 1:1000 in 50 ul Liquor buffer+

10% Sea-Blocking buffer(Pierce) / well

50 ul sample (for Aβ 40 1:5 diluted, for standard

1:10 diluted) / well

Incubate at 4 °C 48 hr

Wash with 250 ul wash buffer 5min x3(equ. HRP buffer and TMB to RT)

Mix 1.2ul SA-Poly-HRP(Amersham) in 12 ml HRP buffer

Apply 100ul / well and incubate at RT 30 min

Wash with wash buffer 5min x 3

Wash with wash buffer 5 min x 3

Detection with TMB-substration buffer (Pierce), 100ul / well

Optimize by individual, when color appears

Stop the reaction with 1M H_2SO_4 50 ul / well

Measureing with Multiskan(Thermo MultiScan) by instruction

6. References

Aksenova, M. V., Aksenov, M. Y., Butterfield, D. A., and Carney, J. M. (1996). alpha-1-antichymotrypsin interaction with A beta (1-40) inhibits fibril formation but does not affect the peptide toxicity. Neurosci Lett **211**, 45-48.

Alber, T. (1992). Structure of the leucine zipper. Curr Opin Genet Dev **2**, 205-210.

Allinquant, B., Hantraye, P., Mailleux, P., Moya, K., Bouillot, C., and Prochiantz, A. (1995). Downregulation of amyloid precursor protein inhibits neurite outgrowth in vitro. J Cell Biol **128**, 919-927.

Amaratunga, A., Leeman, S. E., Kosik, K. S., and Fine, R. E. (1995). Inhibition of kinesin synthesis in vivo inhibits the rapid transport of representative proteins for three transport vesicle classes into the axon. J Neurochem **64**, 2374-2376.

Ando, K., Iijima, K. I., Elliott, J. I., Kirino, Y., and Suzuki, T. (2001). Phosphorylation-dependent regulation of the interaction of amyloid precursor protein with Fe65 affects the production of beta-amyloid. J Biol Chem **276**, 40353-40361.

Annaert, W., and De Strooper, B. (2002). A cell biological perspective on Alzheimer's disease. Annu Rev Cell Dev Biol **18**, 25-51.

Baek, S. H., Ohgi, K. A., Rose, D. W., Koo, E. H., Glass, C. K., and Rosenfeld, M. G. (2002). Exchange of N-CoR corepressor and Tip60 coactivator complexes links gene expression by NF-kappaB and beta-amyloid precursor protein. Cell **110**, 55-67.

Barnham, K. J., McKinstry, W. J., Multhaup, G., Galatis, D., Morton, C. J., Curtain, C. C., Williamson, N. A., White, A. R., Hinds, M. G., Norton, R. S., et al. (2003). Structure of the Alzheimer's disease amyloid precursor protein copper binding domain. A regulator of neuronal copper homeostasis. J Biol Chem **278**, 17401-17407.

Bayer, T. A., Cappai, R., Masters, C. L., Beyreuther, K., and Multhaup, G. (1999). It all sticks together--the APP-related family of proteins and Alzheimer's disease. Mol Psychiatry **4**, 524-528.

Beher, D., Elle, C., Underwood, J., Davis, J. B., Ward, R., Karran, E., Masters, C. L., Beyreuther, K., and Multhaup, G. (1999). Proteolytic fragments of Alzheimer's disease-associated presenilin 1 are present in synaptic organelles and growth cone membranes of rat brain. J Neurochem **72**, 1564-1573.

Beher, D., Hesse, L., Masters, C. L., and Multhaup, G. (1996). Regulation of amyloid protein precursor (APP) binding to collagen and mapping of the binding sites on APP and collagen type I. J Biol Chem **271**, 1613-1620.

Borg, J. P., Ooi, J., Levy, E., and Margolis, B. (1996). The phosphotyrosine interaction domains of X11 and FE65 bind to distinct sites on the YENPTY motif of amyloid precursor protein. Mol Cell Biol **16**, 6229-6241.

Borg, J. P., Yang, Y., De Taddeo-Borg, M., Margolis, B., and Turner, R. S. (1998). The X11alpha protein slows cellular amyloid precursor protein processing and reduces Abeta40 and Abeta42 secretion. J Biol Chem **273**, 14761-14766.

Brady, S. T. (1985). A novel brain ATPase with properties expected for the fast axonal transport motor. Nature **317**, 73-75.

Breen, K. C., Bruce, M., and Anderton, B. H. (1991). Beta amyloid precursor protein mediates neuronal cell-cell and cell-surface adhesion. J Neurosci Res **28**, 90-100.

Brown, M. S., Ye, J., Rawson, R. B., and Goldstein, J. L. (2000). Regulated intramembrane proteolysis: a control mechanism conserved from bacteria to humans. Cell **100**, 391-398.

Bush, A. I., Pettingell, W. H., Jr., de Paradis, M., Tanzi, R. E., and Wasco, W. (1994). The amyloid beta-protein precursor and its mammalian homologues. Evidence for a zinc-modulated heparin-binding superfamily. J Biol Chem **269**, 26618-26621.

Buxbaum, J. D., Liu, K. N., Luo, Y., Slack, J. L., Stocking, K. L., Peschon, J. J., Johnson, R. S., Castner, B. J., Cerretti, D. P., and Black, R. A. (1998). Evidence that tumor necrosis factor alpha converting enzyme is involved in regulated alpha-secretase cleavage of the Alzheimer amyloid protein precursor. J Biol Chem **273**, 27765-27767.

Caceres, J., and Brandan, E. (1997). Interaction between Alzheimer's disease beta A4 precursor protein (APP) and the extracellular matrix: evidence for the participation of heparan sulfate proteoglycans. J Cell Biochem **65**, 145-158.

Caille, I., Allinquant, B., Dupont, E., Bouillot, C., Langer, A., Muller, U., and Prochiantz, A. (2004). Soluble form of amyloid precursor protein regulates proliferation of progenitors in the adult subventricular zone. Development **131**, 2173-2181.

Cao, X., and Sudhof, T. C. (2001). A transcriptionally [correction of transcriptively] active complex of APP with Fe65 and histone acetyltransferase Tip60. Science **293**, 115-120.

Cao, X., and Sudhof, T. C. (2004). Dissection of amyloid-beta precursor protein-dependent transcriptional transactivation. J Biol Chem **279**, 24601-24611.

Capell, A., Kaether, C., Edbauer, D., Shirotani, K., Merkl, S., Steiner, H., and Haass, C. (2003). Nicastrin interacts with gamma-secretase complex components via the N-terminal part of its transmembrane domain. J Biol Chem **278**, 52519-52523.

Chartier-Harlin, M. C., Araria-Goumidi, L., and Lambert, J. C. (2004). [Genetic complexity of Alzheimer's disease]. Rev Neurol (Paris) **160**, 251-255.

Clarris, H. J., Cappai, R., Heffernan, D., Beyreuther, K., Masters, C. L., and Small, D. H. (1997). Identification of heparin-binding domains in the amyloid precursor protein of Alzheimer's disease by deletion mutagenesis and peptide mapping. J Neurochem **68**, 1164-1172.

Coulson, E. J., Paliga, K., Beyreuther, K., and Masters, C. L. (2000). What the evolution of the amyloid protein precursor supergene family tells us about its function. Neurochem Int **36**, 175-184.

Crain, B. J., Hu, W., Sze, C. I., Slunt, H. H., Koo, E. H., Price, D. L., Thinakaran, G., and Sisodia, S. S. (1996). Expression and distribution of amyloid precursor protein-like protein-2 in Alzheimer's disease and in normal brain. Am J Pathol **149**, 1087-1095.

Cras, P., Kawai, M., Lowery, D., Gonzalez-DeWhitt, P., Greenberg, B., and Perry, G. (1991). Senile plaque neurites in Alzheimer disease accumulate amyloid precursor protein. Proc Natl Acad Sci U S A 88, 7552-7556.

De Strooper, B. (2003). Aph-1, Pen-2, and Nicastrin with Presenilin generate an active gamma-Secretase complex. Neuron **38**, 9-12.

De Strooper, B., and Annaert, W. (2000). Proteolytic processing and cell biological functions of the amyloid precursor protein. J Cell Sci **113** (Pt 11), 1857-1870.

De Strooper, B., Craessaerts, K., Dewachter, I., Moechars, D., Greenberg, B., Van Leuven, F., and Van den Berghe, H. (1995). Basolateral secretion of amyloid precursor protein in Madin-Darby canine kidney cells is disturbed by alterations of intracellular pH and by introducing a mutation associated with familial Alzheimer's disease. J Biol Chem **270**, 4058-4065.

Dewachter, I., and Van Leuven, F. (2002). Secretases as targets for the treatment of

Alzheimer's disease: the prospects. Lancet Neurol **1**, 409-416.

Dotti, C. G., and Simons, K. (1990). Polarized sorting of viral glycoproteins to the axon and dendrites of hippocampal neurons in culture. Cell **62**, 63-72.

Duilio, A., Faraonio, R., Minopoli, G., Zambrano, N., and Russo, T. (1998). Fe65L2: a new member of the Fe65 protein family interacting with the intracellular domain of the Alzheimer's beta-amyloid precursor protein. Biochem J 330 **(Pt 1)**, 513-519.

Edbauer, D., Winkler, E., Regula, J. T., Pesold, B., Steiner, H., and Haass, C. (2003). Reconstitution of gamma-secretase activity. Nat Cell Biol **5**, 486-488.

Eggert, S., Paliga, K., Soba, P., Evin, G., Masters, C. L., Weidemann, A., and Beyreuther, K. (2004). The proteolytic processing of the amyloid precursor protein gene family members APLP-1 and APLP-2 involves alpha-, beta-, gamma-, and epsilon-like cleavages: modulation of APLP-1 processing by n-glycosylation. J Biol Chem **279**, 18146-18156.

Ferreira, A., Caceres, A., and Kosik, K. S. (1993). Intraneuronal compartments of the amyloid precursor protein. J Neurosci **13**, 3112-3123.

Fiore, F., Zambrano, N., Minopoli, G., Donini, V., Duilio, A., and Russo, T. (1995). The regions of the Fe65 protein homologous to the phosphotyrosine interaction/phosphotyrosine binding domain of Shc bind the intracellular domain of the Alzheimer's amyloid precursor protein. J Biol Chem **270**, 30853-30856.

Fortini, M. E. (2002). Gamma-secretase-mediated proteolysis in cell-surface-receptor signalling. Nat Rev Mol Cell Biol **3**, 673-684.

Gao, Y., and Pimplikar, S. W. (2001). The gamma -secretase-cleaved C-terminal fragment of amyloid precursor protein mediates signaling to the nucleus. Proc Natl Acad Sci U S A **98**, 14979-14984.

Gindhart, J. G., Jr., and Goldstein, L. S. (1996). Tetratrico peptide repeats are present in the kinesin light chain. Trends Biochem Sci **21**, 52-53.

Glenner, G. G., and Wong, C. W. (1984). Alzheimer's disease: initial report of the purification and characterization of a novel cerebrovascular amyloid protein. Biochem Biophys Res Commun **120**, 885-890.

Goldstein, L. S., and Philp, A. V. (1999). The road less traveled: emerging principles of kinesin motor utilization. Annu Rev Cell Dev Biol **15**, 141-183.

Goldstein, L. S., and Yang, Z. (2000). Microtubule-based transport systems in neurons: the roles of kinesins and dyneins. Annu Rev Neurosci **23**, 39-71.

Gotz, J. (2001). Tau and transgenic animal models. Brain Res Brain Res Rev **35**, 266-286.

Grziwa, B., Grimm, M. O., Masters, C. L., Beyreuther, K., Hartmann, T., and Lichtenthaler, S. F. (2003). The transmembrane domain of the amyloid precursor protein in microsomal membranes is on both sides shorter than predicted. J Biol Chem **278**, 6803-6808.

Gu, Y., Misonou, H., Sato, T., Dohmae, N., Takio, K., and Ihara, Y. (2001). Distinct intramembrane cleavage of the beta-amyloid precursor protein family resembling gamma-secretase-like cleavage of Notch. J Biol Chem **276**, 35235-35238.

Gunawardena, I. D., Burnett, A., Makeham, V., and Harris, J. P. (2001). Why do some patients with > 80% stenosis of the internal carotid artery not undergo surgery? A retrospective review. ANZ J Surg **71**, 659-661.

Haass, C., Koo, E. H., Capell, A., Teplow, D. B., and Selkoe, D. J. (1995). Polarized sorting of beta-amyloid precursor protein and its proteolytic products in MDCK cells is regulated by two independent signals. J Cell Biol **128**, 537-547.

Harr, S. D., Uint, L., Hollister, R., Hyman, B. T., and Mendez, A. J. (1996). Brain

expression of apolipoproteins E, J, and A-I in Alzheimer's disease. J Neurochem **66**, 2429-2435.

Hayashi, Y., Kashiwagi, K., Ohta, J., Nakajima, M., Kawashima, T., and Yoshikawa, K. (1994). Alzheimer amyloid protein precursor enhances proliferation of neural stem cells from fetal rat brain. Biochem Biophys Res Commun **205**, 936-943.

Heber, S., Herms, J., Gajic, V., Hainfellner, J., Aguzzi, A., Rulicke, T., von Kretzschmar, H., von Koch, C., Sisodia, S., Tremml, P., et al. (2000). Mice with combined gene knock-outs reveal essential and partially redundant functions of amyloid precursor protein family members. J Neurosci **20**, 7951-7963.

Heery, D. M., Kalkhoven, E., Hoare, S., and Parker, M. G. (1997). A signature motif in transcriptional co-activators mediates binding to nuclear receptors. Nature **387**, 733-736.

Hirasawa, A., Saito-Ohara, F., Inoue, J., Aoki, D., Susumu, N., Yokoyama, T., Nozawa, S., Inazawa, J., and Imoto, I. (2003). Association of 17q21-q24 gain in ovarian clear cell adenocarcinomas with poor prognosis and identification of PPM1D and APPBP2 as likely amplification targets. Clin Cancer Res **9**, 1995-2004.

Ho, A., and Sudhof, T. C. (2004). Binding of F-spondin to amyloid-beta precursor protein: a candidate amyloid-beta precursor protein ligand that modulates amyloid-beta precursor protein cleavage. Proc Natl Acad Sci U S A **101**, 2548-2553.

Hock, C., Konietzko, U., Papassotiropoulos, A., Wollmer, A., Streffer, J., von Rotz, R. C., Davey, G., Moritz, E., and Nitsch, R. M. (2002). Generation of antibodies specific for beta-amyloid by vaccination of patients with Alzheimer disease. Nat Med **8**, 1270-1275.

Hock, C., Konietzko, U., Streffer, J. R., Tracy, J., Signorell, A., Muller-Tillmanns, B., Lemke, U., Henke, K., Moritz, E., Garcia, E., et al. (2003). Antibodies against beta-amyloid slow cognitive decline in Alzheimer's disease. Neuron **38**, 547-

Homayouni, R., Rice, D. S., Sheldon, M., and Curran, T. (1999). Disabled-1 binds to the cytoplasmic domain of amyloid precursor-like protein 1. J Neurosci **19**, 7507-7515.

Howell, B. W., Lanier, L. M., Frank, R., Gertler, F. B., and Cooper, J. A. (1999). The disabled 1 phosphotyrosine-binding domain binds to the internalization signals of transmembrane glycoproteins and to phospholipids. Mol Cell Biol **19**, 5179-5188.

Hussain, I., Powell, D., Howlett, D. R., Tew, D. G., Meek, T. D., Chapman, C., Gloger, I. S., Murphy, K. E., Southan, C. D., Ryan, D. M., et al. (1999). Identification of a novel aspartic protease (Asp 2) as beta-secretase. Mol Cell Neurosci **14**, 419-427.

Janus, C. (2003). Vaccines for Alzheimer's disease: how close are we? CNS Drugs **17**, 457-474.

Kaether, C., Skehel, P., and Dotti, C. G. (2000). Axonal membrane proteins are transported in distinct carriers: a two-color video microscopy study in cultured hippocampal neurons. Mol Biol Cell **11**, 1213-1224.

Kamal, A., Almenar-Queralt, A., LeBlanc, J. F., Roberts, E. A., and Goldstein, L. S. (2001). Kinesin-mediated axonal transport of a membrane compartment containing beta-secretase and presenilin-1 requires APP. Nature **414**, 643-648.

Kamal, A., and Goldstein, L. S. (2000). Connecting vesicle transport to the

cytoskeleton. Curr Opin Cell Biol **12**, 503-508.

Kamal, A., Stokin, G. B., Yang, Z., Xia, C. H., and Goldstein, L. S. (2000). Axonal transport of amyloid precursor protein is mediated by direct binding to the kinesin light chain subunit of kinesin-I. Neuron **28**, 449-459.

Kang, J., Lemaire, H. G., Unterbeck, A., Salbaum, J. M., Masters, C. L., Grzeschik, K. H., Multhaup, G., Beyreuther, K., and Muller-Hill, B. (1987). The precursor of Alzheimer's disease amyloid A4 protein resembles a cell-surface receptor. Nature **325**, 733-736.

Kim, T. W., Wu, K., Xu, J. L., McAuliffe, G., Tanzi, R. E., Wasco, W., and Black, I. B. (1995). Selective localization of amyloid precursor-like protein 1 in the cerebral cortex postsynaptic density. Brain Res Mol Brain Res **32**, 36-44.

Kimberly, W. T., Esler, W. P., Ye, W., Ostaszewski, B. L., Gao, J., Diehl, T., Selkoe, D. J., and Wolfe, M. S. (2003). Notch and the amyloid precursor protein are cleaved by similar gamma-secretase(s). Biochemistry **42**, 137-144.

Kimberly, W. T., LaVoie, M. J., Ostaszewski, B. L., Ye, W., Wolfe, M. S., and Selkoe, D. J. (2003). Gamma-secretase is a membrane protein complex comprised of presenilin, nicastrin, Aph-1, and Pen-2. Proc Natl Acad Sci U S A **100**, 6382-6387.

King, G. D., and Scott Turner, R. (2004). Adaptor protein interactions: modulators of amyloid precursor protein metabolism and Alzheimer's disease risk? Exp Neurol **185**, 208-219.

Kinoshita, A., Whelan, C. M., Smith, C. J., Berezovska, O., and Hyman, B. T. (2002). Direct visualization of the gamma secretase-generated carboxyl-terminal domain of the amyloid precursor protein: association with Fe65 and translocation to the nucleus. J Neurochem **82**, 839-847.

Kitaguchi, N., Takahashi, Y., Tokushima, Y., Shiojiri, S., and Ito, H. (1988). Novel precursor of Alzheimer's disease amyloid protein shows protease inhibitory activity. Nature **331**, 530-532.

Klafki, H., Abramowski, D., Swoboda, R., Paganetti, P. A., and Staufenbiel, M. (1996). The carboxyl termini of beta-amyloid peptides 1-40 and 1-42 are generated by distinct gamma-secretase activities. J Biol Chem **271**, 28655-28659.

Koike, H., Tomioka, S., Sorimachi, H., Saido, T. C., Maruyama, K., Okuyama, A., Fujisawa-Sehara, A., Ohno, S., Suzuki, K., and Ishiura, S. (1999). Membrane-anchored metalloprotease MDC9 has an alpha-secretase activity responsible for processing the amyloid precursor protein. Biochem J **343** Pt 2, 371-375.

Koo, E. H., Sisodia, S. S., Archer, D. R., Martin, L. J., Weidemann, A., Beyreuther, K., Fischer, P., Masters, C. L., and Price, D. L. (1990). Precursor of amyloid protein in Alzheimer disease undergoes fast anterograde axonal transport. Proc Natl Acad Sci U S A **87**, 1561-1565.

Lammich, S., Kojro, E., Postina, R., Gilbert, S., Pfeiffer, R., Jasionowski, M., Haass, C., and Fahrenholz, F. (1999). Constitutive and regulated alpha-secretase cleavage of Alzheimer's amyloid precursor protein by a disintegrin metalloprotease. Proc Natl Acad Sci U S A **96**, 3922-3927.

LaVoie, M. J., Fraering, P. C., Ostaszewski, B. L., Ye, W., Kimberly, W. T., Wolfe, M. S., and Selkoe, D. J. (2003). Assembly of the gamma-secretase complex involves early formation of an intermediate subcomplex of Aph-1 and nicastrin. J Biol Chem **278**, 37213-37222.

LaVoie, M. J., and Selkoe, D. J. (2003). The Notch ligands, Jagged and Delta, are sequentially processed by alpha-secretase and presenilin/gamma-secretase and release signaling fragments. J Biol Chem **278**, 34427-34437.

Li, Q., and Sudhof, T. C. (2004). Cleavage of amyloid-beta precursor protein and amyloid-beta precursor-like protein by BACE 1. J Biol Chem **279**, 10542-10550.

Li, Z. W., Stark, G., Gotz, J., Rulicke, T., Gschwind, M., Huber, G., Muller, U., and Weissmann, C. (1996). Generation of mice with a 200-kb amyloid precursor protein gene deletion by Cre recombinase-mediated site-specific recombination in embryonic stem cells. Proc Natl Acad Sci U S A **93**, 6158-6162.

Lorent, K., Overbergh, L., Moechars, D., De Strooper, B., Van Leuven, F., and Van den Berghe, H. (1995). Expression in mouse embryos and in adult mouse brain of three members of the amyloid precursor protein family, of the alpha-2-macroglobulin receptor/low density lipoprotein receptor-related protein and of its ligands apolipoprotein E, lipoprotein lipase, alpha-2-macroglobulin and the 40,000 molecular weight receptor-associated protein. Neuroscience **65**, 1009-1025.

Lyckman, A. W., Confaloni, A. M., Thinakaran, G., Sisodia, S. S., and Moya, K. L. (1998). Post-translational processing and turnover kinetics of presynaptically targeted amyloid precursor superfamily proteins in the central nervous system. J Biol Chem **273**, 11100-11106.

Ma, J., Brewer, H. B., Jr., and Potter, H. (1996). Alzheimer A beta neurotoxicity: promotion by antichymotrypsin, ApoE4; inhibition by A beta-related peptides. Neurobiol Aging **17**, 773-780.

Martin-Morris, L. E., and White, K. (1990). The Drosophila transcript encoded by the beta-amyloid protein precursor-like gene is restricted to the nervous system. Development **110**, 185-195.

Masters, C. L., Multhaup, G., Simms, G., Pottgiesser, J., Martins, R. N., and Beyreuther, K. (1985). Neuronal origin of a cerebral amyloid: neurofibrillary tangles of Alzheimer's disease contain the same protein as the amyloid of plaque cores and blood vessels. Embo J **4**, 2757-2763.

Masters, C. L., Simms, G., Weinman, N. A., Multhaup, G., McDonald, B. L., and Beyreuther, K. (1985). Amyloid plaque core protein in Alzheimer disease and Down syndrome. Proc Natl Acad Sci U S A **82**, 4245-4249.

Matsuda, S., Yasukawa, T., Homma, Y., Ito, Y., Niikura, T., Hiraki, T., Hirai, S., Ohno, S., Kita, Y., Kawasumi, M., et al. (2001). c-Jun N-terminal kinase (JNK)-interacting protein-1b/islet-brain-1 scaffolds Alzheimer's amyloid precursor protein with JNK. J Neurosci **21**, 6597-6607.

Mattaj, I. W., and Englmeier, L. (1998). Nucleocytoplasmic transport: the soluble phase. Annu Rev Biochem **67**, 265-306.

Mattson, M. P., and Chan, S. L. (2003). Neuronal and glial calcium signaling in Alzheimer's disease. Cell Calcium **34**, 385-397.

McIlvain, J. M., Jr., Burkhardt, J. K., Hamm-Alvarez, S., Argon, Y., and Sheetz, M. P. (1994). Regulation of kinesin activity by phosphorylation of kinesin-associated proteins. J Biol Chem **269**, 19176-19182.

McLoughlin, D. M., and Miller, C. C. (1996). The intracellular cytoplasmic domain of the Alzheimer's disease amyloid precursor protein interacts with phosphotyrosine-binding domain proteins in the yeast two-hybrid system. FEBS Lett **397**, 197-200.

McNamara, M. J., Ruff, C. T., Wasco, W., Tanzi, R. E., Thinakaran, G., and Hyman, B. T. (1998). Immunohistochemical and in situ analysis of amyloid precursor-like protein-1 and amyloid precursor-like protein-2 expression in Alzheimer disease and aged control brains. Brain Res **804**, 45-51.

Monni, O., Barlund, M., Mousses, S., Kononen, J., Sauter, G., Heiskanen, M., Paavola, P., Avela, K., Chen, Y., Bittner, M. L., and Kallioniemi, A. (2001). Comprehensive copy number and gene expression profiling of the 17q23 amplicon in human breast cancer. Proc Natl Acad Sci U S A **98**, 5711-5716.

Mueller, H. T., Borg, J. P., Margolis, B., and Turner, R. S. (2000). Modulation of amyloid precursor protein metabolism by X11alpha /Mint-1. A deletion analysis of protein-protein interaction domains. J Biol Chem **275**, 39302-39306.

Muller, U., and Kins, S. (2002). APP on the move. Trends Mol Med **8**, 152-155.

Multhaup, G. (1994). Identification and regulation of the high affinity binding site of the Alzheimer's disease amyloid protein precursor (APP) to glycosaminoglycans. Biochimie **76**, 304-311.

Multhaup, G., Mechler, H., and Masters, C. L. (1995). Characterization of the high affinity heparin binding site of the Alzheimer's disease beta A4 amyloid precursor protein (APP) and its enhancement by zinc(II). J Mol Recognit **8**, 247-257.

Multhaup, G., Schlicksupp, A., Hesse, L., Beher, D., Ruppert, T., Masters, C. L., and Beyreuther, K. (1996). The amyloid precursor protein of Alzheimer's disease in the reduction of copper(II) to copper(I). Science **271**, 1406-1409.

Muresan, Z., and Muresan, V. (2004). A phosphorylated, carboxy-terminal fragment of beta-amyloid precursor protein localizes to the splicing factor compartment. Hum Mol Genet **13**, 475-488.

Nagase, T., Seki, N., Ishikawa, K., Ohira, M., Kawarabayasi, Y., Ohara, O., Tanaka, A., Kotani, H., Miyajima, N., and Nomura, N. (1996). Prediction of the coding sequences of unidentified human genes. VI. The coding sequences of 80 new genes (KIAA0201-KIAA0280) deduced by analysis of cDNA clones from cell line KG-1 and brain. DNA Res **3**, 321-329, 341-354.

Ninomiya, H., Roch, J. M., Sundsmo, M. P., Otero, D. A., and Saitoh, T. (1993). Amino acid sequence RERMS represents the active domain of amyloid beta/A4 protein precursor that promotes fibroblast growth. J Cell Biol **121**, 879-886.

Nunan, J., Williamson, N. A., Hill, A. F., Sernee, M. F., Masters, C. L., and Small, D. H. (2003). Proteasome-mediated degradation of the C-terminus of the Alzheimer's disease beta-amyloid protein precursor: effect of C-terminal truncation on production of beta-amyloid protein. J Neurosci Res **74**, 378-385.

Ohsawa, I., Takamura, C., and Kohsaka, S. (2001). Fibulin-1 binds the amino-terminal head of beta-amyloid precursor protein and modulates its physiological function. J Neurochem **76**, 1411-1420.

Ono, Y., Kinouchi, T., Sorimachi, H., Ishiura, S., and Suzuki, K. (1997). Deletion of an endosomal/lysosomal targeting signal promotes the secretion of Alzheimer's disease amyloid precursor protein (APP). J Biochem (Tokyo) **121**, 585-590.

Panza, F., D'Introno, A., Colacicco, A. M., Basile, A. M., Capurso, C., Kehoe, P. G., Capurso, A., and Solfrizzi, V. (2004). Vascular risk and genetics of sporadic late-onset Alzheimer's disease. J Neural Transm **111**, 69-89.

Pastor, P., and Goate, A. M. (2004). Molecular genetics of Alzheimer's disease. Curr Psychiatry Rep **6**, 125-133.

Perez, R. G., Zheng, H., Van der Ploeg, L. H., and Koo, E. H. (1997). The beta-amyloid precursor protein of Alzheimer's disease enhances neuron viability and modulates neuronal polarity. J Neurosci **17**, 9407-9414.

Qiu, W. Q., Walsh, D. M., Ye, Z., Vekrellis, K., Zhang, J., Podlisny, M. B., Rosner, M. R., Safavi, A., Hersh, L. B., and Selkoe, D. J. (1998). Insulin-degrading enzyme regulates extracellular levels of amyloid beta-protein by degradation. J

Biol Chem **273**, 32730-32738.
Rechsteiner, M., and Rogers, S. W. (1996). PEST sequences and regulation by proteolysis. Trends Biochem Sci **21**, 267-271.
Rossjohn, J., Cappai, R., Feil, S. C., Henry, A., McKinstry, W. J., Galatis, D., Hesse, L., Multhaup, G., Beyreuther, K., Masters, C. L., and Parker, M. W. (1999). Crystal structure of the N-terminal, growth factor-like domain of Alzheimer amyloid precursor protein. Nat Struct Biol **6**, 327-331.
Russo, C., Dolcini, V., Salis, S., Venezia, V., Zambrano, N., Russo, T., and Schettini, G. (2002). Signal transduction through tyrosine-phosphorylated C-terminal fragments of amyloid precursor protein via an enhanced interaction with Shc/Grb2 adaptor proteins in reactive astrocytes of Alzheimer's disease brain. J Biol Chem **277**, 35282-35288.
Sabo, S. L., Ikin, A. F., Buxbaum, J. D., and Greengard, P. (2001). The Alzheimer amyloid precursor protein (APP) and FE65, an APP-binding protein, regulate cell movement. J Cell Biol **153**, 1403-1414.
Sabo, S. L., Lanier, L. M., Ikin, A. F., Khorkova, O., Sahasrabudhe, S., Greengard, P., and Buxbaum, J. D. (1999). Regulation of beta-amyloid secretion by FE65, an amyloid protein precursor-binding protein. J Biol Chem **274**, 7952-7957.
Saito-Ohara, F., Imoto, I., Inoue, J., Hosoi, H., Nakagawara, A., Sugimoto, T., and Inazawa, J. (2003). PPM1D is a potential target for 17q gain in neuroblastoma. Cancer Res **63**, 1876-1883.
Sandbrink, R., Banati, R., Masters, C. L., Beyreuther, K., and Konig, G. (1993). Expression of L-APP mRNA in brain cells. Ann N Y Acad Sci **695**, 183-189.
Sandbrink, R., Masters, C. L., and Beyreuther, K. (1994). Beta A4-amyloid protein precursor mRNA isoforms without exon 15 are ubiquitously expressed in rat tissues including brain, but not in neurons. J Biol Chem **269**, 1510-1517.
Sandbrink, R., Monning, U., Masters, C. L., and Beyreuther, K. (1997). Expression of the APP gene family in brain cells, brain development and aging. Gerontology **43**, 119-131.
Scheinfeld, M. H., Ghersi, E., Laky, K., Fowlkes, B. J., and D'Adamio, L. (2002). Processing of beta-amyloid precursor-like protein-1 and -2 by gamma-secretase regulates transcription. J Biol Chem **277**, 44195-44201.
Scheinfeld, M. H., Matsuda, S., and D'Adamio, L. (2003). JNK-interacting protein-1 promotes transcription of A beta protein precursor but not A beta precursor-like proteins, mechanistically different than Fe65. Proc Natl Acad Sci U S A **100**, 1729-1734.
Schenk, D., Barbour, R., Dunn, W., Gordon, G., Grajeda, H., Guido, T., Hu, K., Huang, J., Johnson-Wood, K., Khan, K., et al. (1999). Immunization with amyloid-beta attenuates Alzheimer-disease-like pathology in the PDAPP mouse. Nature **400**, 173-177.
Scheuermann, S., Hambsch, B., Hesse, L., Stumm, J., Schmidt, C., Beher, D., Bayer, T. A., Beyreuther, K., and Multhaup, G. (2001). Homodimerization of amyloid precursor protein and its implication in the amyloidogenic pathway of Alzheimer's disease. J Biol Chem **276**, 33923-33929.
Schlessinger, J. (2002). Ligand-induced, receptor-mediated dimerization and activation of EGF receptor. Cell **110**, 669-672.
Schroeter, E. H., Ilagan, M. X., Brunkan, A. L., Hecimovic, S., Li, Y. M., Xu, M., Lewis, H. D., Saxena, M. T., De Strooper, B., Coonrod, A., et al. (2003). A presenilin dimer at the core of the gamma-secretase enzyme: insights from parallel analysis of Notch 1 and APP proteolysis. Proc Natl Acad Sci U S A **100**, 13075-13080.

Selkoe, D., and Kopan, R. (2003). Notch and Presenilin: regulated intramembrane proteolysis links development and degeneration. Annu Rev Neurosci **26**, 565-597.

Selkoe, D. J. (1994). Cell biology of the amyloid beta-protein precursor and the mechanism of Alzheimer's disease. Annu Rev Cell Biol **10**, 373-403.

Selkoe, D. J. (2002). Alzheimer's disease is a synaptic failure. Science **298**, 789-791.

Selkoe, D. J., Yamazaki, T., Citron, M., Podlisny, M. B., Koo, E. H., Teplow, D. B., and Haass, C. (1996). The role of APP processing and trafficking pathways in the formation of amyloid beta-protein. Ann N Y Acad Sci **777**, 57-64.

Seubert, P., Oltersdorf, T., Lee, M. G., Barbour, R., Blomquist, C., Davis, D. L., Bryant, K., Fritz, L. C., Galasko, D., Thal, L. J., and et al. (1993). Secretion of beta-amyloid precursor protein cleaved at the amino terminus of the beta-amyloid peptide. Nature **361**, 260-263.

Shirotani, K., Edbauer, D., Capell, A., Schmitz, J., Steiner, H., and Haass, C. (2003). Gamma-secretase activity is associated with a conformational change of nicastrin. J Biol Chem **278**, 16474-16477.

Simons, A., Ruppert, T., Schmidt, C., Schlicksupp, A., Pipkorn, R., Reed, J., Masters, C. L., White, A. R., Cappai, R., Beyreuther, K., et al. (2002). Evidence for a copper-binding superfamily of the amyloid precursor protein. Biochemistry **41**, 9310-9320.

Sinha, S., Anderson, J. P., Barbour, R., Basi, G. S., Caccavello, R., Davis, D., Doan, M., Dovey, H. F., Frigon, N., Hong, J., et al. (1999). Purification and cloning of amyloid precursor protein beta-secretase from human brain. Nature **402**, 537-540.

Sisodia, S. S., Koo, E. H., Hoffman, P. N., Perry, G., and Price, D. L. (1993). Identification and transport of full-length amyloid precursor proteins in rat peripheral nervous system. J Neurosci **13**, 3136-3142.

Skovronsky, D. M., Pijak, D. S., Doms, R. W., and Lee, V. M. (2000). A distinct ER/IC gamma-secretase competes with the proteasome for cleavage of APP. Biochemistry **39**, 810-817.

Slunt, H. H., Thinakaran, G., Von Koch, C., Lo, A. C., Tanzi, R. E., and Sisodia, S. S. (1994). Expression of a ubiquitous, cross-reactive homologue of the mouse beta-amyloid precursor protein (APP). J Biol Chem **269**, 2637-2644.

Small, D. H., Mok, S. S., and Bornstein, J. C. (2001). Alzheimer's disease and Abeta toxicity: from top to bottom. Nat Rev Neurosci **2**, 595-598.

Small, D. H., Nurcombe, V., Moir, R., Michaelson, S., Monard, D., Beyreuther, K., and Masters, C. L. (1992). Association and release of the amyloid protein precursor of Alzheimer's disease from chick brain extracellular matrix. J Neurosci **12**, 4143-4150.

Suzuki, N., Cheung, T. T., Cai, X. D., Odaka, A., Otvos, L., Jr., Eckman, C., Golde, T. E., and Younkin, S. G. (1994). An increased percentage of long amyloid beta protein secreted by familial amyloid beta protein precursor (beta APP717) mutants. Science **264**, 1336-1340.

Takasugi, N., Tomita, T., Hayashi, I., Tsuruoka, M., Niimura, M., Takahashi, Y., Thinakaran, G., and Iwatsubo, T. (2003). The role of presenilin cofactors in the gamma-secretase complex. Nature **422**, 438-441.

Tanaka, S., Nakamura, S., Ueda, K., Kameyama, M., Shiojiri, S., Takahashi, Y., Kitaguchi, N., and Ito, H. (1988). Three types of amyloid protein precursor mRNA in human brain: their differential expression in Alzheimer's disease. Biochem Biophys Res Commun **157**, 472-479.

Tanzi, R. E., McClatchey, A. I., Lamperti, E. D., Villa-Komaroff, L., Gusella, J. F., and

Neve, R. L. (1988). Protease inhibitor domain encoded by an amyloid protein precursor mRNA associated with Alzheimer's disease. Nature **331**, 528-530.

Tarr, P. E., Roncarati, R., Pelicci, G., Pelicci, P. G., and D'Adamio, L. (2002). Tyrosine phosphorylation of the beta-amyloid precursor protein cytoplasmic tail promotes interaction with Shc. J Biol Chem **277**, 16798-16804.

Tienari, P. J., De Strooper, B., Ikonen, E., Simons, M., Weidemann, A., Czech, C., Hartmann, T., Ida, N., Multhaup, G., Masters, C. L., et al. (1996). The beta-amyloid domain is essential for axonal sorting of amyloid precursor protein. Embo J **15**, 5218-5229.

Tomita, S., Ozaki, T., Taru, H., Oguchi, S., Takeda, S., Yagi, Y., Sakiyama, S., Kirino, Y., and Suzuki, T. (1999). Interaction of a neuron-specific protein containing PDZ domains with Alzheimer's amyloid precursor protein. J Biol Chem **274**, 2243-2254.

Trommsdorff, M., Borg, J. P., Margolis, B., and Herz, J. (1998). Interaction of cytosolic adaptor proteins with neuronal apolipoprotein E receptors and the amyloid precursor protein. J Biol Chem **273**, 33556-33560.

Vale, R. D., Reese, T. S., and Sheetz, M. P. (1985). Identification of a novel force-generating protein, kinesin, involved in microtubule-based motility. Cell **42**, 39-50.

Vassar, R., Bennett, B. D., Babu-Khan, S., Kahn, S., Mendiaz, E. A., Denis, P., Teplow, D. B., Ross, S., Amarante, P., Loeloff, R., et al. (1999). Beta-secretase cleavage of Alzheimer's amyloid precursor protein by the transmembrane aspartic protease BACE. Science **286**, 735-741.

Vekrellis, K., Ye, Z., Qiu, W. Q., Walsh, D., Hartley, D., Chesneau, V., Rosner, M. R., and Selkoe, D. J. (2000). Neurons regulate extracellular levels of amyloid beta-protein via proteolysis by insulin-degrading enzyme. J Neurosci **20**, 1657-1665.

Verhey, K. J., Meyer, D., Deehan, R., Blenis, J., Schnapp, B. J., Rapoport, T. A., and Margolis, B. (2001). Cargo of kinesin identified as JIP scaffolding proteins and associated signaling molecules. J Cell Biol **152**, 959-970.

von Koch, C. S., Zheng, H., Chen, H., Trumbauer, M., Thinakaran, G., van der Ploeg, L. H., Price, D. L., and Sisodia, S. S. (1997). Generation of APLP2 KO mice and early postnatal lethality in APLP2/APP double KO mice. Neurobiol Aging **18**, 661-669.

von Rotz, R. C., Kohli, B. M., Bosset, J., Meier, M., Suzuki, T., Nitsch, R. M., and Konietzko, U. (2004). The APP intracellular domain forms nuclear multiprotein complexes and regulates the transcription of its own precursor. J Cell Sci *117*, 4435-4448.

Walsh, D. M., Fadeeva, J. V., LaVoie, M. J., Paliga, K., Eggert, S., Kimberly, W. T., Wasco, W., and Selkoe, D. J. (2003). gamma-Secretase cleavage and binding to FE65 regulate the nuclear translocation of the intracellular C-terminal domain (ICD) of the APP family of proteins. Biochemistry **42**, 6664-6673.

Wasco, W., Bupp, K., Magendantz, M., Gusella, J. F., Tanzi, R. E., and Solomon, F. (1992). Identification of a mouse brain cDNA that encodes a protein related to the Alzheimer disease-associated amyloid beta protein precursor. Proc Natl Acad Sci U S A **89**, 10758-10762

Wasco, W., Gurubhagavatula, S., Paradis, M. D., Romano, D. M., Sisodia, S. S., Hyman, B. T., Neve, R. L., and Tanzi, R. E. (1993). Isolation and characterization of APLP2 encoding a homologue of the Alzheimer's associated amyloid beta protein precursor. Nat Genet **5**, 95-100.

Weidemann, A., Eggert, S., Reinhard, F. B., Vogel, M., Paliga, K., Baier, G., Masters,

C. L., Beyreuther, K., and Evin, G. (2002). A novel epsilon-cleavage within the transmembrane domain of the Alzheimer amyloid precursor protein demonstrates homology with Notch processing. Biochemistry **41**, 2825-2835.

Weidemann, A., Konig, G., Bunke, D., Fischer, P., Salbaum, J. M., Masters, C. L., and Beyreuther, K. (1989). Identification, biogenesis, and localization of precursors of Alzheimer's disease A4 amyloid protein. Cell **57**, 115-126.

Williamson, T. G., Mok, S. S., Henry, A., Cappai, R., Lander, A. D., Nurcombe, V., Beyreuther, K., Masters, C. L., and Small, D. H. (1996). Secreted glypican binds to the amyloid precursor protein of Alzheimer's disease (APP) and inhibits APP-induced neurite outgrowth. J Biol Chem **271**, 31215-31221.

Williamson, T. G., Nurcombe, V., Beyreuther, K., Masters, C. L., and Small, D. H. (1995). Affinity purification of proteoglycans that bind to the amyloid protein precursor of Alzheimer's disease. J Neurochem **65**, 2201-2208.

Wolfe, M. S., Xia, W., Ostaszewski, B. L., Diehl, T. S., Kimberly, W. T., and Selkoe, D. J. (1999). Two transmembrane aspartates in presenilin-1 required for presenilin endoproteolysis and gamma-secretase activity. Nature **398**, 513-517.

Yamazaki, T., Selkoe, D. J., and Koo, E. H. (1995). Trafficking of cell surface beta-amyloid precursor protein: retrograde and transcytotic transport in cultured neurons. J Cell Biol **129**, 431-442.

Yan, R., Bienkowski, M. J., Shuck, M. E., Miao, H., Tory, M. C., Pauley, A. M., Brashier, J. R., Stratman, N. C., Mathews, W. R., Buhl, A. E., et al. (1999). Membrane-anchored aspartyl protease with Alzheimer's disease beta-secretase activity. Nature **402**, 533-537.

Zambrano, N., Buxbaum, J. D., Minopoli, G., Fiore, F., De Candia, P., De Renzis, S., Faraonio, R., Sabo, S., Cheetham, J., Sudol, M., and Russo, T. (1997). Interaction of the phosphotyrosine interaction/phosphotyrosine binding-related domains of Fe65 with wild-type and mutant Alzheimer's beta-amyloid precursor proteins. J Biol Chem **272**, 6399-6405.

Zhang, Y., Yang, Y., Yeh, S., and Chang, C. (2004). ARA67/PAT1 functions as a repressor to suppress androgen receptor transactivation. Mol Cell Biol **24**, 1044-1057.

Zhang, Z., Lee, C. H., Mandiyan, V., Borg, J. P., Margolis, B., Schlessinger, J., and Kuriyan, J. (1997). Sequence-specific recognition of the internalization motif of the Alzheimer's amyloid precursor protein by the X11 PTB domain. Embo J **16**, 6141-6150.

Zheng, P., Eastman, J., Vande Pol, S., and Pimplikar, S. W. (1998). PAT1, a microtubule-interacting protein, recognizes the basolateral sorting signal of amyloid precursor protein. Proc Natl Acad Sci U S A **95**, 14745-14750.